



HAL
open science

Micro-structured membrane as a 3D biodegradable scaffold : development, characterization and cell-matrix interaction

Pritam Das

► **To cite this version:**

Pritam Das. Micro-structured membrane as a 3D biodegradable scaffold : development, characterization and cell-matrix interaction. Biomechanics [physics.med-ph]. Université Paul Sabatier - Toulouse III; Universiteit Twente (Enschede, Nederland); Univerità della Calabria (Rende, Italia), 2018. English. NNT : 2018TOU30282 . tel-02417498

HAL Id: tel-02417498

<https://theses.hal.science/tel-02417498v1>

Submitted on 18 Dec 2019

HAL is a multi-disciplinary open access archive for the deposit and dissemination of scientific research documents, whether they are published or not. The documents may come from teaching and research institutions in France or abroad, or from public or private research centers.

L'archive ouverte pluridisciplinaire **HAL**, est destinée au dépôt et à la diffusion de documents scientifiques de niveau recherche, publiés ou non, émanant des établissements d'enseignement et de recherche français ou étrangers, des laboratoires publics ou privés.

Université Fédérale



Toulouse Midi-Pyrénées

THÈSE

En vue de l'obtention du DOCTORAT DE L'UNIVERSITÉ DE TOULOUSE

Délivré par l'Université Toulouse 3 - Paul Sabatier

Cotutelle internationale : University of Calabria, Rende, Italy
Et University of Twente, Enschede, The Netherlands

Présentée et soutenue par

Pritam DAS

Le 14 décembre 2018

**Membrane micro-structurée utilisable comme support au
développement de cellule humaine : Développement,
caractérisation et interaction cellule-matrice**

Ecole doctorale : **MEGEP - Mécanique, Energétique, Génie civil, Procédés**

Spécialité : **Génie des Procédés et de l'Environnement**

Unité de recherche :

LGC - Laboratoire de Génie Chimique

Thèse dirigée par

Patrice BACCHIN et Jean Francois LAHITTE

Jury

M. Antoine Venault, Rapporteur
Mme Cécile Legallais, Rapporteur
Mme Loredana De Bartolo, Examinateur
M. Andries D. van der Meer, Examinateur
Mme Sylvie Lorthoïs, Examinateur
M. Patrice BACCHIN, Directeur de thèse

Micro-structured membrane as a 3D biodegradable scaffold:

Development, characterization and cell-matrix interaction

Dissertation

To obtain

The degree of joint Doctorate from

University Paul Sabatier, France

University of Calabria, Italy

University of Twente, The Netherlands

On the authority of the corresponding rector magnificus,

On account of the decision of the graduation committee,

To be publicly defended

On Friday 14th December 2018 at 10 am.

By

Pritam Das

Born 23rd September 1990 in Serampore, West Bengal, India

Composition of the thesis Committee

Reviewers (Jury):

- Cécile Legallais, Research director, CNRS, Université Technologique de Compiègne, France
- Antoine Venault, Associate Professor, Chung Yuan Christian University, Taiwan

Examiners (Jury):

- Loredana De Bartolo, Senior researcher, ITM CNR, Italy
- Sylvie Lorthois, Research director, IMFT, CNRS, France
- Andries Van Der Meer, Assistant Professor, University of Twente, Netherlands
- Patrice Bacchin, Professor, Université de Toulouse, France

Guests:

- Barbara Garmy-Susini, Research director, Inserm, France
- Jean François Lahitte, Associate Professor, Université de Toulouse, France
- Rob Lammertink, Professor, University of Twente, Netherlands

This research work is presented in this thesis has been funded by Erasmus Mundus Doctorate in Membrane Engineering (EUDIME)-5th Ed. Under the division of Education, Audio-visual and Culture Executive Agency (EACEA) grant. - <http://www.eudime.unical.it>. And the research work was Co-supervised corresponding to the three Universities as follows-

Patrice Bacchin	Professor	Thesis Director	Chemical Engineering	University Paul Sabatier, France (Home)
Jean-François Lahitte	Associate Professor	Thesis co-director	(“)	(“)
Jean-Christophe Remigy	Professor		(“)	(“)
Clémence Coetsier	Assistant Professor		(“)	(“)
Barbara Garmy-Susini	Research Director			Inserm, France
Loredana De Bartolo	Senior Researcher		Institute on Membrane Technology	University of Calabria, Italy (Host1)
Simona Salerno	Researcher		(“)	(“)
Andries D. van der Meer	Assistant Professor		Applied Stem Cell Technology	University of Twente, Netherlands (Host 2)
Rob G. H. Lammertink	Professor		Membrane Science and Technology	(“)

UNIVERSITÀ
DELLA CALABRIA



UNIVERSITY OF TWENTE.

© All rights reserved. No parts of this thesis may be reproduced, stored in a retrieval system or transmitted in any form or by any means without permission of the author.

**I would like to dedicate
this work to my family,
friends and my beloved
teachers whose constant
guide, support and
affection is my real asset
and remains always in
my heart.**

***“All power is within you. You can do anything and
everything. Believe in that. Do not believe that you
are weak.
Strength is life, weakness is death.”***

-Swami Vivekananda

Micro-structured membrane as a 3D biodegradable scaffold:

Development, characterization and cell-matrix interaction

Summary of the thesis in English

Over the last decades, three-dimensional (3D) scaffolds are unfolding many promising applications in tissue engineering and regenerative medicine field by providing suitable microenvironment for the incorporation of cells or growth factors to regenerate damaged tissues or organs. The three-dimensional polymeric porous scaffolds with higher porosities having homogeneous interconnected pore network are highly useful for tissue engineering.

In this context, a poly (ϵ - caprolactone) PCL/chitosan CHT blend membrane with a double porous morphology was developed by modified liquid induced phase inversion technique. The membrane shows: (i) surface macrovoids (big pores) which could be easily accessible for cells invasion and viability; (ii) interconnected microporous (small pores) network to transfer essential nutrients, oxygen, growth factors between the macrovoids and throughout the scaffolds. The physico-chemical properties (pore size, surface chemistry and biodegradability) of the materials have been characterized. This study shows how it is possible to tune the membrane properties by changing the PCL/CHT ratio.

Human mesenchymal stem cell (hMSCs) culture was performed on the membranes and the cell viability and proliferation was investigated by MTT assay and oxygen uptake rate experiments. The experiments demonstrate that the membranes are biocompatible and can be colonized by the cells at micron scale. Confocal microscopy images show that the cells are able to adhere and penetrate inside the macrovoids of the membranes. Both cell proliferation and oxygen uptake increase with time especially on membranes with lower chitosan concentration. The presence of chitosan in the blend produces an increase of porosity that affect the entrapment of the cells inside the porous bulk of the membranes. Successful cellular proliferation of hMSCs could be useful to enhance longevity of other primary cells by production of corresponding growth factors.

To test the dynamic behavior of cells on the membranes, an organ-on-chip (OOC) device has been developed with human umbilical endothelial cells (HUVECs) seeded on the membrane. The hydraulic resistance of the cellular barrier on the membrane has been quantified for real time trans-endothelial pressure (TEP) 20 cmH₂O at 37 degree C and with living cells after 1 day and 3 day of post seeding. Results suggests this kind of polymeric scaffolds can be useful in future as an in vivo patch to repair disrupted vessels.

Résumé de la thèse en français

Les matériaux à structure tridimensionnelle laissent entrevoir de nombreuses applications prometteuses dans le domaine de l'ingénierie tissulaire et de la médecine régénérative en fournissant un micro-environnement approprié pour l'incorporation de cellules ou de facteurs de croissance afin de régénérer des tissus ou organes endommagés.

Dans ce contexte, une membrane a été élaborée à partir d'un mélange de poly (-caprolactone) PCL / chitosan CHT à partir d'une technique d'inversion de phase permettant un apport localisé de non solvant. La technique permet d'obtenir une double morphologie poreuse : (i) des macrovides en surface (gros pores) facilement accessibles pour l'invasion et la viabilité des cellules; (ii) un réseau macroporeux interconnecté (petits pores) pour transférer les nutriments, l'oxygène, le facteur de croissance à travers le matériau. Les propriétés physico-chimiques (taille des pores, chimie de surface et biodégradabilité) des matériaux ont été caractérisées. Il est montré comment il est possible d'ajuster les propriétés de la membrane en modifiant le rapport PCL / CHT.

Des cultures de cellules souches mésenchymateuses humaines (CSMh) ont été réalisées sur la membrane. La viabilité et la prolifération cellulaires ont été étudiées par des essais de test au MTT et de taux d'absorption d'oxygène. Les expériences démontrent que la membrane est biocompatible et peut être colonisée par les cellules. La microscopie confocale montre que les cellules sont capables de pénétrer à l'intérieur des macrovides de la membrane. La prolifération cellulaire de CSM dans ce matériau pourrait être utile pour augmenter la longévité d'autres cellules primaires en modifiant les CSM pour produire des facteurs de croissance.

Pour tester le comportement dynamique des cellules sur la membrane, un dispositif d'organe sur puce a été développé avec des cellules endothéliales ombilicales humainesensemencées sur la membrane. Les résistances hydrauliques de la barrière cellulaire sur la membrane ont été quantifiées en temps réel pour une pression trans-endothéliale (PTE), 20 cm H₂O à 37 ° C et avec des cellules vivantes après 1 jour et 3 jours après l'ensemencement. Les résultats suggèrent que ce type d'échafaudages polymères peut être utile à l'avenir comme patch in vivo pour réparer des vaisseaux endommagés.

Riassunto della tesi in italiano

Negli ultimi decenni, scaffolds tridimensionali (3D) si stanno rivelando particolarmente promettenti in diverse applicazioni nel campo dell'ingegneria tissutale e della medicina rigenerativa, poiché forniscono un microambiente adatto per l'incorporazione di cellule o fattori di crescita per rigenerare tessuti o organi danneggiati. Scaffolds porosi polimerici tridimensionali, con porosità più elevate e con un reticolo omogeneo di pori interconnessi, sono particolarmente utili per l'ingegneria tissutale.

A questo proposito è stata realizzata, mediante una modifica della tecnica di inversione di fase indotta da non solvente, una membrana da una miscela polimerica di poli(ϵ -caprolattone) e chitosano (PCL/CHT), avente una morfologia con doppia porosità. La membrana sviluppata mostra: (i) macrovuoti o macropori di superficie che potrebbero essere facilmente accessibili per l'intrappolamento e la vitalità cellulare; (ii) una rete interconnessa microporosa per il trasporto di nutrienti essenziali, ossigeno e fattori di crescita tra i macropori ed attraverso la membrana. Sono state caratterizzate le proprietà chimico-fisiche (dimensione dei pori, chimica della superficie e biodegradabilità) delle membrane realizzate. Questo studio dimostra come sia possibile regolare le proprietà della membrana variando il rapporto PCL/CHT.

E' stata realizzata una coltura di cellule staminali mesenchimali umane (hMSCs) sulle membrane sviluppate e sono state valutate la vitalità e la proliferazione cellulare, mediante dosaggi di vitalità con MTT, e mediante esperimenti di valutazione delle velocità di consumo di ossigeno. I risultati ottenuti dimostrano che le membrane sono biocompatibili e possono essere colonizzate dalle cellule a livello micrometrico. Immagini di microscopia confocale mostrano come le cellule siano in grado di aderire e penetrare all'interno dei macropori delle membrane. Sia la proliferazione cellulare che il consumo di ossigeno aumentano nel tempo specialmente su membrane con più alte concentrazioni di chitosano. La presenza di CHT nella miscela polimerica causa un aumento della porosità che influenza l'intrappolamento delle cellule nella matrice porosa delle membrane. Una proliferazione proficua delle hMSC potrebbe essere utile per migliorare la longevità di altre cellule primarie mediante la produzione di fattori di crescita corrispondenti.

Per testare il comportamento dinamico delle cellule sulle membrane, è stato sviluppato un dispositivo di organo su chip (OOC) con cellule endoteliali umane ombelicali (HUVEC) seminate sulla membrana. La resistenza idraulica della barriera cellulare sulla membrana è stata quantificata per la pressione trans-endoteliale in tempo reale (TEP) di 20 cm H₂O a 37 °C e con cellule vitali dopo 1 e 3 giorni di coltura. I risultati suggeriscono che questo tipo di scaffolds polimerici può essere utile in futuro come patch in vivo per riparare vasi danneggiati.

Samenvatting van de scriptie in het Nederlands

Gedurende de laatste decennia ontvouwen driedimensionale (3D) scaffolds vele veelbelovende toepassingen op het gebied van tissue engineering en regeneratieve geneeskunde door het verschaffen van een geschikte micro-omgeving voor de opname van cellen of groeifactoren om beschadigde weefsels of organen te regenereren. De driedimensionale polymere poreuze scaffolds met hogere porositeiten met homogeen onderling verbonden porie-netwerk zijn zeer bruikbaar voor tissue-engineering.

In deze context, een poly (ϵ -caprolacton) PCL / chitosan CHT-blendmembraan met een dubbele poreuze morfologie werd gevormd door gemodificeerde vloeistofgeïnduceerde fase-inversietechniek: (i) oppervlakte-macrololten (grote poriën) die gemakkelijk toegankelijk zouden kunnen zijn voor invasie en levensvatbaarheid van cellen; (ii) onderling verbonden macroporeuze (kleine poriën) netwerk om essentiële voedingsstoffen, zuurstof, groeifactor over te dragen tussen de macrololten en door de steigers heen. De fysisch-chemische eigenschappen (poriegrootte, oppervlaktechemie en biologische afbreekbaarheid) van de materialen zijn gekarakteriseerd. Deze studie laat zien hoe het mogelijk is om de membraaneigenschappen af te stemmen door de PCL / CHT-ratio te veranderen.

Humane mesenchymale stamcel (hMSCs) kweek werd op het membraan uitgevoerd en de levensvatbaarheid en proliferatie van de cel werd onderzocht met behulp van MTT-test en zuurstofopnamesnelheidsexperimenten. De experimenten tonen aan dat het membraan biocompatibel is en door de cellen kan worden gekoloniseerd. Confocale microscopie toont aan dat de cellen in de macrololten (micrometrische poriën) van het membraan kunnen penetreren. Succesvolle cellulaire proliferatie van hMSC's zou nuttig kunnen zijn om de levensduur van andere primaire cellen te verbeteren door productie van overeenkomstige groeifactoren.

Om het dynamische gedrag van cellen op het membraan te testen, is een Organ-on-chip (OOC) -apparaat ontwikkeld met humane navelstreng endotheelcellen (HUVEC's) die op het membraan zijn gezaaid.

De hydraulische weerstand van de cellulaire barrière op het membraan is gekwantificeerd voor real-time trans-endotheliale druk (TEP) 20 cm H₂O bij 37 °C en met levende cellen na 1 dag en 3 dagen na uitzaaiing. Resultaten suggereren dat dit soort polymere scaffolds in de toekomst bruikbaar kunnen zijn als een in vivo patch om verstoorde vaten te repareren.

Contents

Chapter 1: General Introduction.....	1
<hr/>	
1.1 Tissue engineering paradigm.....	1
1.2 General principle of tissue engineering	2
1.3 Current Research approach	5
1.4 Polymer materials as biomaterials for tissue engineering	6
1.5 Advantage of Three-dimensional polymer scaffolds on cellular adhesion.....	10
1.5.1 Porous scaffolds and effect of pore size and pore morphology	11
1.5.2 Previous approach to develop porous morphology and it's limitations.....	12
1.5.3 Evolution of double porous morphology	13
1.6 Necessity of Organ-on-chips (OOCs) for tissue engineering	14
1.7 Research Framework and outline	16
1.8 Project funding and collaborations.....	19
Chapter 2: Double porous poly (ϵ-caprolactone)/chitosan membrane as tissue engineering scaffold: development, characterization and biodegradation	20
<hr/>	
2.1 Summary of the Chapter	20
2.2 Introduction	20
2.3 Materials.....	22
2.4 Methods	23
2.4.1 Development of the membrane with a double porosity level	23
2.4.2 Viscosity measurements of the polymer solution	26
2.4.3 Scanning electron microscopic (SEM) analysis	26
2.4.4 Attenuated total reflection (ATR)-Fourier transformed infrared (FTIR) spectroscopic analysis and mapping.....	26
2.4.5 X-ray diffraction (XRD) analysis.....	26
2.4.6 Differential scanning calorimetric (DSC) measurements.....	27
2.4.7 Enzymatic degradation of the blend.....	27
2.5 Results.....	28
2.5.1 Polymer-solvent-nonsolvent optimization.....	28
2.5.2 Morphology of the double porous material	31

2.5.3	Chemical characterization by ATR-FTIR spectra.....	33
2.5.4	Crystalline and thermal properties	37
2.5.5	Enzymatic degradation	40
2.6	Discussion	43
2.6.1	Microscopic PCL/CHT chemical structure	44
2.6.2	Mesoscopic morphological structuration of the membrane.....	46
2.7	Conclusions.....	50
2.8	Acknowledgements	51
	Chapter 3: Double porous, biodegradable poly (ϵ - caprolactone)/chitosan 3D membrane scaffolds: understanding hMSCs attachment, proliferation and invasion by varying pore size and morphology of the scaffolds	52
<hr/>		
3.1	Summary of the chapter.....	52
3.2	Introduction	53
3.3	Materials and methods.....	56
3.3.1	Membrane fabrication with 3D double porosity	56
3.3.2	Membrane characterization	57
3.3.3	Cell Culture.....	58
3.3.3.1	Effective surface area (ESA %) for cell viability.....	58
3.3.3.2	Cell morphology by SEM analysis	58
3.3.3.3	Cell morphology by CLSM.....	59
3.3.3.4	Cell Proliferation	59
3.3.3.5	Oxygen uptake rate (OUR) measurements	60
3.3.4	Statistical analysis	60
3.4	Results.....	60
3.4.1	Membrane properties	60
3.5	Discussion	72
3.6	Conclusions.....	76

Chapter 4: Fabrication of tuneable micro-structured flat sheet membrane in Organ-on-chip to monitor trans-endothelial hydraulic resistance	78
<hr/>	
4.1 Summary of the chapter.....	78
4.2 Introduction	79
4.3 Materials and Methods:	81
4.3.1 Materials	81
4.3.2 Methods	82
4.3.2.1 Double porous membrane scaffolds fabrication	82
4.3.2.2 Membrane characterization by SEM	82
4.3.2.3 Organ-on-chip fabrication.....	82
4.3.2.4 Hydraulic resistance measurements in different pressure by Fluigent set up ...	83
4.3.2.5 Flux before and after the cell seeding by Fluigent set up.....	84
4.3.2.5.1 Flux before cell seeding	84
4.3.2.5.2 Cell seeding	85
4.3.2.5.3 Flux after Cell seeding and staining.....	85
4.3.2.5.4 Calculation of the hydraulic resistance of HUVECs	86
4.3.2.5.5 Statistical analysis.....	86
4.4 Results and discussion:.....	87
4.4.1 Membrane morphological characteristics	87
4.4.2 Permeate flux and Hydraulic resistance of the membrane at different pressure regime	89
4.4.2.1 Permeate flux and Hydraulic resistance of the membranes without cells.....	89
4.4.2.2 Permeate flux and Hydraulic resistance of membranes with cell cultures	92
4.4.3 Microscopic observation of cells on the membrane	95
4.5 Conclusion	97
4.6 Acknowledgment:	98
4.7 Supplementary materials	98
4.7.1 Verification of the absence of leakage with fluorescent dye.....	98
4.7.2 Permeate flux of the membrane in Amicon cell	99
5 <i>General conclusion and perspectives</i>	102
<hr/>	
5.1 General conclusion	102
5.2 Perspectives	105
6 References	108

7	Scientific Output	121
7.1	Publications	121
7.2	Conferences	121
8	Thank You.....	122
9	About the Author	124

Chapter 1: General Introduction

1.1 Tissue engineering paradigm

Tissue engineering is an interdisciplinary field that should find many applications to develop tissue regeneration or reconstruction via applying the principle of engineering and biology. It also refers to regenerative medicine by which biofunctional human tissues can be constructed by cells in a laboratory. The ultimate goal of tissue engineering is to use those tissue to replace human organs which were damaged by diseases, genetic abnormalities or traumatic injury. Tissue engineering relies on three important factors (Fig. 1).

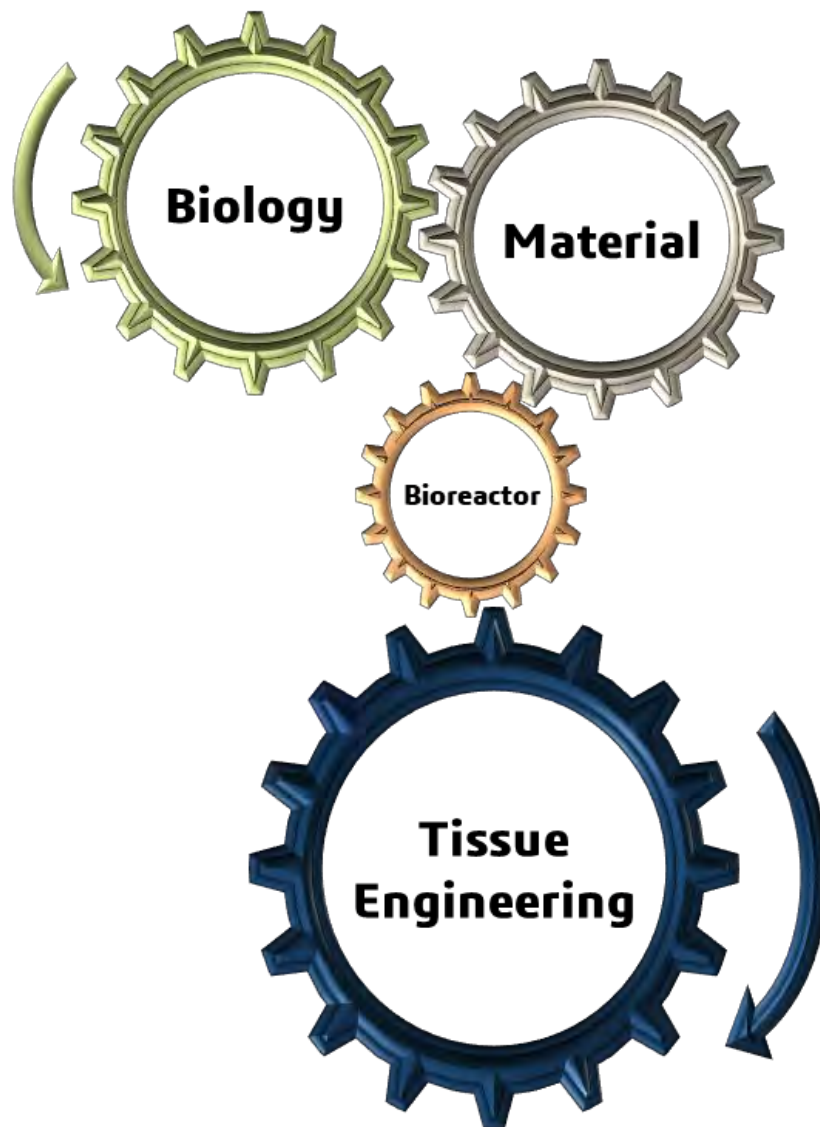


Fig. 1. Role of Biological Science, Material Science and Bioreactors on tissue engineering.

Biology; which refers to use the right cells to construct the target tissue and also the right biomolecule to keeps those cells healthy and productive. Materials; or biomaterials which refers to provide the right environment to support the cellular growth. The material can be sometimes degrade overtime or remains inside the body to provide support to the organs. And Bioreactors; where the tissue construct can be prepared by using the cells and material with proper conditioning. The bioreactor can be inside the laboratory, which called as *in vitro* condition, or it can be inside the physiological condition, which called as *in vivo* condition [1].

The rapid reconstruction of biomaterials remains an important challenge, emphasizing the need to reproduce smart biomedical device for tissue engineering and regenerative medicine application [2–5]. Progress in our conception of regenerative biomaterials and their roles in new tissue formation, can potentially open a new frontier in the fast-growing field of regenerative medicine [6–9]. The range and degree of biomaterial sophistication have also dramatically increased as more knowledge has accumulated through materials science, matrix biology and tissue engineering [10]. Broadly speaking, biomaterials can be defined as material devices or implants used to repair/replace native body tissues or as scaffolding materials, adopted to construct manmade tissues and organs.

1.2 General principle of tissue engineering

The general principle of tissue engineering can be simply defined by seeding living cell on a three-dimensional porous biomaterial/bioscaffold. Although there are numbers of other technique to do that but porous biomaterials always dominates the field in the recent years. The basic role of biomaterials in tissue engineering is to provide temporary mechanical support and mass transport to encourage cell adhesion, proliferation and differentiation and to control the size and shape of the regenerated tissue. Let say, if we prepare a target tissue construct by seed some living cells on three-dimensional porous scaffolds in a bioreactors, they will continuously need proper nutrients and conditioning (**Fig. 2**).

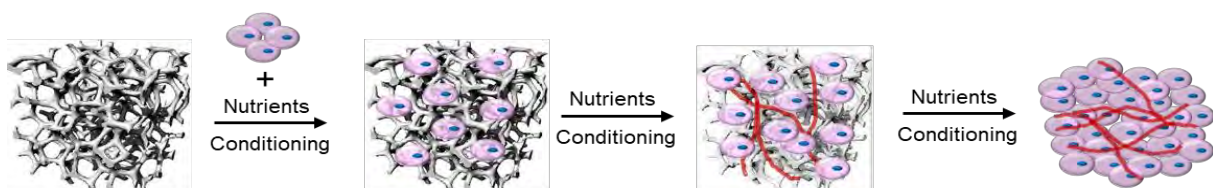


Fig. 2. Three-dimensional porous scaffolds to prepare tissue construct.

Although the development of the tissue construct (let say in month scale) from cells involves number of important processes which can be serve by the porous scaffolds (**Fig. 3**):

- The cells with the right condition will grow with time
- The scaffold will degrade (if biodegradable) overtime which allows the cell to replace the scaffolds
- As the scaffolds degrade, the mechanical property will decrease in the initial days but it will increase again due to the growing mechanical support by the tissue construct
- As the cell grow, they will start suffocate themselves to transport oxygen through cellular channel. That is how they will prepare the blood vessel rather rapidly by the mechanism called angiogenesis.
- There will be another process which is called the inflammation, a normal process of healing. Inflammation will grow due to presence of the scaffold which will go away after certain time.

At the end, we have the desired tissue construct where the scaffolds will be completely gone.

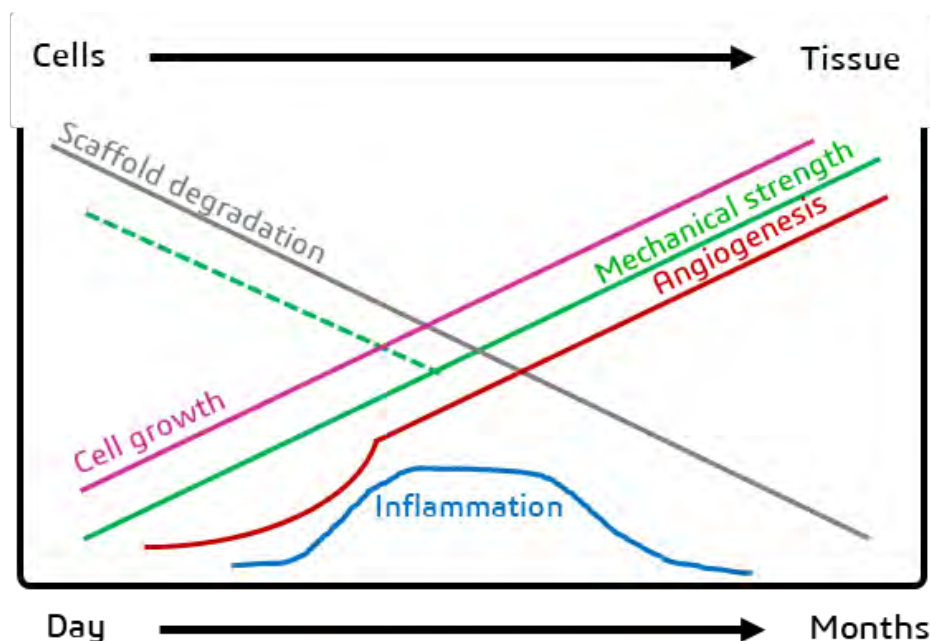


Fig. 3. Functions involves tissue formation from cells. (Inspired by a talk of Prof. Buddy D Ratner, University of Washington, USA)

Preferably, a bioactive scaffold for tissue engineering should meet the design criteria:

- biocompatible (surface should permit cell adhesion and growth, material should produce negligible inflammation)
- cellular transportation and ingrowth (three dimensional porous structure should be capable of cell migration through the bulk which will avoid overcrowding on the surface)
- interconnected porosity (to transfer cell signalling and to develop cell-polymer interaction via extracellular matrix regeneration) [11]
- adjustable biodegradability (scaffolds should resorb once it has served its purpose of providing a template for the regeneration, the degradation rate should be tuneable to match the rate of tissue regeneration by the cell type of interest)
- mechanical property (suitable for hard or soft tissue grafts e.g. generation of cartilage, bone, artificial blood vessel, among others) [12].

1.3 Current Research approach

Cardiovascular diseases (CVD) refer to a group of diseases involving the heart and blood vessels. Due to uncontrolled life, excessive smoking, obesity, diabetes, heart disease is the number one silent killer in the world for both men and women [13]. The initial stimulus is damage to the endothelium (Luminal side) and followed by damaging the smooth muscle cell layer due to the toxic chemical release in the blood stream (Fig. 4).

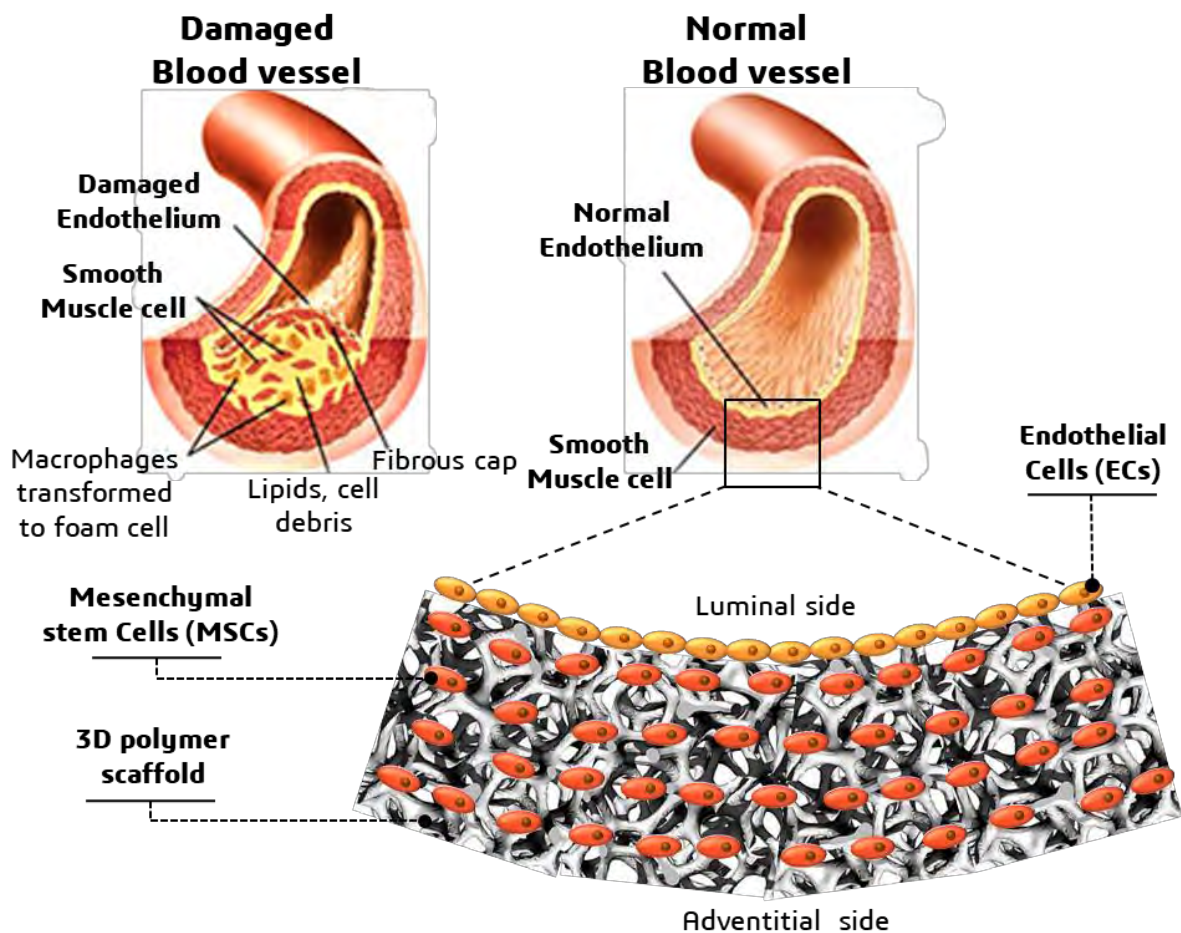


Fig. 4. Schematic of the current research approach.

In medical terminology which is referred as a chronic state of Atherosclerosis. The main objective of this thesis is to produce and investigate a novel three-dimensional biomaterial that can deliver potential tissue engineering scaffolds for cardiovascular system diseases (CVD). Here we intend to regenerate the blood vessel by tissue engineering technology where two different kind cells can be seeded strategically. Human endothelial cell (ECs) can be seeded on the surface (on the luminal side) and human

mesenchymal stem cells (MSCs) inside the bulk. Using of MSCs has two main beneficial effect: once the MSCs are modified by gene therapy, they can produce the growth factors (VEGFs) to enhance the endothelium which is very important as the damaged vessel could not produce the VEGFs naturally. MSCs proliferation and viability are highly depend on the environmental cues like material stiffness, growth medium and other physical and mechanical forces. With proper environmental condition, they can change their phenotype to smooth muscle cells. At the end the scaffold will be completely absorb inside the body where we have our blood vessel construct. That will be a perfect mimicking of the human blood vascular system.

1.4 Polymer materials as biomaterials for tissue engineering

On material point of view, polymeric scaffolds, both synthetic and natural, are of great interest as tissue engineering scaffolds due to their wide range of properties that can assuredly meet the above specifications via proper tuning to match the desired specific target [5,11,14]. The structure, property and application of all the commercially available synthetic/natural polymers are listed in **Table. 1**.

The field of biomaterials resulted from a marriage of disciplines in tissue engineering field including the life sciences, medicine, materials science, and engineering. The use of biomaterials for tissue and organ regeneration is called tissue engineering. Tissue engineers study other materials in addition to polymers, and many of these materials, e.g. Polycaprolacton (PCL), Polylactic acid (PLA), Polyglycolic acid (PGA), Poly Lactic-co-Glycolic Acid (PLGA), Chitosan (CHT), Collagen (Col), hydroxyapatite, will be crucial for the success of the field. The value of polymers is tremendous and polymers with similar chemical characteristics behave differently in certain situations. For example, polyethylene and ultrahigh molecular weight polyethylene behave differently as orthopaedic biomaterials for knee and hip replacement. Ultrahigh molecular weight polyethylene exhibits reduced wearing and debris formation compared with polyethylene. This broad spectrum of materials provides scientists and engineers with not only many choices of existing polymers, but also the opportunity to design polymers better suited to the tissue of interest. In addition to the issues of mechanical properties of the materials, we must concern ourselves with the surface morphology, porosity, degradation, and chemistry of the

materials. As we will see below, all these parameters play a significant role in cell attachment, proliferation, differentiation and secretion of the proper ratios of extracellular matrix molecules.

We also must consider biological parameters as we design new polymers. Regardless of other inherent properties, the material must be biocompatible. This requirement means that the material must not be immediately attacked or encapsulated by the body. As a result, there are many questions that need to be answered in the search for new and improved materials:

- Will the body recognize the polymer as grossly foreign and respond by walling off the foreign body?
- Will the material elicit an immune response?
- Will cells that are able to regenerate the endothelium of the vasculature adhere, proliferate and remain differentiated once they are in contact with the polymer?
- Do we need to include bioactive factors that are covalently attached to the backbone of the polymeric material?
- On the other hand, do we need to consider controlled release of a bioactive factor or factors to coax the seeded cells to remain differentiated or secrete proper extracellular matrix molecules?

All of these questions are design parameters that must be taken into account as we develop new scaffolding for tissue regeneration.

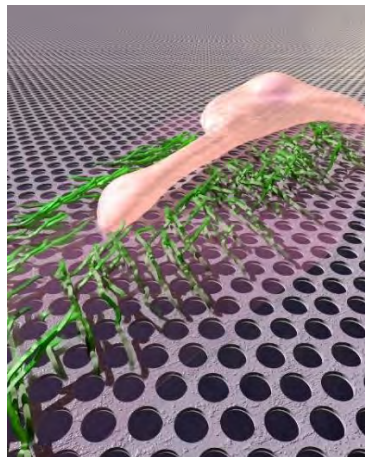
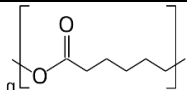
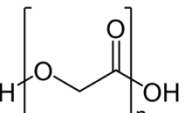
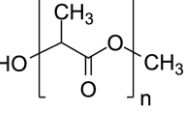
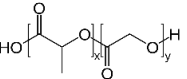
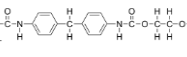
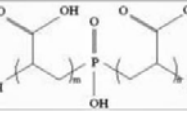


Fig. 5. Schematic representation of new tissue formation on a porous biomaterial (source: ACS biomaterials and engineering).

To this end, material scientists and engineers have a great challenge ahead of them. We must embrace not only traditional materials issues, but also biology. Stem cell research has given us a new angle to approach tissue engineering. As a result, we may be able to harness the potential of stem cells to develop tissues and organs as nature does during foetal development. We will need to create materials that are biocompatible, support cell adhesion, growth, and differentiation. These materials will need to temporarily replace mechanical function, and degrade at rates appropriate to tissue regeneration. One example of the marriage between biology and polymer synthesis involves the use of molecular biology to incorporate biological signals into the backbone of polymers [15–17].

Table 1. List of commercial polymer with structure, property and applications.

Polymer	Structure	Property	Biomedical Application
Synthetic			
PCL [18,19]		High dynamic modulus [20] Improved Structure Biodegradable form Fibre based devices Membrane based devices	Orthopaedic fixation devices Tissue engineering application (FDA approved) Tissue regeneration membrane Long-term contraceptive device
PGA [21,22]		Regenerate biological tissue Useful mechanical properties	First biodegradable synthetic suture in 1969 Bone internal fixation devices
PLLA [23,24]		High tensile strength Improved suture Fiber-based devices Injectable form	Orthopaedic fixation devices High-strength fibers (FDA approved) Blood vessel conduits
PLGA [25,26]		High degradation Form of meshes	First commercially developed monofilament suture Skin graft Drug delivery vehicle
PU [27]		High porous & no adverse effect	Tissue engineering application
PCA [28]		Absorb or encapsulate a wide range of drug or protein molecules Major component of skin and other musculoskeletal tissues	First biodegradable polymers used for developing nanoparticles for drug delivery application Tissue adhesives for topical skin application (FDA approved) Wound dressings

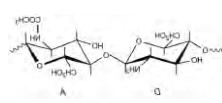
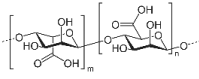
Natural			
Chitosan [18,19,29]		ECM like functionality High biodegradation High growth factor protein affinity	Guided tissue regeneration Coatings of orthopaedic implants Patterned medical membranes
Alginate [30,31]		Biodegradation Scaffolds based devices	Periodontal tissue regeneration Bone tissue engineering
Collagen [32,33]	See Link [33]	Membrane-film based devises ECM like functionality	Angiogenic properties Bone regeneration
Gelatin [31,34]	See Link [34]	Scaffolds based devises ECM like functionality	Nerve regeneration Bone tissue engineering implants
HA [35,36]	See Link [37]	Promote angiogenesis, Sponge as a carrier vehicle for osteo-inductive protein	Wound dressing application Synthetic bone graft

Table. 2. Scaffolds' fabrication technique.

Method	Polymers	Unique factors
Fibrous scaffold fabrication		
Nanofiber electrospinning process [38,39]	PCL, PGA, PLA, PLGA copolymers, collagen, elastin, and so forth	High surface area, biomechanical, and biocompatibility, moderate degradability
Microfiber wet-spinning Process [40,41]	PLGA, PLA, chitosan, and PCL	Biocompatible fibres with good mechanical properties
Nonwoven fibre by melt-blown Process [42,43]	Polyesters, PGA	Submicron fiber size, highly porous scaffold
Functional scaffold fabrication		
Growth factor's release process [44,45]	Collagen, gelatin, alginate, chitosan, fibrin, PLGA, PLA, and PEG	Membranes, hydrogels, foams, microsphere, and particles
Biodegradable porous scaffold fabrication		
Solvent casting/salt leaching Method [46,47]	Absorbable polymer (PLLA, PLGA, collagen, etc.)	Biodegradable controlled porous scaffolds
Ice particle leaching method [48,49]	PLLA & PLGA	Control of pore structure and production of thicker scaffolds
Gas foaming/salt leaching Method [50,51]	PLLA, PLGA & PDLLA	Controlled porosity and pore structure sponge

Microsphere fabrication		
Solvent evaporation technique [52]	PLGA, PLAGA	High-density cell culture, due to the extended surface area
Particle aggregated scaffold [53]	Chitosan, HAP	High mechanical stability
Freeze drying method [54,55]	PLGA, PLLA, PGA, PLGA/PPF, Collagen, and Chitosan	3D porous sponge structure, durable and flexible
Thermally induced phase Separation [56,57]	PEG, PLLA	Highly porous scaffold for cellular transplantation
Injectable gel scaffold fabrication		
Hydrogel-based injectable Scaffolds [58,59]	Hydrophilic/hydrophobic diblock and triblock copolymer combinations of PLA, PGA, PLGA, and PEG. Copolymers of PEO and PPO and polyoxamer. alginates, collagen, chitosan, HA, and fibroin	Biomimetically, exhibit biocompatibility and cause minimal inflammatory responses, thrombosis, and tissue damage
Ceramic-based injectable Scaffolds [60,61]	CP ceramics, HAp, TCP, BCP, and BG	Porosity and bioresorbability
Hydrogel scaffold fabrication		
Micromolding [62,63]	Alginate, PMMA, HA, PEG	Microgels, biologically degradable, mechanical and physical Complexity
Photolithography [64,65]	Chitosan, fibronectin, HA, PEG, PNIAAm, PAA, PMMA, PAam, and PDMAEM	Microwells, microarrays, controlled size and shape
Microfluidics [66–68]	PGS, PEG, calcium alginate, silicon and PDMS	Microbeads, microrods, valves, and pumps
Emulsification [69,70]	Gelatin, HA, and collagen	Microgels, microsensors, cell-based diagnostics

1.5 Advantage of Three-dimensional polymer scaffolds on cellular adhesion

Over the last decades, three-dimensional (3D) scaffolds are unfolding many promising application in tissue engineering and regenerative medicine field by providing suitable microenvironment for the incorporation of cells or growth factors to regenerate damaged tissues or organs [71]. Scaffolding is essential in this endeavour to act as a three-dimensional template for tissue ingrowths by mimicking ECM. These key scaffold characteristics can be tailored to the application by careful selection of the

polymers, additional scaffold components, and the fabrication technique. Typical scaffold designs have included meshes, fibers, sponges and foams, and so forth. These designs are chosen because they promote uniform cell distribution, diffusion of nutrients, and the growth of organized cell communities [72]. The fabrication technique for tissue engineering scaffolds depends almost entirely on the bulk and surface properties of the material and the proposed function of the scaffold. Most techniques involve the application of heat and/or pressure to the polymer or dissolving it in an organic solvent to mould the material into its desired shape. While each method presents distinct advantages and disadvantages, the appropriate technique must be selected to meet the requirements for the specific type of tissue (listed in **Table. 2**).

1.5.1 Porous scaffolds and effect of pore size and pore morphology

The three-dimensional polymeric porous scaffolds with higher porosities having homogeneous interconnected pore network are highly useful for tissue engineering. Sponge or foam porous scaffold have been used in tissue engineering applications [73], especially for growth of host tissue, bone regrowth, or organ vascularization. Their porous network simulates the ECM architecture allowing cells to interact effectively with their environment.

Controlling the porosity and pore size of 3D scaffolds is the key to create an ideal biomaterial scaffold [74]. Open porous and interconnected networks have direct implications on their functionality during biomedical applications which are essential for cell nutrition, proliferation and invasion inside the bulk for tissue vascularization and formation of new tissues. New tissue regeneration and cell morphology with particular phenotypic expression depend on the cell type, scaffold composition and most significantly on pore size and porosity, facilitating the mechanical interlocking between the cells and surrounded scaffold [71,74–76]. If pores are too small, cell proliferation can be limited only on the surface and the transfer of nutrients, growth factors and waste product can be reduced throughout the bulk. Conversely if the pores are too big there is decrease in effective surface area, limiting the initial cell-scaffold interaction which is very important to mediate all subsequent events such as proliferation, differentiation and migration within the scaffold [75,76]. Bigger pores are also responsible to reduce the scaffolds mechanical strength and can drive a faster degradation in vivo before finishing the tissue

construct. Scaffolds should be practically applicable as an implant and consist of sufficient compressive moduli of 10-1500 MPa (for hard tissue graft) or 0.4- 350 MPa (for soft tissue graft) [20]. Hence finding a balance between the optimal pore size and effective surface area is essential for high cell proliferation via both cell attachment on the surface and invasion inside the bulk. Scaffolds with mean pore sizes from 20-1500 μm have been reported for bone tissue engineering application [76]. In porous silicon nitride scaffolds, endothelial cells favourably bind to scaffolds with pores smaller than 80 μm , while fibroblasts favour to bind larger pores ($>90 \mu\text{m}$). In PLLA scaffolds, vascular smooth muscle cells preferentially bind a certain range of pore (63–150 μm) while fibroblasts bind to a wider range (38–150 μm) [77,78]. Kasten et. al. [79] reported the porosity and pore size effect of β -tricalcium phosphate scaffold with pore diameter 5 μm to 600 μm and porosity 25 % to 75 % for osteogenic differentiation of human mesenchymal stem cells where they conclude that the distribution and size of the pores, as well as the surface structure might play an important role for osteogenic differentiation in vivo.

1.5.2 Previous approach to develop porous morphology and it's limitations

Several efforts have so far been developed to control the pore structure characteristics of scaffolds such as porogen leaching, freeze-drying, gas foaming and rapid prototyping [74–76]. Among them porogen leaching offers quite impressive and easy processing technique to control the pore size and porosity. Choi et. al. [12,80] developed a uniform pore structure of chitosan based inverse opal scaffolds by PCL microspheres as porogen and obtained a high proliferation of mouse preosteoblastic cells. Zhang et. al. [74] used a combination of porogen and freeze drying method where they use ice particulate as porogen and mixed with collagen aqueous solution followed by freeze drying. By this method, they obtained pores structure by removing the ice particulate easily without using any toxic organic solvent for leaching. Apart from many possibilities to develop porous 3D scaffolds by porogen leaching, this technique has some significant drawbacks. The porogen materials used in this method can leave replica pores after leaching, most of the time they cannot initiate the formation of interconnected pores. As a result, cells cannot enter the isolated pores and the void space cannot be filled with new tissue. Thus, pores remain in the newly regenerated tissues as defects, compromising the mechanical property without a purpose. Another reason is that the scaffold consists of only one kind of mean pore size which is

responsible to serve both cell invasion and also transfer of nutrients. The nutrients and growth factor could be effectively transported through much smaller pore ($>1 \mu\text{m}$ - $10\mu\text{m}$) and for this use of bigger pores are not worthy enough which in term reduce the effective surface area and mechanical property and enhance the physiological degradation before target time scale.

1.5.3 Evolution of double porous morphology

To overcome these drawbacks, 3D scaffolds with double porosity can be a further step forward where the macrovoids (big pores) are responsible for the invasion and proliferation of the cells and the transport of nutrients and growth factors can be accomplished by smaller interconnected macropores resulting a higher effective surface area than a single big porous surface. Three-dimensional scaffolds with double porosity was previously reported by using paraffin as porogen followed by heat treatment to create PLLA foam matrix [81]. Another group used double porogen method (two different size of porogen) to construct a double porous PHEMA based scaffolds [82]. They used CaCO_3 ($125 - 160 \mu\text{m}$) and PMMA ($200 - 250 \mu\text{m}$) as macroporogen, in conjugation with hydroxyapatite (200 nm) or a solvent as nanoporogen. Both of these method they achieved bigger pores interconnected with smaller pores but the formation of unutilized big pores inside the bulk were inevitable resulting a reduction of compressive moduli ($23 - 50 \text{ KPa}$) far below than the minimum physiological requirements (0.4 MPa) [81]. Moreover, the authors [82] did not report any data with cells.

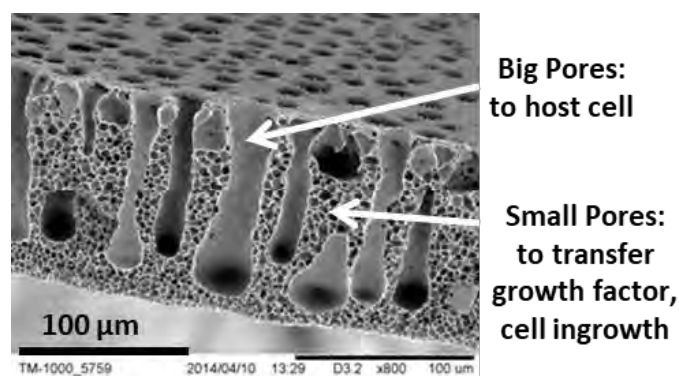


Fig. 6. Double porous membrane scaffolds prepared by modified liquid induced phase inversion method (detail in chapter 2).

Recently researchers from our group report an innovative and smart idea to create double porous 3-D scaffolds via modified liquid induced phase inversion process and found very good results for the application in artificial liver with invasion and migration of hepatic (C3A) cells inside the macrovoids

[83]. They have used Polysulfone (PSU) as a material and dissolve it in a solvent (NMP) followed by casting of the polymer solution. Just before putting inside the non-solvent (water), they have applied a commercial PET track etched isoporous (track-etched, diameter 10 μm) membrane on the casted solution to create open and interconnected macrovoids on the surface [83,84]. Due to the presence of the track-etched membrane, after immersion inside the non-solvent, the solvent exchange was quite heterogeneous leading to the formation of macrovoids (50-60 μm) where the non-solvent has a direct access through the pores of the track-etched membrane. In addition, the part where the non-solvent could not make a direct access, interconnected spongy macropores (1 μm) were formed resulting an overall double porous morphology where the macrovoids were open towards the surface for cell invasion. Apart from many future possibilities and delicacy of that report, the disadvantages were: the hydrophobic properties, lack of functional group and negatively charged surface at physiological pH [85] (repulsion could be possible with the negatively charged cell membranes [86]) of PSU membranes are not ideal for cell adhesion and spreading in comparison with hydrophilic surface, non-degradability could be a problem for the growth of the cells inside the macrovoids and also where we do not want to keep the scaffolds for long time and lastly total removal of NMP (carcinogenic) solvents after formation of the porous scaffold could be difficult which is not suitable for cell culture application.

1.6 Necessity of Organ-on-chips (OOCs) for tissue engineering

The development of new drugs is becoming more difficult, time-consuming and costly. Despite all the trials done before approval of a drug, reactions of patients to the drug can differ greatly. In fact, individuals can even react adversely to a drug. These responses do not always become apparent in the first stages of clinical trials. Participants are often selected on characteristics such as sex, age or ethnicity and thus do not represent the entire population. Also, due to ethical reasons, the effects of drugs on children are hardly investigated. As a result of these limitations, clinical trials often do not show the entire spectrum of responses to a drug. Moreover, many drugs fail during clinical trials, despite showing efficacy during preclinical trials. The notion that we cannot fully rely on animal models is growing. Despite a considerable resemblance in both genetics and physiology between animal models and humans, animal models often do not accurately predict how drugs will perform in humans.

In vitro models have the advantage that they often use only human cells. However, they lack the physiology of a tissue, and thus cell behaviour may differ from the in vivo situation. Trans-well inserts consist of small baskets with a porous, permeable membrane underneath which can be placed in a well plate. This way, the membrane is suspended above the bottom of the well. Cells can be placed on the membrane and exposed to air, while receiving nutrients through the membrane. This already allows more realistic cell culturing than traditional systems. However, the cells do not experience stimuli such as air flow or mechanical stretch. In vitro models that better offer suitable stimuli and can account for individual differences would address many of the issues in tissue engineering. Because of the need of such in vitro models, organs-on-chips (OOCs) have been developed.

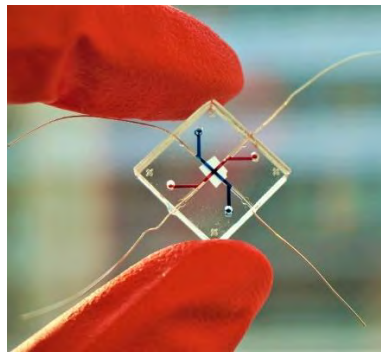


Fig. 7. Organ-on-chip device with microfluidic technologies for mimicking blood brain barrier and gut tissues (Source: Marinke et. al. [87])

These are small microfluidic devices that mimic a particular organ by introducing organ-like features such as fluid flow and mechanical stress [88]. These organ-on-chip models, which contain micrometer-sized, fluid-filled channels in which human cells can be cultured, provide opportunities for engineering a controlled culture environment that resembles the microenvironment of a certain organ by tuning mechanical, biochemical and geometrical aspects [89]. More physiological behaviour is expected from such a combination of cells and engineering, resulting in better predictive value [66]. In addition, organs-on-chips can be engineered in such a way that they allow direct measurements of organ functions as well as pharmacokinetics and pharmacodynamics [66]. Furthermore, as all in vitro models, organs-on-chips hold the potential of parallelization and high-throughput screening. The goal of organs-on-chips is to mimic functional units of a certain organ rather than complete organs, in order to arrive at realistic but simple in vitro models [66,89]. Such a functional unit can comprise one or more tissue types, depending on the organ function that needs to be mimicked.

1.7 Research Framework and outline

The main objective of the thesis is to produce and investigate a novel three-dimensional biomaterial that can deliver potential tissue engineering scaffolds and provide a home like environment for the cells.

- ✓ The bulk microenvironment of the scaffold should be accessible by the cells, it should furnish superior characteristics with tuneable parameters like physico-chemical, morphological and mechanical property in order to use it as a vascular grafts application.
- ✓ The scaffolds should be highly biocompatible in order to enhance the cell viability and bioresorbable in the sense; it will absorb inside the body without releasing any toxic side product once its purpose will be served.
- ✓ It will consists of open pores with interconnected network and the porous structure should be optimum by providing suitable environment for the cells without compromising the overall mechanical property.

The positioning of the current research work to develop the materials is summarized in the Fig. 8.

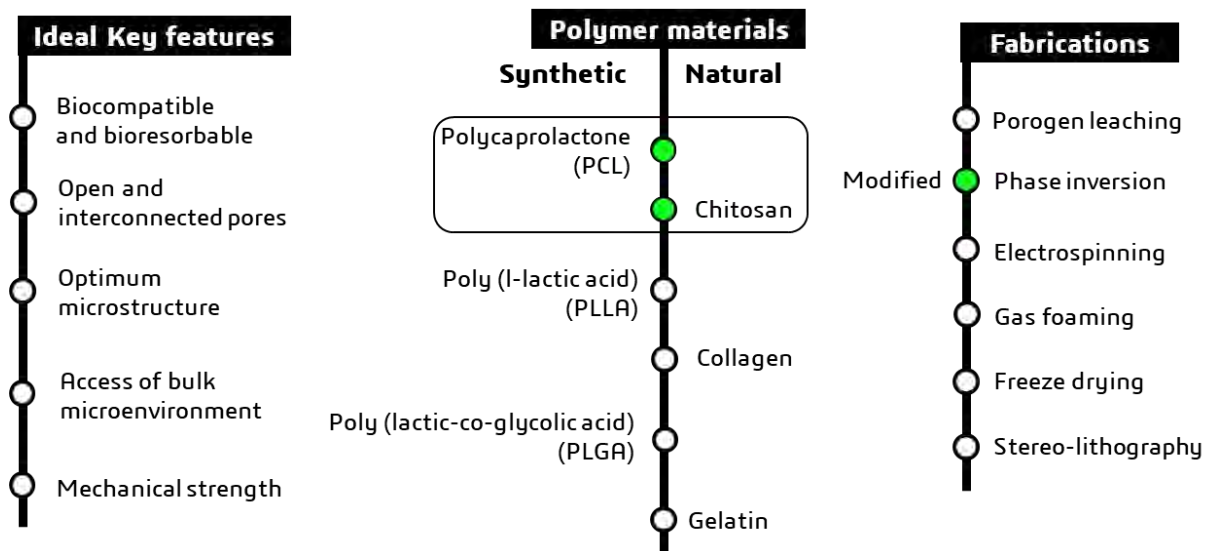


Fig 8: Positioning of the current work (green full circles) with the possibilities offered by the different polymer blend and fabrication techniques to address the ideal key characteristics of a scaffold for tissue engineering.

We choose a combination of synthetic/natural polymer to develop the 3D microstructural biomaterials with modified phase inversion technique in order to obtain the ideal key features. And we progress our work in the following chapters as follows:

Chapter 1: Address the present limitations in the advance biomaterials field for vascular grafts applications and define the state of the art from the recent literature survey. By realising the essentiality of polymeric scaffolds, we understand that certainly three-dimensional scaffolds with aforementioned tuneable features can have a bright outcome not only for the project but also for the upcoming decades.

Chapter 2: Here we discussed a unique three-dimensional scaffold in term of flat sheet polymeric membranes consisting of two different kind of porous structures; so called in the thesis as double porous membranes. Solvent mix of polycaprolactone (PCL) and Chitosan (CHT) was chosen as base material. Due to different chemical nature of the two polymers many challenges in processing technique has to be solve to reach the desired morphology. Furthermore, all the relevant aspects of the material property were explored by physico-chemical and morphological experiments. In addition, the formation mechanism of the double porous membrane is explained with the fundamental basis of 'Hansen solubility parameter' and illustrated in details with the ternary phase diagram.

Chapter 3: This chapter was mainly focused on the real understanding between the scaffolds morphology with cellular adhesion. Human mesenchymal stem cells (hMSCs) were seeded due to its powerful multipotent properties, which uphold huge future possibilities to transform into any cell lineage or by assisting other cell types by endogenous production of growth factors as discussed in the current research approach. Mechanical properties of the scaffolds were observed in dry as well as in wet condition and enzymatic degradation was performed in physiological concentration. Cells were seeded and all the relevant cellular quantitative/qualitative experiments were thoroughly analyzed.

Chapter 4: After having the positive outcome of the previous two chapters, finally we define a real time performance of the membrane scaffolds in Organ-on-chip system by mimic the human physiological condition. Human umbilical vesicle endothelial cells (HUVECs) were used to understand the resistance

of cellular barrier developed by the cells upon the polymer membrane scaffolds as potential in vivo vascular grafts by varying the membrane morphology, pore size and physicochemical properties.

1.8 Project funding and collaborations

The project is funded by Erasmus Mundus Doctorate in Membrane Engineering (EUDIME 5th Ed) – EACEA under European Commission. This program allow the collaborations between three universities of the consortium as follows-

- Home University: Laboratoire de genie chimique (LGC) under University Paul Sabatier, France (Below called as **UPS-3, FR**).
- Host University 1: Institute on membrane technology (ITM-CNR) under University of Calabria, Italy (Below called as **UNICAL, IT**)
- Host University 2: Applied stem cell technology (AST) and Membrane science technology (MST) under University of Twente, The Netherlanfds (Below called as **UTWENTE, NL**).

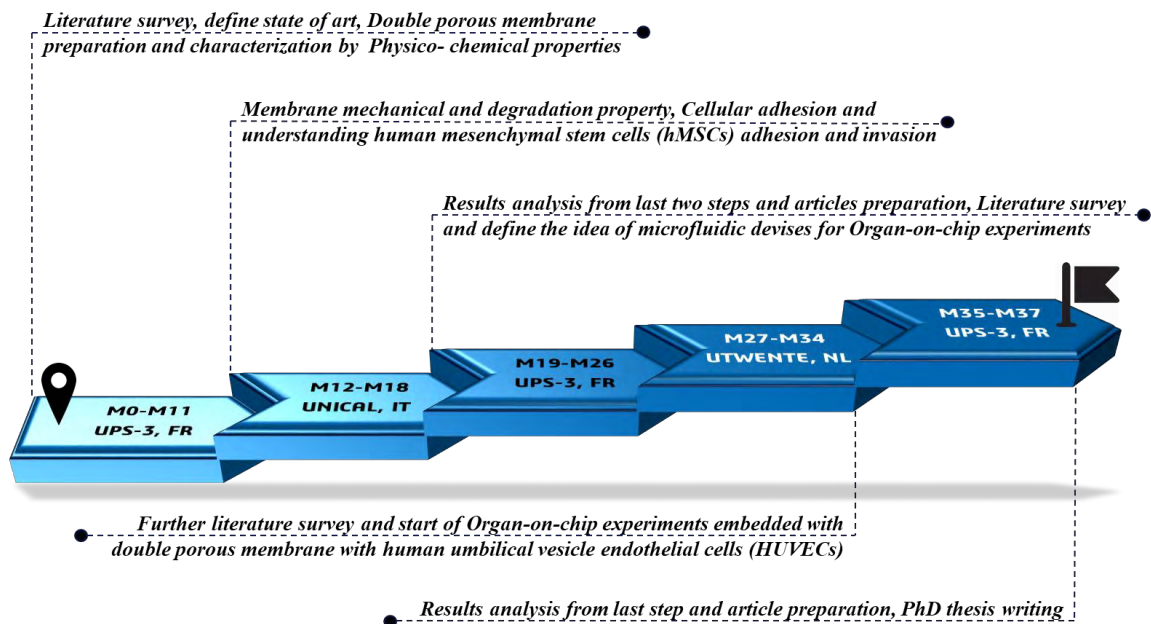


Fig. 6. Progression of the project from starting **M0** (first month) to ending **M37** (after 37 months) and the key work done in the collaborations.

Chapter 2: Double porous poly (ϵ -caprolactone)/chitosan membrane as tissue engineering scaffold: development, characterization and biodegradation

2.1 Summary of the Chapter

Limited capacity of cell hosting and lower dynamic properties are the main problem in membrane based biocompatible and bioresorbable vascular grafts. They are mainly produced as a fiber mesh structure by electrospinning. For the first time, we are reporting poly (ϵ - caprolactone)/chitosan (PCL/CHT) blend membrane with a double porous morphology which could be potentially applicable in future for tissue engineering: (i) surface macrovoids (20 to 110 μm) which can be easily accessible for cell proliferation and differentiation; (ii) macroporous spongy network (7 to 20 μm) to transfer essential nutrients, oxygen, growth factor between the macroporous and the supernatant. PCL/CHT blends with the ratios 100:0, 90:10, 80:20, 70:30 (w/w %) were prepared using a mixture of formic acid/ acetic acid as a solvent. SEM images of the cross section of scaffolds confirmed that macrovoids are connected with each other through the spongy macroporous network. ATR-FTIR, XRD and DSC were performed to check the miscibility of the two polymers and characterize the physico-chemical properties. Enzymatic degradation was tested by lipase (*Pseudomonas cepacia*; 7 U/ml) in Phosphate Buffered Saline (PBS Buffer) at pH 7.4 and 37°C. The SEM images after degradation and the weight loss (%) were observed at predetermined time interval and an almost selective and fast degradation of pure PCL and PCL in the blends within 48 hours was obtained. Data suggest that the blend membrane with double porosity level could be useful in future as a promising membrane scaffold to provide an inner three-dimensional environment for tissue engineering applications.

2.2 Introduction

The 3D structure of the material should enable to host the cells but also to distribute the nutrients and to favor the removal of the products of their metabolism. In the last decades, various scaffolds have been developed more often from an assembly of simple fibers by combining the salient features of synthetic/natural polymers (section [1.4](#)). Among them, the combination PCL/CHT has a many

promising features by modifying the individual features of each other's (**Fig. 1**). The study of PCL/CHT blend with electrospinning method is extensively researched and well adaptable for better cell attachment with good dynamic properties [18,19,29,38,90–95]. However numerous studies report on the difficulties encountered for electrospinning pure chitosan as the structure is mechanically weak, limiting practical processing [25,96–98]. Furthermore, it is difficult to manage the multiple functionality requirements with an assembly of fibers. The use of membranes appears as an interesting alternative to tune the porosity and to manage the mass transport properties. The different level of membrane porosity can be adjusted in order to have both macrovoids to host the cells and interconnected macropores (at micrometer scale) to ensure the transportation of molecules [83]. Solvent mixing with PCL and CHT was more conveniently used compared to melt blending which is quite difficult to perform as CHT decomposes before undergoing melting. Although it is also difficult to make a homogeneous blend in solvent mixing due to high viscosity of CHT in solvent and also scarcity of good mutual solvents. Several efforts were made, like Honma et al. [95,99] produced PCL/CHT blend casting by using common solvent as 1,1,1,3,3,3-hexa-fluoro-2-propanol (HFIP) solution. They showed that PCL/CHT can be processed by using HFIP but this solvent is very expensive, carcinogenic and difficult to remove during washing [100]. Although different approach was reported to find a good mutual solvent [101–106]. Among them a suitable approach could be to dissolve CHT in 0.5 M acetic acid and PCL in glacial acetic acid where the authors [103] were able to obtain a mixture of these two solutions at a low concentration of polymer but it was not effective at high concentration [99] as in our case. In another study, a solvent mixture of formic acid/acetone was reported to be used to develop PCL/CHT nanofibers at high concentration of polymers. In this case, it was forming beads like morphology indicating incomplete dissolution of the polymer [107]. Recently, formic acid/acetic acid mixture [108] with certain ratio has produced a mutual solvent for both polymers with minimal degradation and phase segregation but with faster dissolution. Despite so many combination of solvents, the author [108] have reported that the formic acid/acetic acid mixture produced the bead free and least toxic scaffold and the solvent can be easily removed during washing.

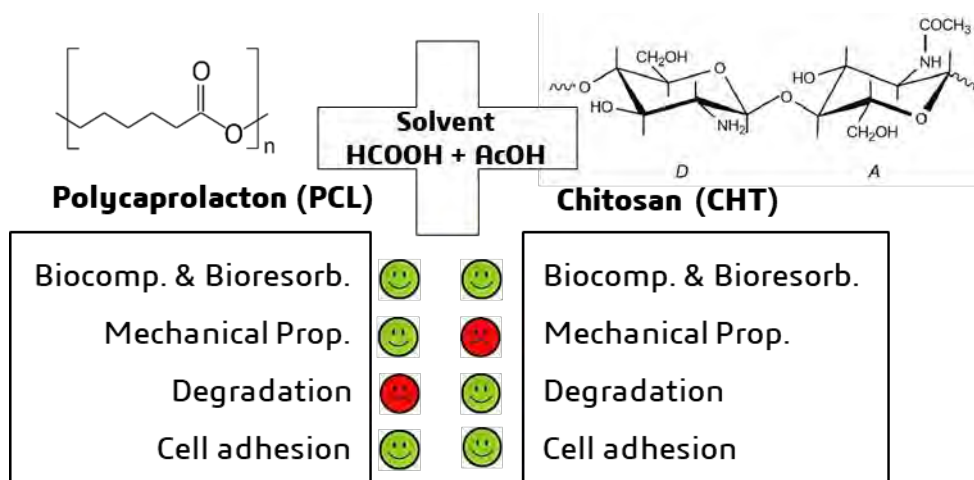


Fig. 1. Solvent mixing of PCL-CHT and their individual properties.

The objective of this chapter is to develop the flat sheet membrane scaffolds with double porosity (open big pores ready to access for cellular invasion and interconnected porous network in order to transfer growth factors and nutrients). By understanding the delicacy of the processing, a smart approach for liquid induced phase inversion was defined e.g. finding a suitable solvent and reaction condition where this two chemically different polymer can be mixed together, maintaining the proper viscosity of the polymer solution and ultimately perform the modified phase inversion in order to obtain the desired morphology. After formation of the membrane, it was very important to determine and characterize the material quality in terms of repeatability and homogeneity. In addition, enzymatic degradation was also performed to understand the bioresorbability of the material.

2.3 Materials

CHT (MW 190-310 kDa, 75-85% de-acetylation degree, CAS Number 9012-76-4) was purchased from Sigma-Aldrich and PCL (MW 80 kDa, CAPA™ 6800, CAS Number 24980-41-4) was purchased from Perstorp Holding AB, Sweden. Isopore® Polyester (PET) membranes (with 10 μm diameter), used as track-etched, were purchased from Sterlitech, USA. Acetic acid, formic acid, sodium hydroxide and sodium azide were purchased from Sigma-Aldrich. Lipase from *Pseudomonas cepacia* (35U/mg, CAS Number 9001-62-1) were purchased from Sigma-Aldrich. Phosphate buffer saline (PBS) was purchased from Fisher Scientific (CAS Number 7778-77-0).

2.4 Methods

2.4.1 Development of the membrane with a double porosity level

The membranes were developed by modified version of the conventional liquid induced phase inversion method by diffusion between a solvent as formic acid/ acetic acid (FA/AA) mixture and a NaOH aqueous solution used as non-solvent. PCL and CHT with a ratio 100/0, 90/10, 80/20 and 70/30 (w/w%) were dissolved in FA/AA (w/w%) mixture. The polymer concentration in the solution was expressed in wt.% as followed:

$$\text{CHT (wt. \%)} = 100 \frac{\text{Mass}_{\text{CHT}}}{\text{Mass}_{\text{CHT}} + \text{Mass}_{\text{PCL}}} \quad (1)$$

$$\text{Polymer (wt. \%)} = 100 \frac{\text{Mass}_{\text{CHT}} + \text{Mass}_{\text{PCL}}}{\text{Mass}_{\text{CHT}} + \text{Mass}_{\text{PCL}} + \text{Mass}_{\text{Solvents}}} \quad (2)$$

The polymer solution was casted on a glass plate using a gardener knife in order to achieve a thickness around 250 μm at 23° C (room temperature). The casted solution was covered by the isopore[®], commercially available track-etched membrane of 10 μm pore diameter (**Fig. 2**), so called in the thesis “*track-etched membrane*” to denote the function taken by this membrane. The track-etched membrane was at first immersed in the solvent mixture to fill the pores with solvent mixture and slowly wiped out to remove excess solvent.

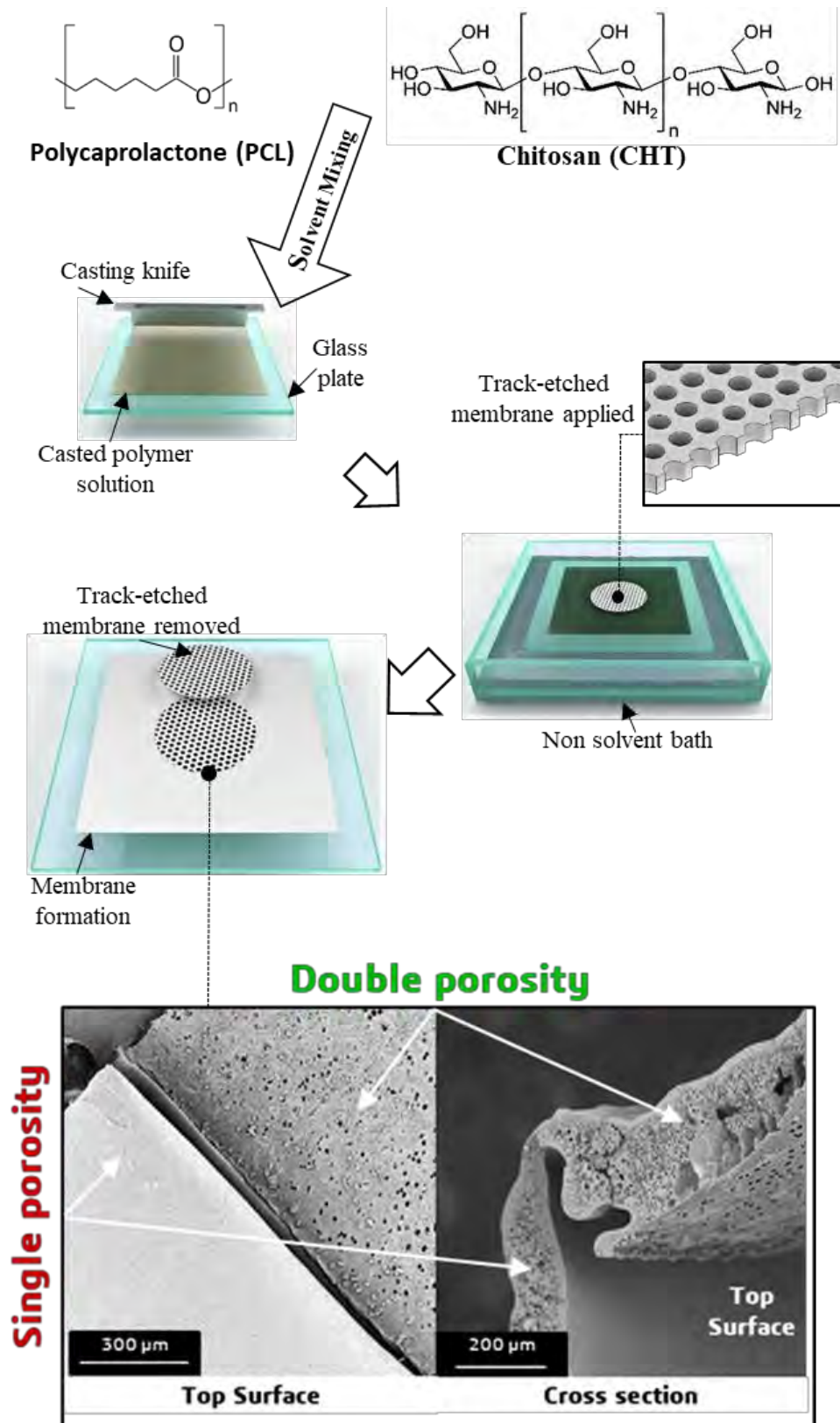


Fig. 2. Double porosity development, using a track-etched membrane, by modified liquid induced phase inversion process with the following steps 1) PCL/CHT membrane casting, 2) application of the track-etched membrane before the non-solvent phase inversion, 3) removal of the track-etched membrane after full precipitation. SEM images of PCL/CHT 100/0 represent double porosity and single porosity membranes on top surface and cross section.

The glass plate was then gently immersed in a non-solvent bath containing NaOH solution at room temperature. Immediately after the immersion, demixing via neutralization of the acidic casted solution was started due to solvent exchange leading to the flat sheet membrane formation within few minutes (PCL) to hours (PCL/CHT 70/30). It should be noted that this quenched phase inversion method leads to a thermodynamically non-equilibrium state of the polymers in the final membrane.

The solvent exchange rate was spatially quite homogeneous where the polymer solution was not covered by the track-etched membrane leading to single porous structure without enough open pores on the top surface. Where the polymer solution was covered by the track-etched membrane, a heterogeneous solvent exchange rate was occurred leading to the formation of double porous structure. The macrovoids were formed where the non-solvent has a direct access to the polymer solution through the pores of the track-etched. A second phase inversion occurs when the non-solvent diffused inside the polymer solution and led to the formation of interconnection between the macropores. This mechanism was described by Strathmann et al. [109] to explain the formation of skinned membrane with macrovoids and sponge structure; the nascent skin playing an equivalent role than our track-etched membrane.

After the membrane formation, when it was turned opaque and detached from the glass plate, the track-etched membrane was removed gently and the PCL/CHT membrane was washed several times in ultrapure water. After that, the membrane was stored in ultrapure water at 4°C.

The surface where the macrovoids were open towards the non-solvent (i.e. where the track-etched membrane was) is denoted as top surface and the other surface, which was facing the glass plate, is denoted as the bottom surface.

By this way, two different kinds of porous structures were formed in the same condition. The area, of the final membrane, which was covered by the track-etched membrane, has shown double porosity. In **Fig. 2**, SEM images of the membrane PCL/CHT 100/0 were indicating the efficient use of the track-etched membrane for the development of the double porosity.

2.4.2 Viscosity measurements of the polymer solution

The viscosity of the polymer solution was measured by Rheometer Anton Paar Physica MCR 301, France. After complete dissolution of the solution, a 0.6 ml volume was injected on a cone plate rheometer (diameter 50 mm). The viscosity was measured at a shear rate from 2 to 100 s⁻¹ at 20°C. All the measurements were performed inside a close chamber in order to avoid the solvent evaporation and dissolution of water from air moisture.

2.4.3 Scanning electron microscopic (SEM) analysis

SEM analysis (Phenom XL, Fondis Biotech, France) were done on both double and single porous membranes to evaluate all the developed blend morphology from the top surfaces and the cross sections. All the samples were coated with gold and analysis were performed at an accelerating voltage of 10kV from 500X to 3000X. The surface porosity was also determined from the SEM images by using ImageJ [110] software and reported in **Table 1**.

2.4.4 Attenuated total reflection (ATR)-Fourier transformed infrared (FTIR) spectroscopic analysis and mapping

FTIR analysis were done by using a Nexus Nicolet (USA) FTIR Microscope system with an ATR diamond crystal at 45° angle. Prior to the examination, 1 cm² sample was cut and measurements were done on both surfaces (three times) of each sample. Each point was scanned sixteen times with a resolution of 8 cm⁻¹ and the spectral range was 650 – 4000 cm⁻¹. The ATR correction was applied on all spectra. We have also done a FTIR chemical mapping on either side of the membrane using an infrared spectrometer IN10MX Thermoscientific (USA) with an ATR germanium crystal of a 25° angle. A square sample of 6 mm² was studied. Data were analyzed on a 50 μm x 50 μm surface for each point (one point was measured every 50 μm) with a spectral resolution of 8 cm⁻¹. Each measurement was scanned by sixteen times and the spectral range was 650 – 4000 cm⁻¹.

2.4.5 X-ray diffraction (XRD) analysis

The crystalline structure of membrane sample (5 mm x 5 mm) was investigated by XRD analysis using a D4 Endeavor X-ray diffractometer (CuKα₁ = 0.154056 nm and CuKα₂ = 0.154044 nm; generator 40

eV; 40 mA, Bruker AXS, Karlsruhe, Germany) from 10° to 100° at a scan speed of 21.7 sec /step that is equal to 0.02° (2-theta).

2.4.6 Differential scanning calorimetric (DSC) measurements

DSC experiments were conducted (DSC TA instrument Q2000, France) in order to evaluate thermal properties of the PCL/CHT blend membranes. The membranes were dried at 37°C and were cut in a dimension of 3 mm². The sample was put inside an aluminum pan and mechanically covered by an aluminum cap. The pre-weighted aluminum pan was placed inside the DSC machine and equilibrate at 20°C. The temperature scanning was performed at a constant heating rate of 10° C min⁻¹, from 20 to 80°C without preheating step, to observe the change of the melting point (MP) by varying the wt.% of CHT in PCL matrix. The change of the melting point of PCL in the blend (pure PCL melting point is 60°C), the melting temperature, T_m , and melting enthalpy, ΔH , were determined. The crystallinity, X_c , can be calculated from the following equation:

$$X_c = W \frac{\Delta H}{\Delta H_u^0} \quad (3)$$

Where ΔH_u^0 is the melting enthalpy of 100% crystalline PCL, which is 166 kJ kg⁻¹ [44], W is the weight fraction of the PCL in the blend and ΔH is the melting enthalpy of the polymer blend obtained from the DSC apparatus.

2.4.7 Enzymatic degradation of the blend

The membranes were dried in vacuum at 37°C until constant weight was reached and were cut in 6 mm x 6 mm pieces. The initial weight (w_i) was taken (in mg up to the fifth decimal point). Then the samples were placed in a 5 ml vials containing 3 ml of PBS 1X solution (1X solution at pH 7.4±0.1 contains: 11.9 mM Phosphates, 137mM NaCl and 2.7 mM KCl), 0.6 mg (7U/ml) of lipase from *Pseudomonas cepacia* (35 U/mg) and NaN₃ (0.05 wt.%). The entire procedure was done in a sterile condition and vials were sealed and stored in incubator at 37°C. The enzyme solution was changed every day in order to maintain the same enzymatic activity during the whole process. The same procedure was done without the enzyme as a control. Three consecutive samples were taken out after 6 hours incubation time and

every one-day intervals until 10 days. After being washed with copious deionized water, they were dried at 37°C in vacuum until constant weight. The final weight, W_f , was taken.

The weight loss, W_{loss} %, was calculated by the following equation:

$$W_{loss}\% = 100 \frac{W_i - W_f}{W_i} \quad (4)$$

Where, W_i , is the initial weight and, W_f , the final weight.

Scanning electron microscopic images of the degraded membranes were taken and the ageing solution was collected to observe the change in pH.

2.5 Results

2.5.1 Polymer-solvent-nonsolvent optimization

Regarding the polymer-solvent phase, Chitosan (CHT) and polycaprolactone (PCL) are two polymers with very different properties and finding a mutual solvent to develop a flat sheet membrane is an important challenge. The solvent optimization have been partially based on viscosity measurement of the polymer blend (**Fig. 3**): the viscosity is an important descriptor of the polymer affinity with the solvent. Moreover, maintaining an optimum viscosity is very important to achieve the double porosity membrane. During the solvent mixing, a visible reduction of the viscosity has been observed by dissolving PCL in the common solvent after 2-3 hours at temperature more than 35-40°C, probably due to the breakage of ester bonds. In order to reduce the decrease of viscosity, different factors were tuned e.g. CHT was dissolved in the solvent mixture at first at 55°C for 12 h, prior the addition of PCL at a temperature below 35°C. As discussed in the background section [2.2](#), Formic acid/Acetic acid mixture at a certain ratio enhances the dissolution [108], but the formic acid is also responsible for the breakage of ester bonds of the PCL. For these reasons, the solvent was optimized for each PCL/CHT polymer blend according the following composition: PCL/CHT 100/0 in 15 wt.% in FA/AA 70/30 (w/w) %, PCL/CHT 90/10 and 80/20 in 14 wt.% in FA/AA 60/40 (w/w) % and PCL/CHT 70/30 of 10 wt.% in FA/AA 50/50 (w/w) % (**Table 1**). In these conditions of composition and temperature, within two hours, a clear, faint yellow and viscous solution was obtained. After this dissolution step, the polymer-solvent

phase was kept at rest for 10-20 minutes before starting the membrane-casting step. Due to high viscosity of CHT in the solvent mixture, we could not go beyond the ratio of PCL/CHT 70/30 as it was difficult to make a homogeneous mixture of polymer solution by mechanical stirrer and to avoid phase segregation between the two polymer phases. Viscosity of CHT was remarkably high in the solvent mixture (**Fig. 3**): dissolving pure CHT above 4 wt.% was difficult by mechanical stirring and concentration lower than 4 wt.% are not sufficient to make a double porous membrane due to a lack of good entanglement between the polymer chain or a phase inversion leading to polymer particles.

The viscosity of the final polymer solution of pure PCL, CHT and the different blends were measured and reported in **Fig. 3**. Results showed that the viscosity of pure CHT of only 4 wt.% solution is significantly higher than viscosity of PCL/CHT 100/0 of 15 wt.% solution in mixed solvent. The solution viscosity of CHT is considerably higher than PCL due to several factors. First of all, the medium molecular weight of CHT (190 kDa – 310 kDa) is higher than the medium molecular weight of PCL (80 kDa). Second, CHT has higher affinity towards the solvents due to presence of the amine groups which interact with acetic acid and formic acid (i.e. solvent) via strong acid/base interactions: CHT polymer chains are deployed in the solvent leading to higher viscosity [111]. On contrary, in acidic solvent, the viscosity of PCL is decreased to some extent due to a decrease of the polymer chain length via breakdown of ester linkages. All these effects are responsible for the high difference of solution viscosity between these two polymers.

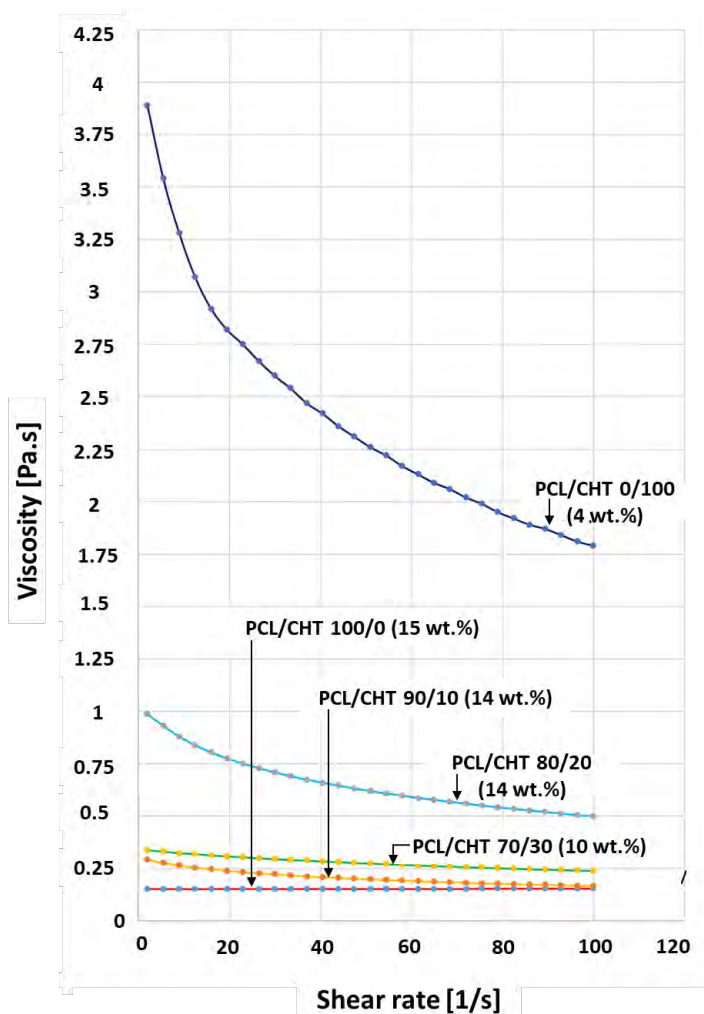


Fig. 3. Viscosity [Pa.s] vs shear rate [1/s] measurement of PCL/CHT 100/0 (15 wt.%), PCL/CHT 90/10 (14 wt.%), PCL/CHT 80/20 (14 wt.%), PCL/CHT 70/30 (10 wt.%) and PCL/CHT 0/100 (4 wt.%) scaffolds respectively in solvent FA/AA mixture (**Table 1**).

Concerning the non-solvent phase, NaOH has been added in the water, used as non-solvent, in order to decrease the interaction between CHT and FA/AA and then to reinforce the non-solvent strength as basic NaOH solution will break the acid/base interaction between the amine group of CHT and the acidic solvent. Concentration of NaOH more than 0.5 M in the non-solvent bath was also responsible to make the membrane fragile by breaking the ester bonds in PCL during membrane formation. A NaOH solution with a concentration lower than 0.2 M was not sufficiently concentrated to allow the formation of macrovoids. We also varied the concentration of the NaOH solution depending upon the viscosity of the casted solution in order to get a consistent macrovoids height of about 50-70 % of the total membrane

thickness. Finally, a 0.3 M NaOH solution was used for PCL/CHT 100/0 of 15 wt.% and a 0.5 M NaOH solution was used for the other PCL/CHT percentage to reduce viscosity.

To our knowledge, we are reporting for the first time the formation of membrane by phase inversion technique with a PCL/CHT blend dissolved in formic acid/acetic acid solvent mixture and precipitated in a non-solvent phase consisting in NaOH aqueous solution. The next sections report the influence of the polymer-solvent-nonsolvent system on the morphological and physico-chemical behaviors of the blends.

2.5.2 Morphology of the double porous material

After the membrane fabrication according to the procedure described in section [2.5.1](#), the top surface and the cross section characteristics were measured from the SEM images (**Fig. 4**). All the scaffolds, which were produced by using the track-etched membrane, are showing double porosity where the macrovoids are open towards the top surface and connected with the macroporous network making a sponge-like structure. From the cross section view, it was observed that the localized arrival of the non-solvent were creating an ellipsoidal macrovoid which was increasing by increasing CHT wt.%. The major axis of the ellipse is around 20 – 110 μm and minor axis (height) of the ellipse is around 15 – 70 μm (**Table 1**). The diameter of interconnected macropores is around $7 \pm 3 \mu\text{m}$ (except the PCL/CHT 70/30 ratio for which the macropores diameter is $20 \pm 5 \mu\text{m}$). The mechanisms that lead to this morphology are discussed in section [2.6.2](#).

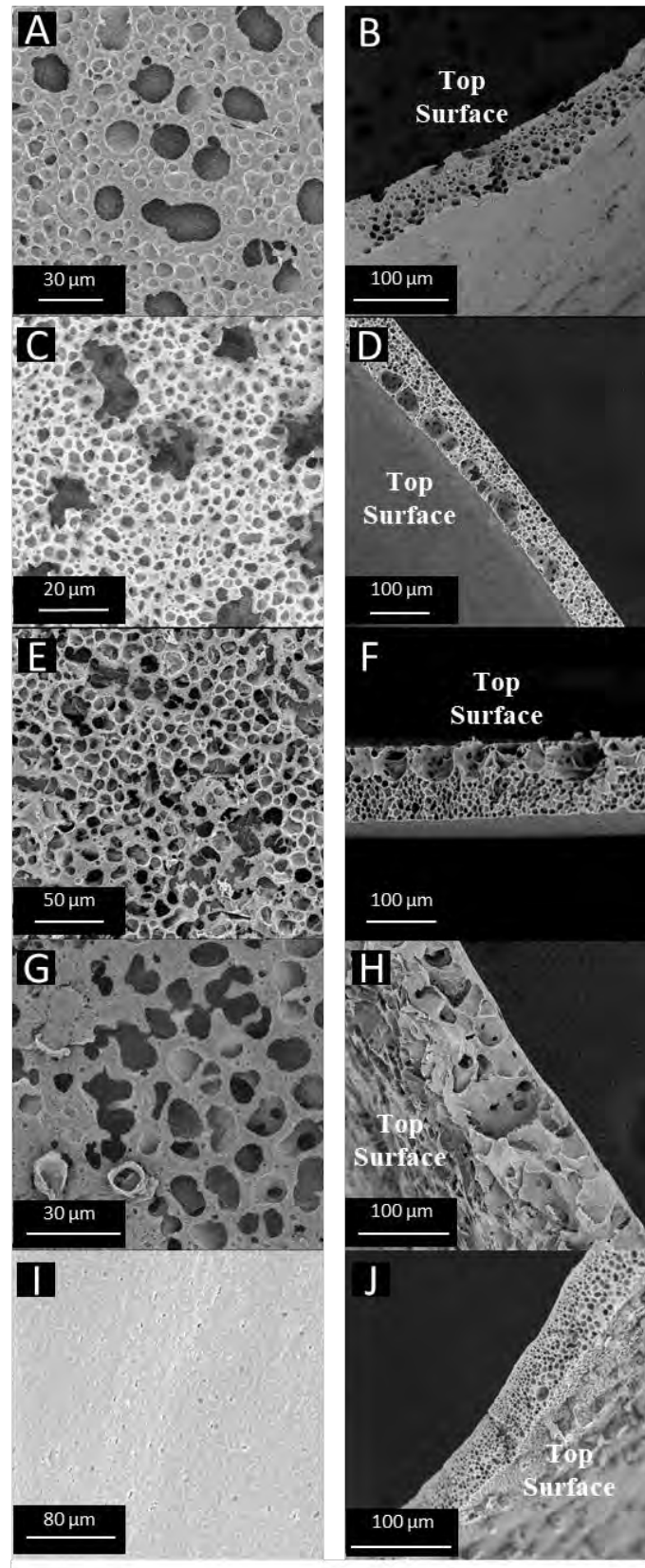


Fig. 4. SEM micrographs of membranes on the top surface and cross section with double porosity after removing the track-etched membrane (isopore dia. $10\mu\text{m}$): (A, B) PCL/CHT 100/0, (C, D) PCL/CHT 90/10, (E, F) PCL/CHT 80/20, (G, H) PCL/CHT 70/30 and with single porosity (made without the track-etched membrane): (I, J) PCL/CHT 100/0, top surface and cross section respectively.

Table 1. Summary of the polymer blend membrane properties with distinct concentration in correlation with viscosity and pore diameter, melting point.

		PCL/CHT percentage Ratio				
		100/0	90/10	80/20	70/30	0/100
	Total Polymer Conc. (w/w%)	15	14	14	10	4
	Solvents HCOOH/AcOH (w/w%)	70/30	60/40	60/40	50/50	50/50
	Nonsolvent NaOH (M)	0.3	0.5	0.5	0.5	-
Macrovoids diameter (μm)*	Major axis	20 \pm 3	80 \pm 5	90 \pm 5	110 \pm 5	-
	Minor axis	15 \pm 3	40 \pm 5	50 \pm 5	70 \pm 5	-
	Macropores diameter (μm)*	7 \pm 3	7 \pm 3	7 \pm 3	20 \pm 5	-
	Surface Porosity (%)*	40 \pm 5	50 \pm 5	53 \pm 5	45 \pm 5	-
	Viscosity of polymer sol. (Pa.s) @shear rate 2 sec ¹ (Fig. 2.)	0.153	0.293	0.987	0.338	3.89
	Degree of Crystallinity (%) (Equ. 3)	34.97	28.55	34.25	40.19	-
	Melting Point of PCL in the Blend (T _m) °C (Fig. 6.B)	61.59	62.78	63.19	61.70	-

*Data were obtained by ImageJ software

2.5.3 Chemical characterization by ATR-FTIR spectra

The representative FTIR spectra of the bottom surface (i.e. polymer materials) are shown in **Fig. 5. (A)**. All the stretching and bending vibrations are found to be well matching with the theoretical values [99]. In crude CHT, the broad peak at 3364 cm⁻¹ was due to N–H and intramolecular hydrogen bonded O–H stretching. The peak at 2880 cm⁻¹ was due to the asymmetric bending of C–H group. The N–H and –C–

O–C peaks were observed at 1651 and 1070 cm^{-1} respectively. In PCL, the peaks at 2946 and 1726 cm^{-1} represent the characteristic peaks for C–H and ester carbonyl groups (C=O), respectively. In PCL/CHT scaffold, by decreasing CHT proportion, the N–H and intramolecular hydrogen bonded O–H stretching of CHT shifted towards higher wavenumber region from 3364 cm^{-1} in PCL/CHT 70/30 to 3437 cm^{-1} in PCL/CHT 90/10. In addition, the C–H stretching of PCL also shifted towards higher wavenumber region from 2943 cm^{-1} in PCL/CHT 70/30 to 2946 cm^{-1} in PCL/CHT 90/10. From all these results, no additional peak was observed indicating that no covalent bonding between the two polymers occurred. However, it is clear that CHT and PCL has some secondary interactions between PCL and CHT as intermolecular hydrogen bonding, that change constantly with the composition [92,112]. These interactions indicate no phase separation occurs between CHT and PCL in accordance with Sarasam et al. [102] and She et al. [106] who observed a negative Flory Huggins parameter for these two polymers.

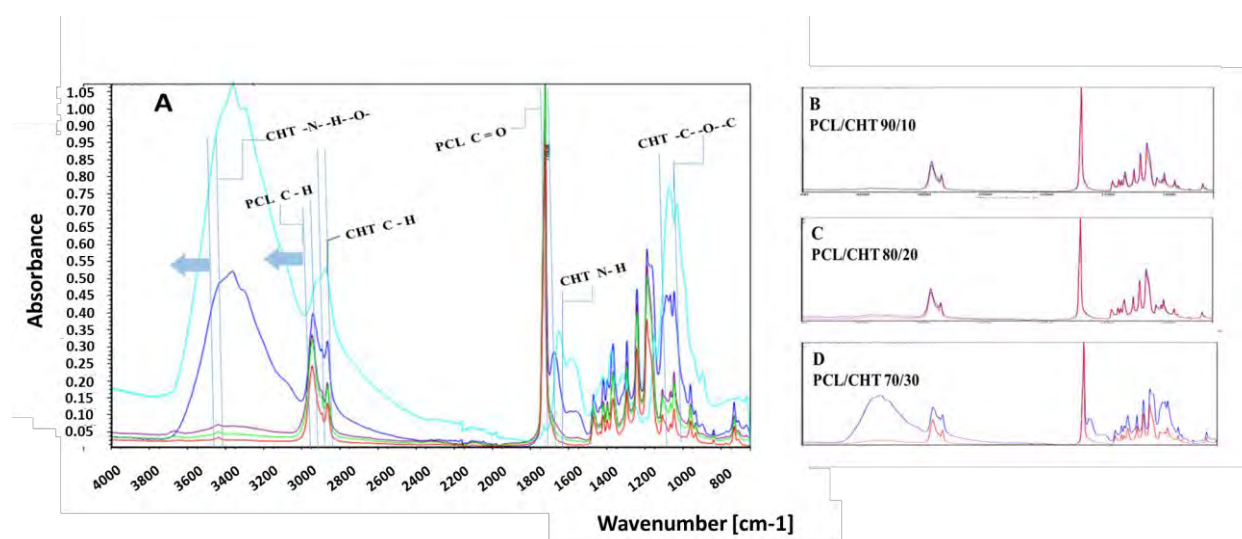


Fig. 5. (A) ATR-FTIR spectra of PCL/CHT scaffold on bottom surface where; PCL/CHT 100/0 in red, PCL/CHT 90/10 in green, PCL/CHT 80/20 in purple, PCL/CHT 70/30 in blue and CHT crude in cyne color respectively. (B, C, D) ATR-FTIR spectra of PCL/CHT scaffold on either side of same membrane where; top surface in red and bottom surface in blue color respectively.

The observations are given for first micrometer depth from the bottom surface as the penetration depth of ATR-FTIR absorption, d_p , for a sample is given by [113]:

$$d_p = \frac{\lambda}{2\pi \sqrt{n_1^2 \sin^2 \theta - n_2^2}} \quad (5)$$

where, λ and θ are the wavelength and incident angle respectively, n_2 , is the refractive index of the sample and n_1 is the refractive index of the ATR crystal. By using the above eq. 5, an incident angle of 45, a refractive index of the polymer of critical angle (θ_c) 1.5 and that of diamond of 2.4, the penetration depths are between 0.5 and 2.0 micrometer, for the wavelength range 1000-4000 cm^{-1} . That means the ATR-FTIR spectra only gather the information from the surface of the scaffolds, whose thickness were around 80 μm .

The comparison of ATR-FTIR spectra on the bottom surface and the top surface for a same membrane is presented in **Fig. 5 (B, C, D)** for the different PCL/CHT compositions. One can note that the intensities of specific bands of PCL are almost the same on the both surface of PCL/CHT 90/10 and PCL/CHT 80/20 membrane indicating almost homogeneous blend. Whereas, in the case of PCL/CHT 70/30, the spectra are not the same with different bands and intensities indicating a segregation of PCL and CHT through the membrane thickness: more CHT is found at the bottom surface than at the top surface. From this ATR-FTIR study, one can conclude no phase separation occurs due to the interaction between PCL and CHT but a segregation could occur through the membrane thickness from the composition of PCL/CHT 70/30.

This segregation was also observed in the **Fig. 6** by ATR-FTIR chemical mapping. Two characteristic bands were observed to highlight the difference of the membrane surface chemistry; C=O (1726 cm^{-1}) for PCL and intramolecular hydrogen bonded N-H and O-H (3364 cm^{-1}) for CHT [93].

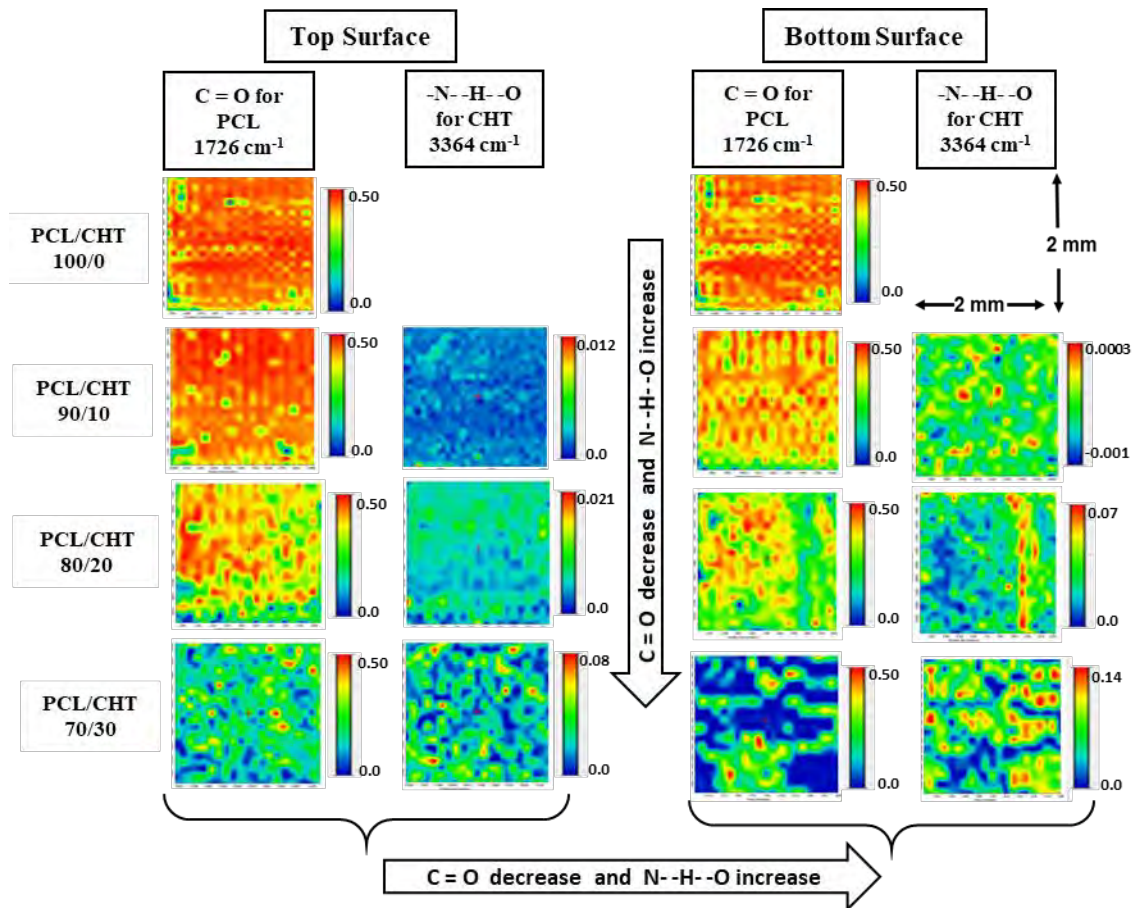


Fig. 6. Chemical mapping of PCL/CHT blends on either surface on the same membrane where; C=O for PCL observed at 1726 cm^{-1} and hydrogen bonded N–H and O–H observed at 3364 cm^{-1} . Red and blue colors indicate the intensity of the corresponding bands, high and low intensity, respectively, corresponding to high and low concentration.

From the chemical FTIR mapping, on top and bottom surface, we can verify that by increasing the concentration of CHT in the blends, the absorbance of C=O decreases and the absorbance of N–H and intramolecular hydrogen bonded O–H increases as expected [93,114]. In well agreement with the **Fig. 5. (B, C, D)**, it appears that PCL intensities of PCL/CHT 100/0 to 80/20 are quite the same on both surface as for CHT on PCL/CHT 90/10. For higher concentration of CHT (PCL/CHT 70/30), CHT is more concentrated at the bottom surface than at the top surface. Moreover, for the bottom surface, the local concentrations of PCL and CHT at the micrometer scale (i.e. each pixel represents a $50 \times 50\ \mu\text{m}$ of analyzed surface) is not homogenous, although PCL and CHT interactions were identified in the FTIR spectra: the high concentration of CHT zone are complementary of those of PCL indicating a segregation of both polymers [102,106,115]. This is less observed on the top surface. The material is thus not

completely homogenous due to the phenomena involved during the membrane formation (see section [2.6](#)).

2.5.4 Crystalline and thermal properties

Crystalline properties of the blend were measured on a 1 cm² dried flat sheet membrane and depicted in **Fig. 7. (A)**. As an amorphous polymer, characteristic broad peak of CHT was hardly observed at 19° in PCL/CHT 80/20 and PCL/CHT 70/30. Characteristic intense peaks at 21.5° and 23.5° at Bragg angles 2-Theta corresponding to the (1 1 0) and (2 0 0) planes in PCL can be observed. Moreover, by increasing CHT wt.%, a slight increase of Bragg angles of the characteristic peak of PCL, indicates an interaction with CHT in agreement with the FTIR data [99,116,117]. It could be interesting to correlate this data with Honma et al. [99], who found differences in the inter-planar spacing of (1 1 0) planes with promoting CHT, the b axes of the PCL orthorhombic cell getting more spread out in the cell. Whereas, no difference was found in the spaces of the (2 0 0) planes. From these results, it can be concluded that significant molecular interaction occurs between PCL and CHT during solvent mixing ; weaker molecular interaction are observed when the blend is produced by melt blending [118] . Generally, in most of the cases, it was reported that by increasing the weight fraction of CHT the intensity of the characteristic peak of PCL should decrease. It is stated that the conjugation with PCL and CHT chains suppresses the crystallization of PCL [99,119–121]. Unlike the other reported data, in our case, this effect was not observed and we found a considerable increase of intensity of the PCL specific peak in the blend by decreasing PCL wt.% like the 29.5° peak which finally disappear for PCL/CHT 70/30.

Apart from the characteristic peaks of PCL and CHT, some other intense peaks were also detected due to the formation of different type of crystals with different D spacing within the crystal lattice [117]. Those gave an overall crystalline behavior to the blend. In the particular case of PCL/CHT 70/30, the intensity of other peaks was very low due to the amount of CHT and the amorphousness of CHT.

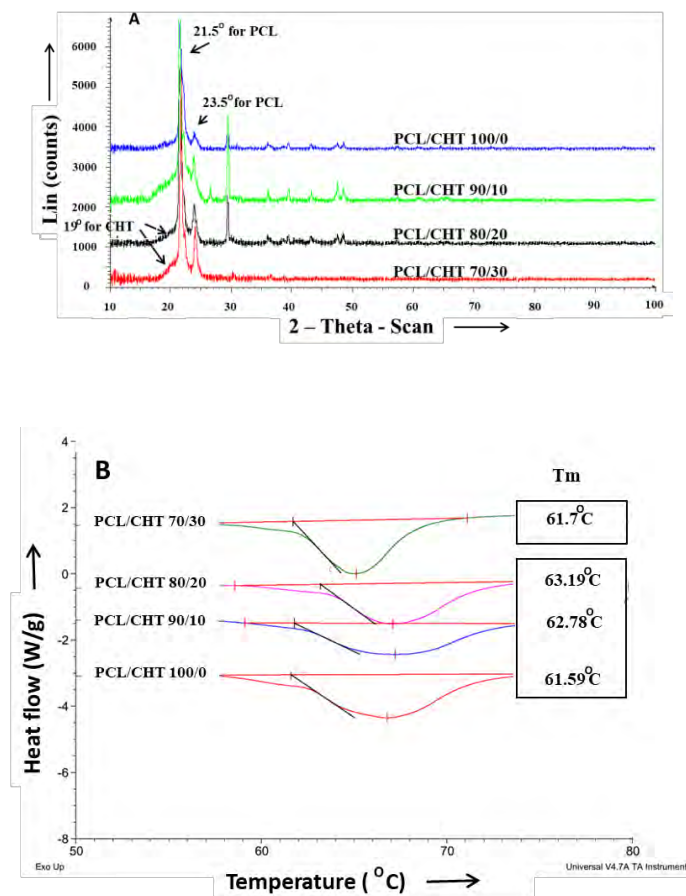


Fig. 7. (A). X-ray diffraction spectra for the different blends, **(B)** Differential scanning calorimetric study of blends as a function of PCL content in the blend.

This observations were also supported by the DSC analysis in **Fig. 7. (B)**. In correlation with the crystallinity, no linear relationship between the wt.% of CHT and the temperature of melting (T_m) of the crystalline PCL was found inside the blend, possibly due to the segregation of these two polymers [93]. In order to check this phenomenon, we calculate the crystallinity (X_c) of the PCL component by applying **Eq. 3**, and results are presented in **Table 1**. We found that by introducing CHT and increasing the CHT wt.%, the crystallinity of PCL in the blend firstly decreased (PCL/CHT 90/10) then increased up to 40%. Generally, pure PCL melts at 60°C and CHT undergoes thermal degradation at around 270°C prior to melting [93]. It is still difficult to determine the glass transition (T_g) of CHT by conventional thermal technique, although some efforts have been done [118,122,123]. Thus, the variation of the melting point of PCL in the blend was monitored by varying the composition of CHT. Unlike other reported data

[93,99,100,103], we found that by increasing the weight fraction of CHT, T_m of the blend increased [117].

The PCL/CHT interaction can be analyzed through the Flory-Huggins interaction parameter χ_{12} . The simplified Nishi-Wang equation [102,124] is used to correlate the melting temperature to the volume fraction of PCL and to the Flory-Huggins parameter with high MW crystalline-amorphous polymer system:

$$\frac{1}{T_m} - \frac{1}{T_{m2}^0} = \frac{-R}{\Delta H_{2u}} \frac{V_{2u}}{V_{1u}} \chi_{12} (1 - \Psi_2)^2 \quad (6)$$

where, subscripts 1 and 2 correspond to CHT and PCL polymer, respectively. T_m and T_{m2}^0 are the equilibrium melting temperature (K) of the blend and pure PCL (333.15 K) respectively. R is the universal gas constant (1.98 cal/mol K), ΔH_{2u} is the heat of fusion per mole of 100% crystalline PCL (3694.67 cal/mol), V_{2u} (99.65 cm³/mol) and V_{1u} (1546.82 cm³/mol) are molar volumes of the repeating unit of polymers and Ψ_2 refers to the volume fraction of PCL in the blend.

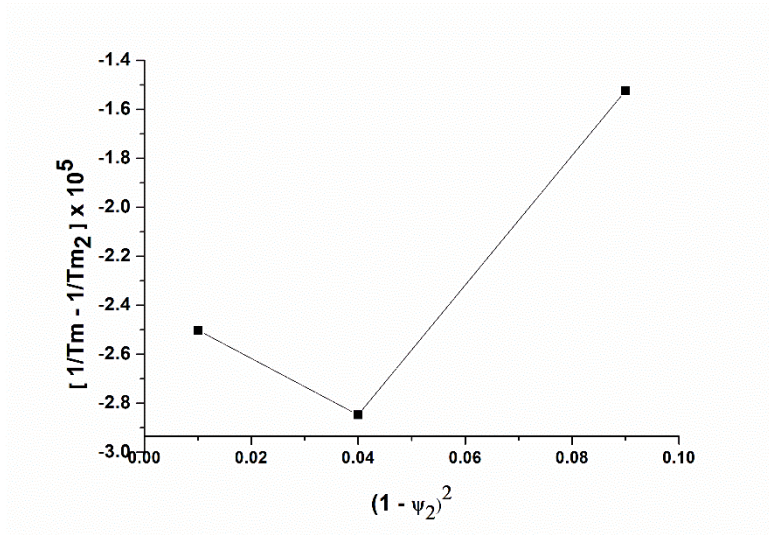


Fig. 8. Nishi – Wang plot. Where T_m and T_{m2} are the equilibrium melting temperature (K) of the blend and pure PCL, respectively, and Ψ_2 is the volume fraction of PCL in the blend.

The Nishi-Wang plot (**Fig. 8.**) shows that our experimental data cannot be represented with a line passing through the origin. Although variations in crystallinity and melting temperature indicate an interaction between PCL and CHT, our samples do not follow the Nishi-Wang law, which assumes homogeneous samples. This result is therefore in agreement with the segregation of the polymers identified by infrared

chemical mapping (**Fig. 6**) which indicates that our samples are heterogeneous: the membranes have a variety of crystallinities and melting temperatures.

2.5.5 Enzymatic degradation

The enzymatic hydrolysis of polymeric biomaterials is a heterogeneous process that is affected by the mode of interaction between the enzymes and polymer chains. It generally involves four steps: (a) diffusion of the enzyme from the bulk solution to the solid surface, (b) adsorption of the enzyme on the substrate, forming an enzyme–substrate complex, (c) hydrolysis reaction catalyzed by the enzyme, forming smaller, soluble polymeric chain and (d) diffusion of the soluble degradation products from the solid substrate to the solution [98]. The rate of the overall degradation is controlled by the slowest step.

The effect of enzymatic degradation by lipase in terms of wt. loss (%) was observed on four batches of samples in **Fig. 9. (A)**. A fast and almost selective degradation of PCL from all the blends within 48 hours was found. The degradation is expected to be faster than in physiological condition as the lipase (*Pseudomonas cepacia*) is concentrated at 7 U/ml while the concentration is about 0.03-0.190 U/ml in human serum [125–127]. Moreover, the enzyme can easily diffuse through the bulk of porous scaffolds as the size of the bulky protein chains of the enzymes (>10 nm) is more than 100 times smaller than the scaffolds pore size (1 to 100 μm) leading to a faster degradation compared to dense, non-porous scaffolds.

First, it has to be noticed that the degradation of the blend in pure water is significantly low (**Fig. 9. (C)**) [128]. Pure PCL showed the lowest degradation ($1.0\% \pm 0.1$ after 90 days) and the degradation increases by increasing the CHT wt.%. PCL/CHT 70/30 showed the highest degradation ($3.7\% \pm 0.2$ after 90 days).

The mechanisms leading to the degradation of the PCL and CHT polymers are significantly different. Generally, PCL, like polyester, degrades similarly to lipid hydrolysis, which is highly facilitated by lipase. Lipases are water-soluble enzymes that hydrolyze ester bonds of water-soluble substrates such as triglycerides, phospholipids, and cholesteryl esters [129]. Increasing the CHT wt.% (or decreasing PCL wt.%) not only increases the amorphousness and hydrophilicity but also increases the macrovoids

size and hence the porous bulk of scaffolds is more accessible by the enzymatic solution leading to faster degradation via formation of a smaller soluble enzyme–substrate complex [130]. On the other hand, CHT, like polysaccharide, consisting of N-acetyl/deacetyl glucosamine, degrades by oxidative-reductive chain scission and lipase has very weak effect on CHT degradation [131–134]. When the degradation is performed without lipase, the ability of the material to absorb water and its water permeability, which was increasing by increasing CHT wt.%, play a key role in the degradation.

The two different trends obtained from enzymatic and non-enzymatic degradation have a very good significance in terms of application and could be highly dependent on the nature of the environment *in vivo*. The diffusion and adsorption of the enzyme in the lymphatic system which is mainly composed of interstitial fluid (94% water and 6% solid particle; proteins, fats, carbohydrate) [135] could be more favorable by increasing CHT wt.%. Whereas, in the case of more concentrated blood vascular system which is mainly composed of 55% plasma (among that 90% is water) and 45% of blood cells and platelets [136], could be less favorable by increasing CHT wt.%.

The surface morphology of degraded membrane after different time intervals is presented in the **Fig. 10**. In case of enzyme degradation, a noticeable damage on surface was observed together with a significant weight loss. It is suggesting that the degradation phenomenon not only depends on the surface of the material [130] but also on the bulk of the material, as the enzyme can reach any zone inside the bulk through the highly porous structure.

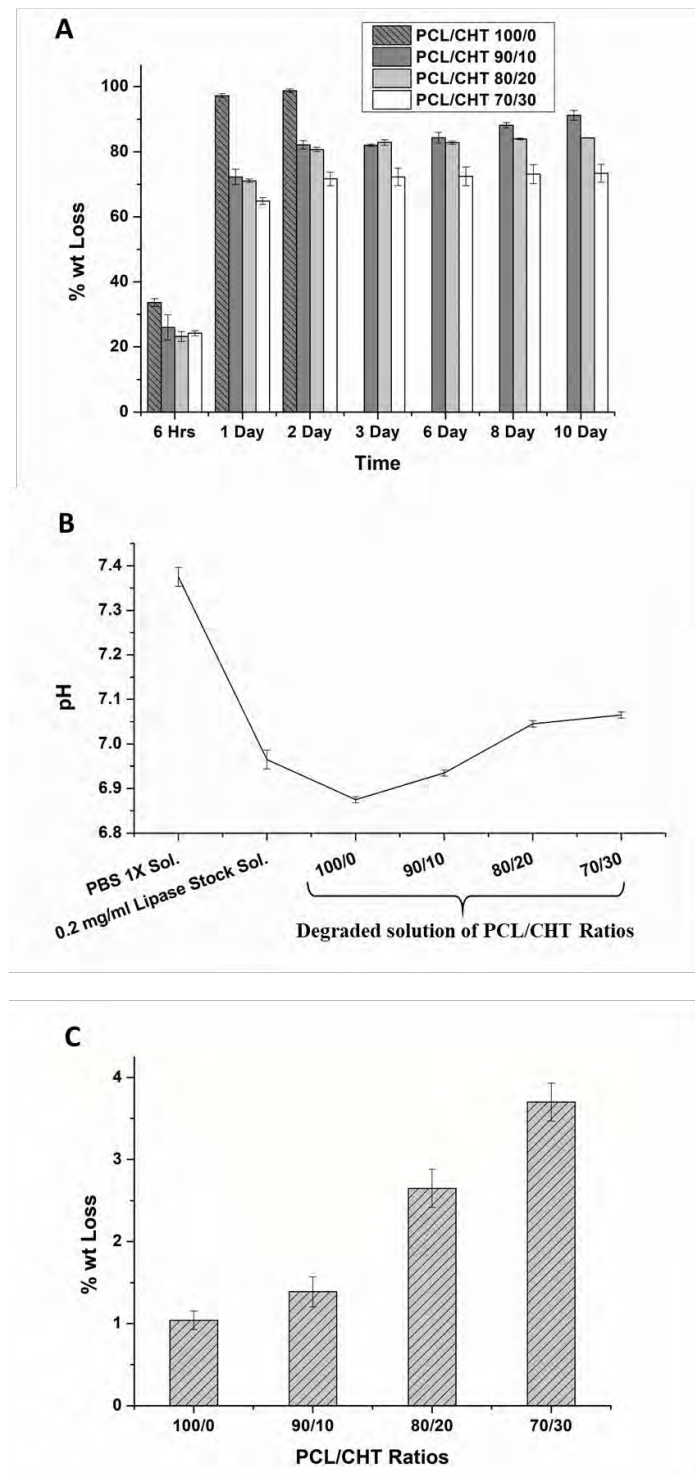


Fig. 9. (A) Weight loss % of the sample with lipase enzyme (*Pseudomonas cepacia*; 7 U/ml) at different time intervals, (B) pH of the enzyme degraded solution after the study and (C) weight loss % of the sample without enzyme after 90 days.

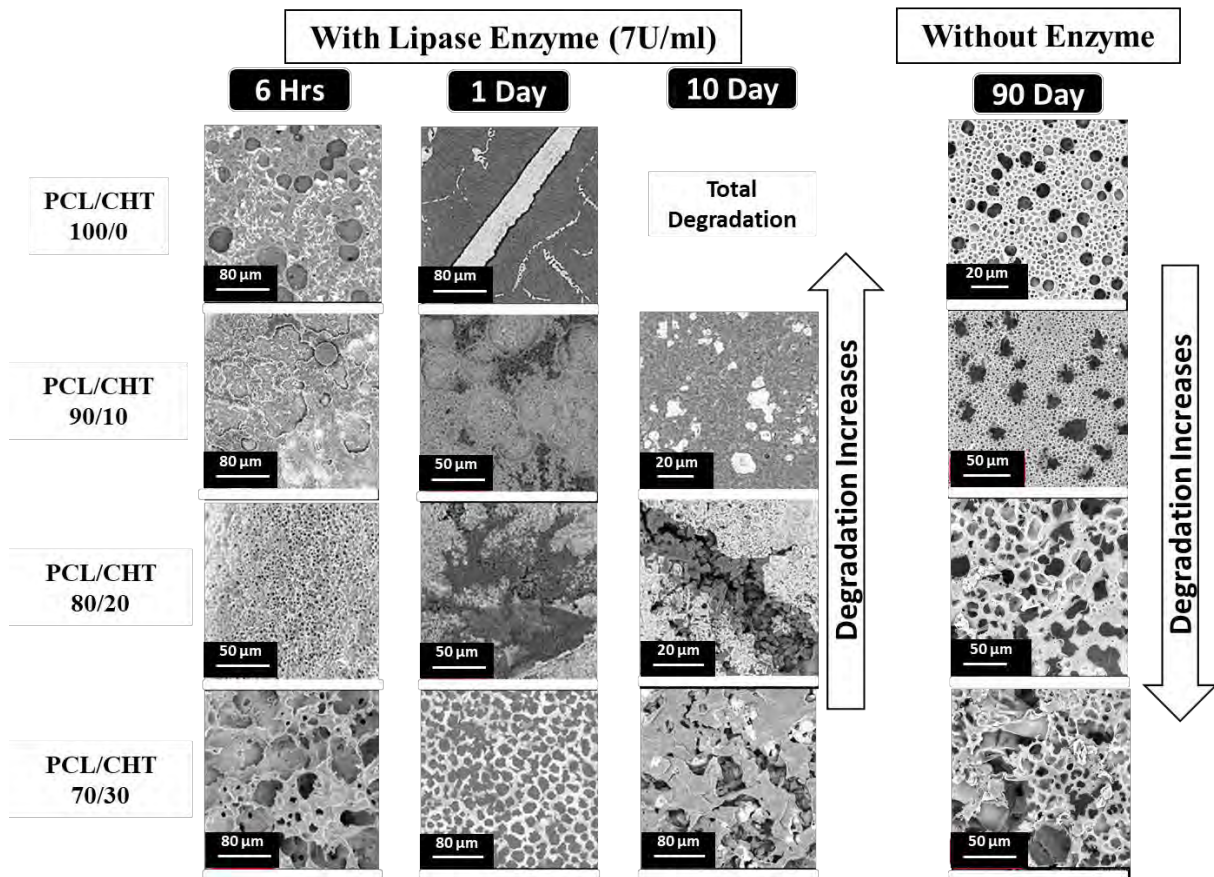


Fig. 10. SEM images of degraded PCL/CHT blends after 6 hrs, 1 day and 10 days with lipase enzyme (*Pseudomonas cepacia*; 7 U/ml) and after 90 days without enzyme.

The change in pH measured in the degraded solution is reported in the **Fig. 9. (B)**. PCL/CHT 100/0 has shown the lowest pH probably due to the presence of highest amount of ester chain degraded acid. When the PCL concentration decreases, the pH increases again but it stays very close to the physiological pH, indicating less toxicity of the degraded solution.

2.6 Discussion

The previous section was presenting the main physico-chemical properties of the membrane and their behavior with the PCL/CHT ratio. From these data, the aim of this section is to discuss the possible mechanisms that control the membrane formation at microscopic scale with the PCL/CHT chemical structure and at mesoscopic scale with the morphological structuration of the membrane porosity.

2.6.1 Microscopic PCL/CHT chemical structure

The IR results demonstrate the presence of weak interactions between PCL and CHT (with a shift of the peak) that allow to avoid phase separation and a total immiscibility between PCL and CHT. The presence of these weak interactions is confirmed by the crystalline properties ([section 2.5.4](#)) with a decrease in crystallinity when mixing PCL and CHT. However, the Nishi - Wang plot ([Fig. 8.](#)) shows that the blend material cannot be considered as fully homogeneous. The chemical analysis ([Fig. 6.](#)) demonstrates also a difference in composition along the membrane thickness: the PCL is more concentrated at the top surface of the membrane (the membrane side in contact with the non-solvent phase).

The solvent and non-solvent power can be evaluated through the interaction distances using the Hansen solubility parameter approach [137]. From the [Table 2](#), the lowest interaction distances are found for PCL and the acids indicating good solvents whereas water is a non-solvent of PCL with highest interaction distance. The CHT shows high interaction distances in the range of 21.6-23.0 for all solvents which are therefore bad solvent (with almost the same non-solvent power) for CHT. However, the solubility of CHT in water at low pH as well as in acids is observed due to the formation of strong acid/base interaction turning CHT to a polyelectrolyte via the protonation of amine groups. The use of NaOH solution as a non-solvent is then crucial, as the base will deprotonate the amine groups leading to insoluble CHT. Thus, NaOH solution is a stronger non-solvent of CHT than pure water.

Table 2. Hansen solubility parameter of CHT, PCL and solvents and the interaction distance. All value are given en MPa^{1/2}.

	δ MPa ^{1/2}	δd MPa ^{1/2}	δp MPa ^{1/2}	δh MPa ^{1/2}	Interaction distance (MPa ^{1/2})		Ref.
					PCL	CHT	
CHT	38,8	22,9	16,6	26,6	23,9	-	[138,139]
PCL	20,3	17,7	6,2	7,8	-	23,9	[140]
water	47,8	15,5	16	42,3	36,1	21,6	[137]
FA	22,6	14,6	10	14	9,6	21,9	[137]
AA	21,4	14,5	8	13,5	8,8	23,0	[137]

This heterogeneity along the membrane thickness can be explained (**Fig. 12.**) by the presence of a NaOH gradient along the thickness of the polymer solution during the phase inversion process (with high NaOH concentration at the top - in contact with the non-solvent phase - and low concentration at the bottom). The NaOH gradient results in an acid concentration gradient along the thickness of the polymer solution due to faster neutralization at the top surface than at the bottom surface, leading to the formation of conjugate bases (FA⁻ and AA⁻, which act as stronger non-solvent). The presence of conjugates increases the gradient of solvent activity. CHT chains have more affinity for the solvent (FA/AA) than PCL and thus the gradient of chemical potential for CHT is more important than the one for PCL [141]. Due to these differences in chemical potential gradient, CHT should move towards the bottom surface to some extent higher than PCL chains. As water is a strong non solvent of PCL, PCL chains will coagulate faster than CHT. The PCL chains will be trapped in contact of water and cannot move anymore.

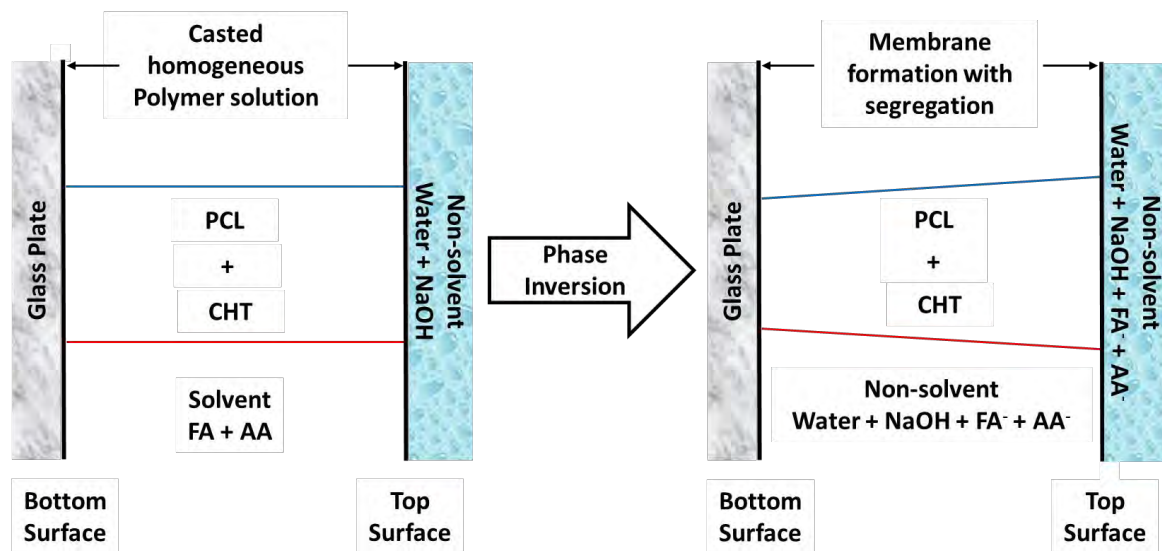


Fig. 12. Schematic representation of the gradient along the thickness and the differential migration of PCL (in blue) and CHT (in red) in the blend after phase inversion (where PCL is polycaprolactone, CHT is chitosan, FA is formic acid, AA is acetic acid, FA^- is formate anion and AA^- acetate anion respectively).

2.6.2 Mesoscopic morphological structuration of the membrane

The equilibrium phase diagram for the ternary system of polymer-solvent-nonsolvent, **Fig. 13. (A)**, can be used to understand the route taken during the membrane precipitation process and the possible consequences for the macrovoids formation. According to the mixture composition, two phases can exist: a one-phase region, where all components are miscible, and a two-phase region, where the system separates into viscous polymer-rich and low viscosity polymer-poor phases (i.e. made of solvent and non-solvent). The liquid-liquid phase boundary is the so-called binodale curve. Every composition inside the binodale curve will demix into two liquid phases which differ in composition but are thermodynamically in equilibrium with each other. The tie line connects a pair of equilibrium compositions in the phase diagram. Thus, at low polymer concentrations where the tie line intersects the binodale, the system is a low viscosity polymer-poor phase dispersed in a high viscosity polymer rich phase. As the solvent leaves the polymer rich phase, the concentration of polymer in the polymer rich phase increases while the polymer-lean phase growth and coalesce. The viscosity of the polymer rich continuously increase up to the gelation point (E), leading to a highly viscous polymer-rich phase where further polymer chain movement is not possible [142,143].

Two extreme cases can be considered according the PCL/CHT percentage. The case 1 (left column in Fig. 13.) corresponds to the pure PCL blend and the case 2 (right column in Fig. 13.) corresponds to the lower PCL/CHT percentage. As previously discussed, one difference between these cases is the use of higher NaOH solution in the non-solvent phase for higher CHT concentration. In this last case, the gelation point should occur for higher polymer concentration, as there is less attractive interaction between CHT and solvent in basic solution.

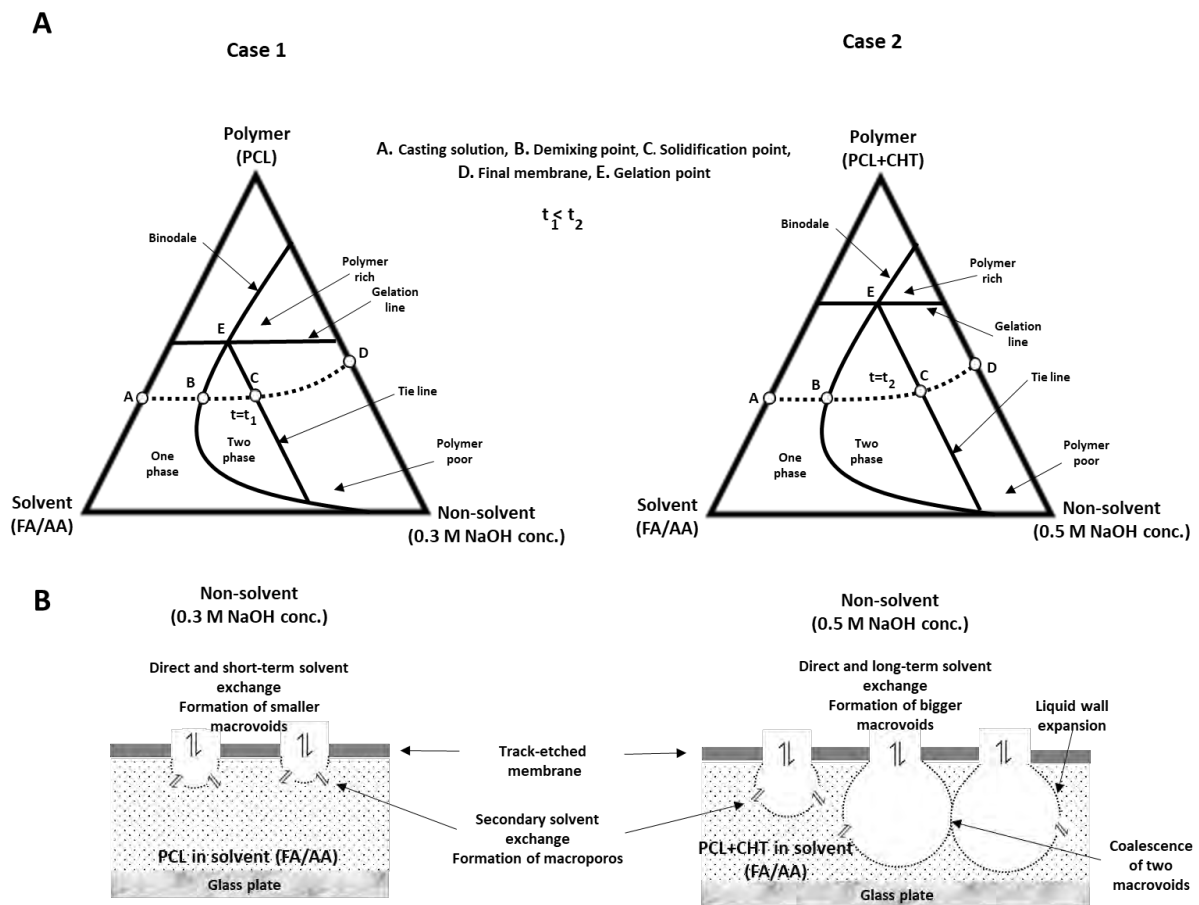


Fig. 13. (A). Schematic phase diagram of the system polymer-solvent-nonsolvent representing the membrane macrovoids formation pathway (A-B-C-D), (B). Illustrative representation of the formation of macrovoids. **Case 1:** formation of smaller macrovoids consisting of polymer as PCL, solvent as FA/AA and non-solvent as NaOH at low concentration and **Case 2:** formation of bigger macrovoids consisting of polymer as PCL+CHT, solvent as FA/AA and non-solvent as NaOH at high concentration (where PCL is polycaprolactone, CHT is chitosan, FA is formic acid, AA is acetic acid respectively).

Regarding the triangular diagram (Fig. 13. (A)), the entire membrane formation process follows the path (A-B-C-D), where A represents the initial casted solution when it is just immersed inside the non-solvent

($t=0$), **B** represents the demixing point where the two liquid phases formation starts. As the two-phase formation proceeds, more and more solvent is neutralized and the viscosity of the polymer-rich phase increases. At one point, the viscosity is high enough to restrict further polymer chain movement and the polymer is considered as solid, representing the solidification point **C** where it intersects the tie line with the gelation point **E**. From **B** to **C**, the polymer lean phase coalesces to form the observed small macrovoid: the extent of the coalescence depends of the time need to go from **B** to **C**.

After that, the membrane structure does not evolve and further solvent exchange results in the removal of solvent. Some shrinkage of the bulk volume could also happen leading to the final membrane structure **D** [142,144]. The composition **D** is in equilibrium between the polymer-rich and polymer-poor phase and the position of point **D** on the polymer/non-solvent line of the phase diagram determines the overall porosity of the membrane. The phase inversion process takes place differently depending on the position of point **C** as depicted in **Fig. 13. (A)**.

Due to the presence of the track-etched membrane on the casted solution, just after immersion, the non-solvent has a restricted access to the polymer solution through the pore of the track-etched membrane, initiating a spatially heterogeneous solvent-nonsolvent exchange [83,84]. The phase inversion starts in the zone where there is a direct contact between the polymer and the non-solvent as soon as the concentration reaches the composition of point **B** in the **Fig. 13. (A)**. As illustrated in the **Fig. 13. (B)**, the phase inversion results in the initiation and growth of a liquid wall (polymer-rich phase). The liquid wall, created from the phase separation, expands radially from the non-solvent invasion point at polymer-poor phase towards the bulk at polymer-rich phase. During the phase separation, the polymer concentration of the liquid wall increases until the liquid gelation (point **E** in **Fig. 13. (A)**) and thus further polymer chain movement stops [142,144]. In a second time, a secondary phase separation occurs through the whole volume of the polymer solution because of the slow diffusion of the non-solvent through the liquid and gel walls. The polymer solution area, protected from direct exposure to the non-solvent due to the presence of the track-etched membrane, undergoes the secondary phase separation. This phase inversion takes place at a slower rate and leads to the formation of a uniform spongy

macroporous network connected by the macrovoids [83,84,142,144]. These phenomena occur up to the point C where the polymer reach phase turn into gel and stop the structure change.

The polymer blend composition, polymer wt.% and non-solvent concentration play an influential role on the macrovoids size and on the membrane porosity. Particularly in the case 2, where CHT is present along with PCL inside the polymer solution, the blend has a higher affinity with solvents than PCL alone. This is due to higher secondary interaction between the CHT functional groups and solvents, higher M.W and the presence of cyclic structure, that result in the CHT chains deployment and high entanglement in the solution [108]. In that case and after the demixing point, the non-solvent first has to disable the secondary interaction between CHT and solvents followed by solvent exchange via acid-base reaction, leading to a delay in solidification ($t=t_2$, path **B-C**). Meantime, more non-solvent invades due to a higher non-solvent concentration and lower polymer wt.% (in the case of PCL/CHT 70/30 with 10 wt.%), leading to further expansion of the liquid wall and eventually coalescence of two neighboring nascent liquid walls before reaching the solidification point C : bigger macrovoids are therefore formed [142,144]. In case 1, due to the presence of PCL alone, after the demixing phase, the solvent exchange starts readily as PCL does not have a strong affinity with the solvents and as water act as a strong non solvent, at the contrary of CHT. Moreover, due to the lower nonsolvent concentration and higher polymer wt.% (pure PCL with 15 wt.%), the liquid wall reaches the solidification point C ($t=t_1$; where $t_1 < t_2$) before significant expansion, resulting in smaller macrovoids.

Remigy et al. [144] and, earlier, Strathmann et al. [142] reported that, due to the heterogeneous and restricted solvent diffusion, the macrovoid generation can also be achieved by a dense skin formation on the polymer solution layer via rapid homogeneous precipitation. In that case, after formation of the dense skin, it disrupts by shrinkage of the homogeneous solid layer and the macrovoid formation starts from the disruption point due to the heterogeneous and restricted access of the non-solvent. In the present work, we cover the polymer solution with track-etched membrane, which acts as a dense skin with restricted access of the non-solvent [83,84]. The use of a track-etched membrane and its removal allows the generation of largely open macrovoids, which were not obtained using the classical phase inversion technique. When no track-etched membrane was used, the membrane material presented single porosity

alike conventional liquid-liquid homogeneous phase inversion and pores were not open enough towards the top surface (Fig. 4. I, J).

2.7 Conclusions

A PCL/CHT membrane with a unique double porosity level has been developed for tissue engineering applications. The membrane has been fabricated with a modified phase inversion technique from PCL/CHT polymer blends in the ratios 100:0, 90:10, 80:20, 70:30 (w/w%) in a solvent mixture of formic acid/acetic acid. Macrovoids at the membrane surface have been formed which are connected through membrane macroporous network. The micro-patterning technique was performed by localized access of the non-solvent inside the polymer solution via applying isoporous, commercial (track-etched) membrane during liquid induced phase inversion. The physico-chemical properties and morphological structure of the membrane have been characterized and the mechanisms at the origin of the membrane formation have been discussed. This membrane exhibits interesting functionalities for tissue engineering applications:

- The membrane possesses a structure with three dimensional double porosity level, thanks to the micro-patterning techniques. The SEM images show that plenty of micrometers macrovoids (20 to 110 μm) are connected through spongy network. Such a structure could ensure bi-functionality for tissue repair: first, macrovoids could act as a holder for the cell and provide better cellular proliferation and colonization, and second, macrovoids, connected through a spongy macroporous network, could be used to store and to supply essential nutrients, growth factors and oxygen for cell survival.

- The morphological analysis of the membrane shows that the macrovoids size increased by increasing the Chitosan concentration. ATR-FTIR chemical spectra confirm the presence of secondary interaction between PCL and Chitosan. From the FTIR chemical mapping, we found a slight segregation of polymers along the thickness in case of high Chitosan wt.%, which is quite natural due to the high affinity of Chitosan with the solvents and chain length difference between the two polymers. From the XRD and DSC studies, we observed an increase of the crystallinity and melting point by increasing CHT wt.%.

-The biodegradability of the material can be adjusted according to the PCL/CHT ratio. The enzymatic degradation of the PCL/CHT double porous scaffold using lipase (from *P. cepacia*), pointed out a faster and almost selective degradation of PCL in the blend. We also measured the pH of the degraded solution after enzymatic experiments; pH was very close to the physiological pH independently of the composition of the material. The degradation rate could coincide with the rate of tissue regeneration (the time scale is between days and months).

2.8 Acknowledgements

We like to thank Corinne Routaboul (Service commun de spectroscopie infrarouge et Raman, Université Paul Sabatier, France) for the scanning of samples on the FTIR micro-spectrometer; we thank Christophe Tenailleau (CIRIMAT, Université Paul Sabatier, France) for the x-ray crystallographic analysis.

Chapter 3: Double porous, biodegradable poly (ϵ -caprolactone)/chitosan 3D membrane scaffolds: understanding hMSCs attachment, proliferation and invasion by varying pore size and morphology of the scaffolds

3.1 Summary of the chapter

In this paper, we developed membranes scaffolds to mimic the biochemical and biophysical properties of human mesenchymal stem cell niches to help direct self-renewal and proliferation providing to cells all necessary chemical, mechanical and topographical cues. The strategy was to create membrane scaffolds with double porosity able to promote the mass transfer of nutrients and to entrapped cells. We developed poly (ϵ - caprolactone)/chitosan blend membrane by modified liquid induced phase inversion technique, consist of double porous morphology: (i) surface macrovoids (big pores) which could be easily accessible for hMSCs invasion and viability; (ii) interconnected macroporous (small pores) network to transfer essential nutrients, oxygen, growth factor between the macrovoids and throughout the scaffolds. The scaffolds were characterized with respect to their composition, structure, mechanical properties and they were finally tested in vitro to assess their potential as platform for tissue engineering. The bioactivity of a 3D scaffolds used in tissue engineering applications depends on density of the available ligands, scaffolds microstructural environment at which specific cell binding occurs. Ligand density is defined by the composition of the scaffolds and the ligand density on the surface is inversely proportional to the surface macrovoid size or proportional to the effective surface area, surface which is exposed for initial attachment of the cells. However, if the macrovoid size is bigger than cell dimension of specific interest, cell invasion inside the bulk takes place influencing the overall cell viability. Herein we varied the mean macrovoid size, effective surface area and surface morphology by varying the PCL/CHT blend composition (100:0, 90:10, 80:20, 70:30). SEM images of the cross section of the scaffolds confirmed that the macrovoids are connected with each other through the interconnected macroporous network and the size of the macrovoids were increased by increasing the CHT wt.%. The cell morphology, viability and oxygen uptake rate (OUR) were evaluated until 21 days.

We found a linear relationship between hMSCs viability with surface mean macrovoid size, effective surface area and surface morphology. The mechanical properties (tensile strength, young modulus and elongation at break) of the membranes observed in dry and in wet condition as well. Enzymatic degradation were performed by using Lipase (*Aspergillus oryzae*) and Lysozyme at the same concentrations of the human serum. The obtained results by culturing hMSCs on this double porous morphology and the relationship with mean macrovoid size, effective surface area and surface morphology will be very useful to advance different aspects of tissue engineering application e.g. to create a 'selective co-culture' or a 3D cell culture environment for tissue regeneration.

3.2 Introduction

An important challenge in tissue engineering and regenerative medicine is the design of a biomaterial able to provide all necessary physical, chemical and mechanical cues that promote cell differentiation and tissue regeneration. Design approach for biomaterials are driven to the interest to reproduce the natural niche of cells that implies cell-cell and cell-extracellular matrix (ECM) contacts in a 3-D environment that ensure the maintenance of cell polarity. In this contest, a great interest is focused on the development of materials able to boost the proliferation and differentiation of mesenchymal stem cells (MSCs), which represent a promising source for cell therapy and regenerative medicine. In particular, bone marrow derived human mesenchymal stem cells (hMSCs) are powerful multipotent progenitor cells and a promising alternative cell source due to their capacity to differentiate into distinctive end-stage cell types, such as those that fabricate specific mesenchymal tissues including bone, cartilage, muscle, bone marrow stroma, tendon/ligament, fat, dermis, and other connective tissues [145–148]. Furthermore MSCs, themselves, secrete a broad spectrum of bioactive macromolecules that are both immunoregulatory and serve to structure regenerative microenvironments in fields of tissue injury [147]. It has been reported that the hMSCs differentiation depend highly on environmental cues such as oxygen and nutrient availability, pore size, scaffold mechanical property, surface morphology and more notably the administration of soluble factors [79,145]. All these intrinsic multipotent parameters of hMSCs make them a potential candidate for a strategic tissue engineering application with greater level of understanding of the interaction between cells and 3D scaffolds mimicking physiological conditions.

Microporous membranes with suitable topographical, mechanical, physico-chemical and permeability properties can act as an artificial stem cell niche providing a bio-instructive extracellular environment characterized by micro- and nano-architecture. Membranes enable to provide an adequate structure in terms of porosity and interconnected pores, which is important for the selective mass transfer of nutrients and metabolites, and on the other hand favour cell attachment on the surface and invasion inside the bulk increasing the effective area for cell accommodation. However, this balance between the optimal pore size and effective cell adhesion area is often compromised in the case of small pores suitable for the transfer of nutrients, growth factors and waste products that limit the cell proliferation to the surface. Conversely, in the case of big pores, it implies an increase of area for cell invasion and migration within the bulk limiting the selective transport of molecules and the initial interaction with the surface, which is crucial to mediate all subsequent events such as proliferation and differentiation [75,76]. Big pores are also responsible to reduce the mechanical strength and can drive a faster degradation in vivo before finishing the tissue construct. To overcome these drawbacks, membranes with double porosity [83,84] can be a further step forward where the macrovoids (big pores) are responsible for the invasion and proliferation of the cells, and the transport of nutrients and growth factors can be accomplished by smaller interconnected micropores resulting a higher effective surface area than a single big porous surface. Previously, we developed a polysulfone (PSU) membrane with double porosity level for the culture of C3A human hepatoma cell line. Although the membrane supported the viability and functionality of the cells for 9 days of culture, the hydrophobic properties of the PSU and non-degradable character limited the cell adhesion and migration representing a drawback for their use in tissue engineering application [83]. Our strategy here is to develop biopolymeric membranes with double porosity through the modified liquid induced phase inversion process by using track-etched. Chitosan and polycaprolactone are two prominent biopolymers currently under study for the fabrication of tissue scaffolds. Chitosan, deliver a crucial subset of biomaterials for use as tissue engineering templates due to their bioactive functionality, biocompatibility, tunable degradation and their intrinsic structural resemblance of native tissue ECM [90,149,150]. It is highly recognised for its innate ability to promote biological recognition in combination with other synthetic biopolymers [90,91,149,150]. It is a linear polysaccharide composed of glucosamine and N-acetyl glucosamine units connected through beta (1-4)

glycosidic bonds and produced from highly abundant natural polymer chitin which not only support cell adhesion and functions, but also provide hydrophilic, non-toxic, high affinity towards proteins, antibacterial, haemostatic, fungistatic, antitumoural and anticholesterimic properties [29,151,152]. Despite many positive features, there are disadvantages linked to the naturally derived biopolymers that include weak mechanical strength in vivo condition, inconsistency in compositions and properties [32] and the inherent variability in the production and the potential, even though small, of the materials to evoke an immune response [153].

Synthetic polyester based polymers such as polycaprolactone (PCL), as matrices and templates in bioengineering present several key advantages relative to naturally derived polymers, offering attractive options for the control of shape, architecture and chemistry to generate potential alternatives that mimic ECM systems with control of biomaterial functions [11,17,154,155]. Another important property of synthetic polymers, such as tensile strength, dynamic modulus and the degradation rate, can be easily tailored for target applications by altering the synthetic/natural proportions in combination with natural polymers. Due to its exceptional qualities, such as its biocompatibility, low immunogenicity, hydrolysis under physiological conditions, and FDA approval for clinical use, PCL is a potential candidate among them which can provide sufficient biocompatibility and biodegradability without producing any toxic side product [155,156]. However, when it used alone, sometimes it lag behind of biofunctional group, compromising not only the cell-matrix interaction but also a slower degradation and eventually higher retention in physiological condition, triggering a probable risk of inflammation [157].

Certainly, a harmonious combination of synthetic/natural biopolymer ratios could be a leading strategy in scaffold design, which not only reduce the limitations of a single component but also provide a greater level of control over the overall material properties for cell guidance and biocompatibility [158–160]. Membranes must have an architecture that must host cells at high density and ensure an adequate transport of nutrients and metabolites. To achieve this goal, membranes should have a macrovoids to accommodate cells, and a macroporosity for diffusion of nutrients. These requirements are essential for cell nutrition, proliferation and invasion inside the bulk for tissue vascularization and formation of new tissues. Here for the first time we report about the design and application of a 3D double porous

membrane scaffold of PCL-CHT prepared by modified liquid induced phase inversion technique for the culture of hMSCs. Considering that the hMSCs proliferation and differentiation strongly depend on environmental cues such as oxygen and nutrient availability, pore size, mechanical property, surface morphology and more notably the administration of soluble factors [79,145], our strategy was to develop membranes with macrovoids (20-110 μm) which are open towards the surface for hMSCs proliferation and invasion, and interconnected microporous (1-5 μm) to transfer essential nutrients, growth factors and cell catabolites. Membranes were characterised in order to evaluate the structural, mechanical and physico-chemical properties before their use in contact with cells. In particular, we investigated the efficacy of the double porous membranes to promote adhesion, proliferation and invasion of hMSCs as well as the metabolic oxygen requirements.

3.3 Materials and methods

3.3.1 Membrane fabrication with 3D double porosity

The membranes were prepared using a modified liquid induced phase inversion technique using formic acid/ acetic acid as solvent and NaOH as non-solvent as stated in section [2.4.1](#). Briefly, poly (ϵ -caprolactone) (MW 80 KDa, CAPATM 6800, Perstorp Holding AB, Sweden) and CHT (MW 190-310 KDa, 75-85 % degree of de-acetylation, Sigma-Aldrich), with a ratio 100/0 (15 wt.%), 90/10 (14 wt.%), 80/20 (14 wt.%) and 70/30 (10 wt.%) (w/w %) were dissolved in FA/AA (w/w %) mixture and then the polymer solution was casted on a glass plate by a gardener knife in order to achieve a thickness around 250 μm at room temperature. Then the track-etched, a polyethylene terephthalate (PET) isoporous membrane (Sterlitech, USA) with pore diameter 10 μm , was rinsed by the solvent, slowly wiped to remove excess solvent, and gently applied on the casted polymer solution. The glass plate was then slowly immersed inside the non-solvent bath containing NaOH aqueous solution at room temperature.

After formation of the membrane when it was turned opaque and detached from the glass plate, the track-etched membrane was removed gently and the newly formed membrane was washed several times in pure water. Then, the membrane was stored in ultrapure water in 4 $^{\circ}\text{C}$ temperature. The surface where the macrovoids were open towards the non-solvent are denoted as top surface and the other surface, which was facing the glass plate, denoted as the bottom surface.

3.3.2 Membrane characterization

After the preparation, the double porous membranes were characterised in order to determine their morphological, physico-chemical and mechanical property.

The surface morphology and cross section were analyzed by scanning electron microscopy (SEM, Quanta 200F, FEI, USA). Diameter of the macrovoids and macropore size distribution were evaluated by ImageJ software on the SEM images. The pore size of the passing pores were determined by Capillary Flow Porometer (CFP 1500 AEXL, Porous Materials Inc., PMI, Ithaca, New York, USA).

The membrane surface wettability was assessed by water contact angle measurements and the sessile drop method, using CAM 200 contact angle meter (KSV Instruments, Helsinki, Finland).

The mechanical properties were determined by Zwick/Roell Z2.5 tensile testing machine (Germany), by applying a pre-load of 0.05 MPa at constant 4 mm/min elongation rate. Tensile strength (N/mm²), Young's modulus E (N/mm²) and elongation at break ϵ (%) were determined at room temperature on ten different samples (1x5 cm) from each batch, considering the different cross-section thickness, in dry and wet conditions. Wet samples were analysed after an incubation of 6 hours in PBS buffer. Real-time longitudinal deformation measurements were obtained and analysed by testXpert[®] testing software.

The membrane biodegradation was evaluated by enzymatic incubation in two different solutions of Lipase from *Aspergillus oryzae* (0.12 U/ml) and human Lysozyme (1300 U/ml), respectively, in PBS buffer and 0.5 mg/ml NaN₃, to emulate the enzymatic activities of human serum. Before the incubation, three different samples (2x1.5 cm) from each batch were dried in vacuum oven at 37° C for 72 hours and then their initial weight (w_i) precisely measured. Then the samples were immersed in 1ml of enzymatic solutions that were freshly changed every seven days. At predetermined time intervals, the samples were washed with copious distilled water, dried in vacuum oven at 37 °C for 72 hours, and their final weight (w_f) precisely measured. The weight loss index (W_{loss} %) was determined by the following equation:

$$(W_{loss} \%) = [(W_i - W_f) / (W_i)] \times 100 \quad (1)$$

3.3.3 Cell Culture

Human bone marrow Mesenchymal Stem Cells (hMSCs) StemPro™ BM (Thermo Fisher Scientific) were used for cell culture on the double porous membranes. Before the cell seeding, the membrane scaffolds were sterilized by incubation in ethanol for 2 hours, extensive washes in sterile water, and UV-irradiation for 4 hours. Then they were conditioned for 2 hours with culture medium constituted by MesenPRO RS™ (Thermo Fisher Scientific) supplemented with 2mM glutamine, 1% gentamycin sulphate/amphotericin-B, and 2% serum. hMSCs were seeded at P:6 on the membrane scaffolds at 3.5×10^3 cell/cm² density, and incubated at 37° C in a 5% CO₂/20% O₂ atmosphere (v/v) with 95% relative humidity. Culture medium was changed every 48 hours, and cells maintained up to 21 days.

3.3.3.1 Effective surface area (ESA %) for cell viability

We determine the effective surface area (ESA %) on the SEM images of the scaffolds by imageJ analysis. Where we calculate the total area of the macrovoids on a unit surface and subtract it from the total unit surface area as follows:

$$\text{Effective surface area (ESA \%)} = \left(\frac{\text{Total unit surface area} - \text{Total area of the macrovoids on that surface}}{\text{Total unit surface area}} \right) \times 100 \quad (2)$$

3.3.3.2 Cell morphology by SEM analysis

hMSCs after 7 and 21 days of culture on double porous membrane scaffolds were examined by SEM (SEM, Quanta 200F, FEI, USA) after proper fixation and dehydration. Samples were gently washed with PBS buffer, and then incubated for 30 minute in 3% glutaraldehyde and 1% formaldehyde mixture. Successively, they were fixed for 30 minutes in 1% OsO₄, and progressively dehydrated in ethanol solutions.

3.3.3.3 Cell morphology by CLSM

Confocal Laser Scanning Microscopy (CLSM, Fluoview FV300, Olympus Italia) was used to investigate the cell morphology of hMSCs after 7 and 21 days of culture on the double porous membranes, after proper immunostaining of specific markers. Cell samples were gently washed with PBS buffer, and fixed with 4% paraformaldehyde solution for 30 minutes, and with acetone for 5 minutes. Successively they were permeabilized in 0.5% Triton-X100, and saturated with 5% donkey normal serum. In order to visualize the cell distribution on the double porous membranes, the cytoskeleton protein vimentin and cell surface antigen CD90 were stained. Vimentin was stained by using a rabbit polyclonal anti-human vimentin (Santa Cruz Biotechnology, Santa Cruz, CA), and a CyTM2-conjugated AffiniPure donkey anti-rabbit IgG (Jackson ImmunoResearch Europe Ltd., Cambridge, UK); CD90 was marked by using a mouse monoclonal anti-human CD90 (eBioscience, San Diego, CA), and a CyTM3-conjugated AffiniPure donkey anti-mouse IgG (Jackson ImmunoResearch Europe Ltd., Cambridge, UK). Primary antibodies were incubated overnight at 4° C, the secondary ones for 2 hours at room temperature. Counterstaining of nuclei was performed with 0.2 µg/ml of 4',6-diamidin-2 phenyl indole (DAPI) (Molecular Probes Inc., Eugene, OR) for 30 min. Finally, the samples were washed with PBS, mounted in slide with coverslip, and visualised with CLSM.

The presence of hMSCs inside the macrovoids of the double porous membranes and the change of cell morphology from the surface towards the bulk of the membrane scaffolds was monitored with scan depth determination by CLSM in the z-scan mode (step size: 0.5 µm) (Fluoview 5.0 software, Olympus Corporation).

3.3.3.4 Cell Proliferation

Cell proliferation was assessed by the 3-(4,5-dimethylthiazol-2-yl)-2,5 diphenyl tetrazolium bromide (MTT) assay. After 7, 14 and 21 days of culture on the different double porous membranes, hMSCs were incubated in 5 mg/ml of MTT solution for 4 hours at 37° C. The yellow tetrazolium MTT salt was reduced by the mitochondrial dehydrogenase in living cells to purple formazan crystals. This precipitate was extracted by using 1 ml per sample of a lysis solution constituted of 10% sodium dodecyl sulphate,

0.6% acetic acid in DMSO, in mild stirring for 30 min at 37° C. Then formazan product was quantified by spectrophotometry at 570 nm wavelength.

3.3.3.5 Oxygen uptake rate (OUR) measurements

The Oxygen uptake rate (OUR) of hMSCs cultured on the different double porous membrane scaffolds was continuously monitored up to 21 days by the pre-calibrated sensor dish reader (SDR; OxoDish®-DW, PreSens Precision Sensing GmbH), a high-throughput, 24-channel reader for non-invasive detection of O₂ in special multi-dishes. O₂ detecting sensors, placed at the bottom of each well, and containing a luminescent dye, were excited every 5 minutes by the SDR placed below the multi-dish. The luminescence lifetime was read out noninvasively through the transparent bottom, and the dissolved oxygen detected with a resolution of ± 0.4% O₂ at 20.9% O₂, and a response time <30 sec. Tests were done in the 24 well special multi-dishes in which were placed the different samples with cells and samples without cells as controls.

3.3.4 Statistical analysis

All tests were performed in triplicate and reported as mean ± standard deviation. Statistical significance of collected data was determined according to ANOVA followed by Bonferroni *t*-test (*p* < 0.05).

3.4 Results

3.4.1 Membrane properties

The developed membrane scaffolds displayed different morphological, physico-chemical, mechanical and biodegradation properties (**Table 1**). SEM images revealed on the top surface macrovoids that are interconnected with a highly porous macropore spongy network (**Fig. 1**). Macrovoids with mean size of 13±4 μm were found on PCL double porous membrane. The increase of CHT concentration in the polymeric blend increased gradually the mean diameter of macrovoids at the active surface to values of 15±5 μm, 21±11 μm and 35±25 μm for PCL/CHT 90/10, PCL/CHT 80/20 and PCL/CHT 70/30, respectively (**Fig. 2, Table 1**). The cross section of the membranes revealed inside the bulk macrovoids with bigger volume and mean diameters of 22±3 μm, 34±10 μm, 27±13 μm and 46±4 μm for PCL/CHT 100/0, PCL/CHT 90/10, PCL/CHT 80/20 and PCL/CHT 70/30, respectively. Interconnected micropores in the range of 1-5 μm were visible for all the developed membranes and size distribution become wider

with the increase of CHT concentration in the blended membranes. Smallest pores of 0.015 μm , 0.034 μm , 0.026 μm and 1.55 μm were measured for PCL/CHT 100/0, PCL/CHT 90/10, PCL/CHT 80/20 and

Table. 1. Morphological, physico-chemical and mechanical properties of the PCL/CHT double porous membranes.

	100/0	90/10	80/20	70/30
Polymer wt (%)	15	14	14	10
Macrovoids diameter (μm)	13 \pm 4 (surface) 22 \pm 3 (bulk)	15 \pm 5 (surface) 34 \pm 10 (bulk)	21 \pm 11 (surface) 27 \pm 13 (bulk)	35 \pm 25 (surface) 46 \pm 4 (bulk)
Mean Flow Pore Diameter (μm)	0.0222	0.0693	0.0496	1.551
Effective Surface Area (%)	88 \pm 1	84 \pm 1	74 \pm 2	69 \pm 2
Porosity (%)	39	46	48	55
Thickness (μm)	45 \pm 0.9	50 \pm 1	60 \pm 0.4	55 \pm 0.6
Tensile modulus E (N/mm²)	140.9 \pm 14.1 (dry) 131.6 \pm 2.2 (wet)	114.6 \pm 4.8 (dry) 58.5 \pm 4.1 (wet)	72.8 \pm 6.5 (dry) 29.5 \pm 0.8 (wet)	111.9 \pm 4.6 (dry) 10.1 \pm 2.7 (wet)
Ultimate tensile strenght Rm (N/mm²)	8.3 \pm 0.7 (dry) 8.1 \pm 0.2 (wet)	3.7 \pm 0.4 (dry) 2.5 \pm 0.3 (wet)	2.4 \pm 0.2 (dry) 1.3 \pm 0.1(wet)	2.1 \pm 0.2 (dry) 0.5 \pm 0.2 (wet)
Elongation at break ϵ (%)	127.6 \pm 50 (dry) 146.9 \pm 68.4 (wet)	13.1 \pm 2.2 (dry) 17.6 \pm 8.8 (wet)	6.9 \pm 0.8 (dry) 15.8 \pm 5.1 (wet)	2.1 \pm 0.4 (dry) 9.1 \pm 1.2 (wet)
WCA (°)	66.5 \pm 1	88.1 \pm 5	110.4 \pm 2	111.1 \pm 3

PCL/CHT 70/30, respectively. Consistently the surface porosity was also depending on the ratio of CHT reaching values of 55% for PCL/CHT 70/30 membranes. Depending upon the mean macrovoids size and their density on the surface area, we calculated the effective surface area (ESA %) to understand the physico-chemical, degradation properties and cell viability on the scaffolds. We found the ESA were 88 \pm 1 %, 84 \pm 1 %, 74 \pm 2 % and 69 \pm 2 % for PCL, PCL/CHT 90/10, PCL/CHT 80/20 and PCL/CHT 70/30 respectively.

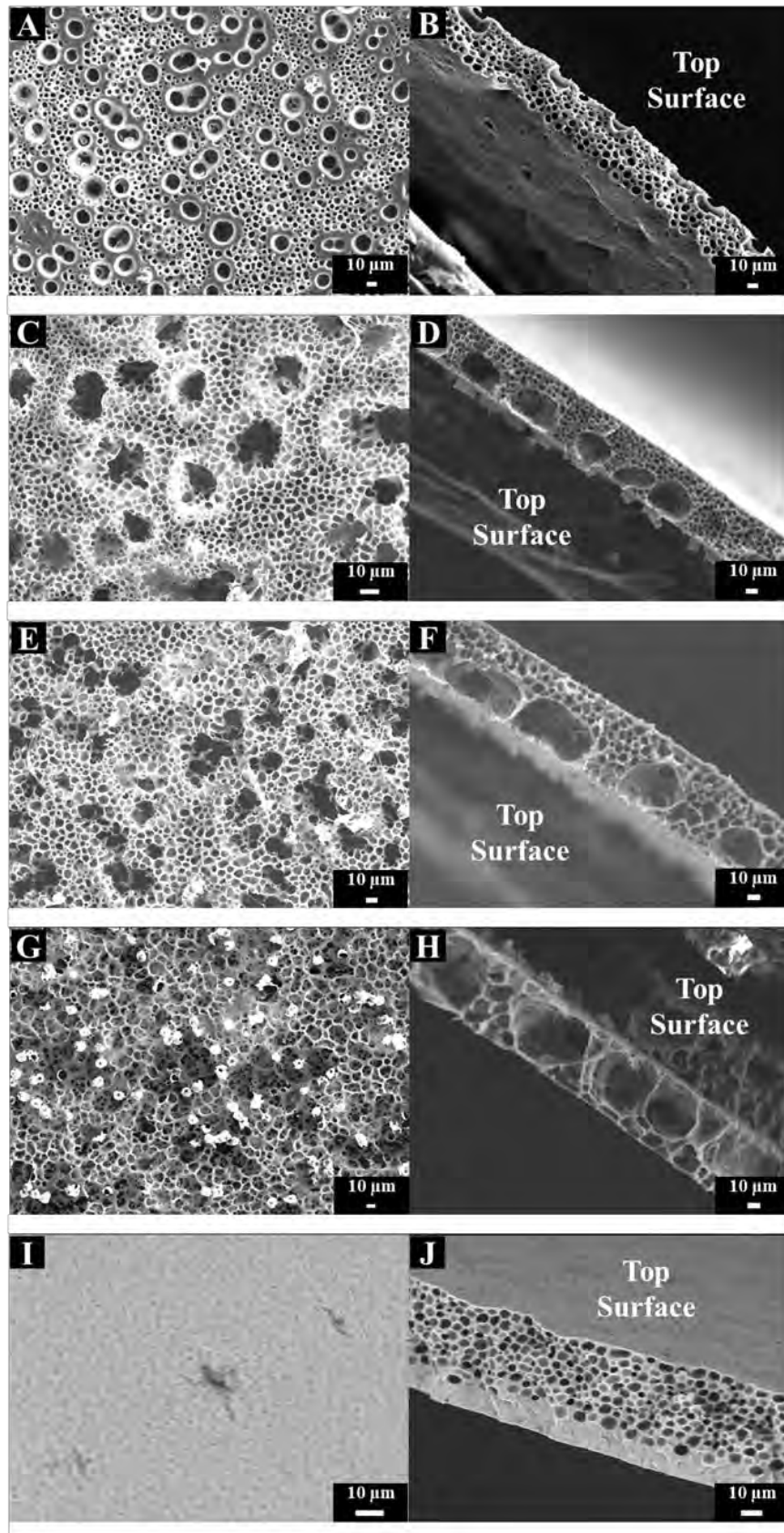


Fig. 1. SEM images: top surface (A, C, E, G, I) and cross sections (B, D, F, H, J) of PCL/CHT double porous membranes 100/0 (A, B), 90/10 (C, D), 80/20 (E, F), 70/30 (G, H) made by using the track-etched, and PCL/CHT 90/10 with single porosity (I, J), made without the track-etched.

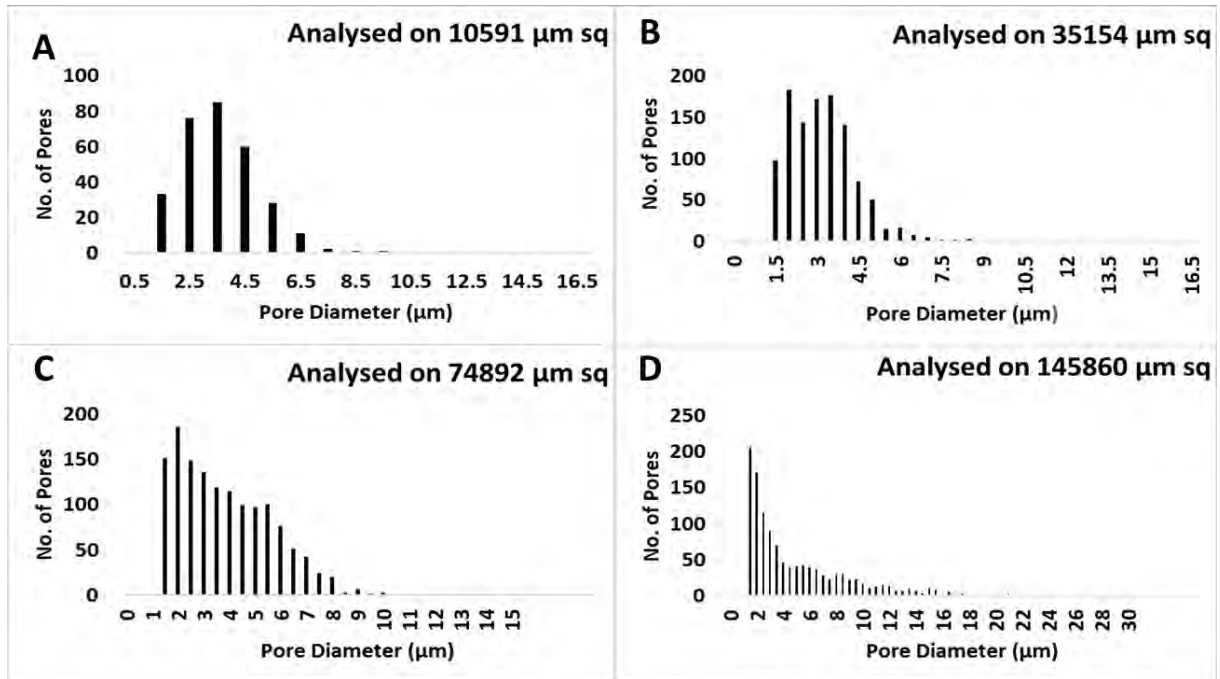


Fig. 2. Small pore size distribution on the top surface of PCL/CHT membranes 100/0 (A), 90/10 (B), 80/20 (C) and 70/30 (D). All data were analysed on SEM images by imageJ software.

The mechanical properties of the membranes were evaluated in dry and in wet conditions by measuring the tensile modulus E , the ultimate tensile strength and the elongation at break (**Table 1**). PCL double porous membranes displayed stable elastic properties in both dry and wet conditions, as evidenced by the moderate tensile modulus E (140.9 ± 14.1 and 131.6 N/mm² in dry and wet conditions, respectively) in combination with elongation at break higher than 100 %. The increase of CHT wt% in the blended double porous membranes caused a gradual decrease of the tensile modulus with respect to the pure PCL ones, reaching low values of the ultimate tensile strength and the elongation at break on the blended membrane of PCL-CHT 70/30, as a result of the gain of more rigid and fragile properties. Passing from the dry to the wet conditions, the tensile modulus and the ultimate tensile strength decreased, and the elongation at break increased (**Table 1**). PCL double porous membrane displayed a water contact angle of 66.5° . A significant increase of water contact angle was observed increasing CHT wt% in the blended double porous membranes (**Table 1**).

The biodegradable properties of the membranes were investigated by using separately lipase and lysozyme solutions at concentrations similar to human serum. The weight loss of all membranes

increased with time as shown in **Fig. 3**. As expected, the degradation of membranes augmented with the decrease of PCL concentration giving rise the highest percentage of weight loss with the PCL/CHT 70/30 membranes. The membrane weight loss in lipase solution was quite fast and higher than that of lysozyme solution. After 10 days of incubation in lipase the PCL/CHT 70/30 membrane was completely degraded on the contrary only 8% of weight loss was measured in lysozyme solution.

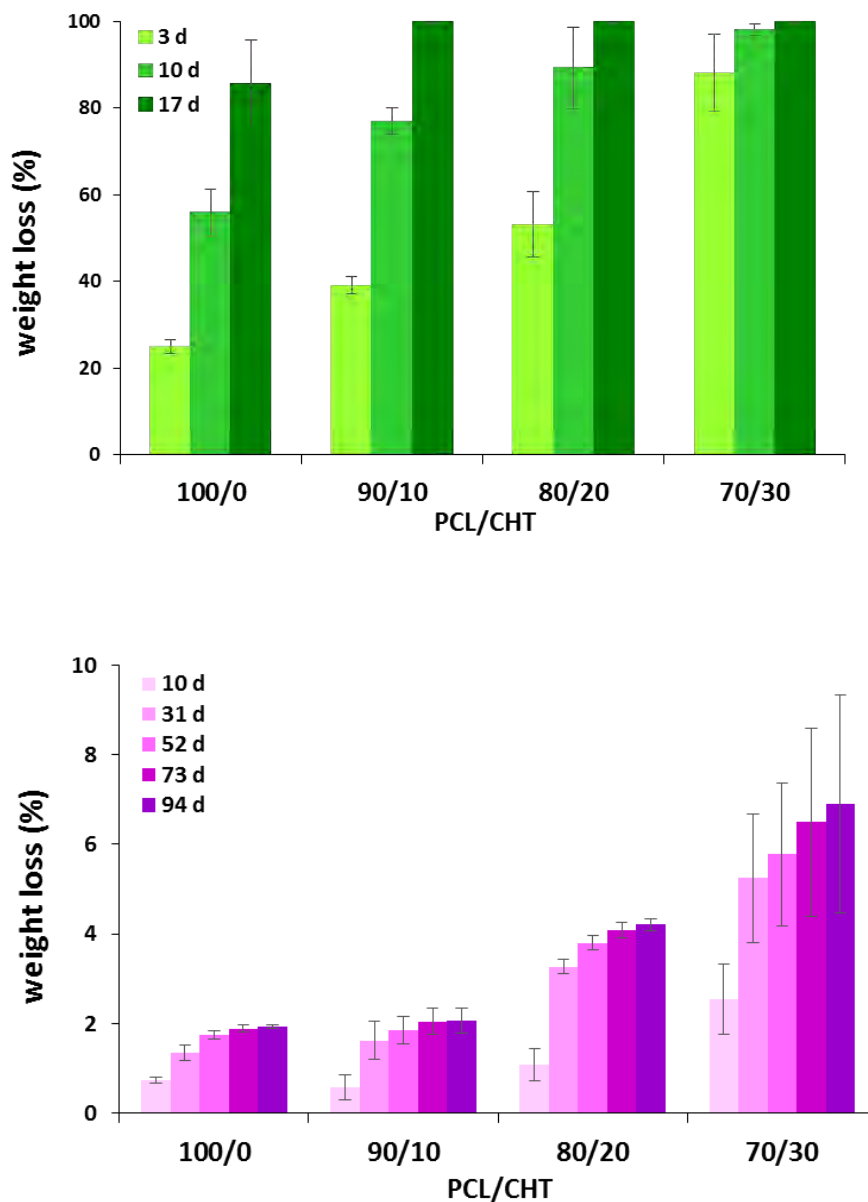


Fig. 3. Weight loss (%) of PCL/CHT double porous membranes with different time interval (days) by enzymatic degradation in presence of Lipase (*Aspergillus oryzae* with 0.112 U/ml) (A) and Lysozyme (0.013 mg/ml) (B).

3.3. Proliferation and invasion of hMSCs in the double porous scaffolds

The capability of the developed membranes to promote the adhesion and proliferation of mesenchymal stem cells was evaluated in the culture time. Cells adhered over the membrane surfaces and appeared flattened with elongated filopodia as highlighted by SEM's images (**Fig. 4**). During the culture time they proliferated covering the membrane surfaces as shown in **Fig. 5**. In case of PCL/CHT 100/0 and PCL/CHT 90/10 the hMSCs exhibited a spindle-like morphology. On the other two blends, by increasing the concentration of CHT, the cells became less flattened, showing a spherical-like morphology, and remaining confined into the macrovoids of the double porous membranes.

The expression of specific markers of hMSCs cultured on the different membranes is shown in **Fig. 6**. Cells on all investigated membranes were positive for the cytoskeleton protein vimentin (in green) and cell surface protein CD90 (in red). In agreements with the SEM's observations, here we also found that on PCL/CHT 100/0 and PCL/CHT 90/10 cells were only on the surface taking a spindle like morphology. On the contrary, on PCL/CHT 80/20 and PCL/CHT 70/30, cells were on the surface by taking a spherical or star like morphology and also inside the macrovoids by acquiring a globular morphology due to the limited area available for cell adhesion and organization.

For a deeper understanding of the cell invasion phenomenon inside the scaffolds, we accrued the CLSM images in Z-scanning mode from surface towards the bulk (**Fig. 7**). From the images it can clearly observed that for PCL/CHT 100/0 and PCL/CHT 90/10 cells were adhered on the surface and no cells were found in the bulk. On the other hand, on PCL/CHT 80/20 and PCL/CHT 70/30 cells were distributed on both surface and bulk acquiring a completely globular morphology in the bulk. Moreover, the cell invasion in the latter two scaffolds increased from 7 days to 21 days.

The cell experiment results demonstrated a remarkable effect of macrovoids size and surface morphology on cell proliferation and behaviour. **Fig. 8** report the quantitative cell viability by MTT assay after 7 days 14 days and 21 days. Here we found that PCL/CHT 100/0 was showing a highest rate of cell viability after 7 days and 14 days, which is even higher than the control represented by

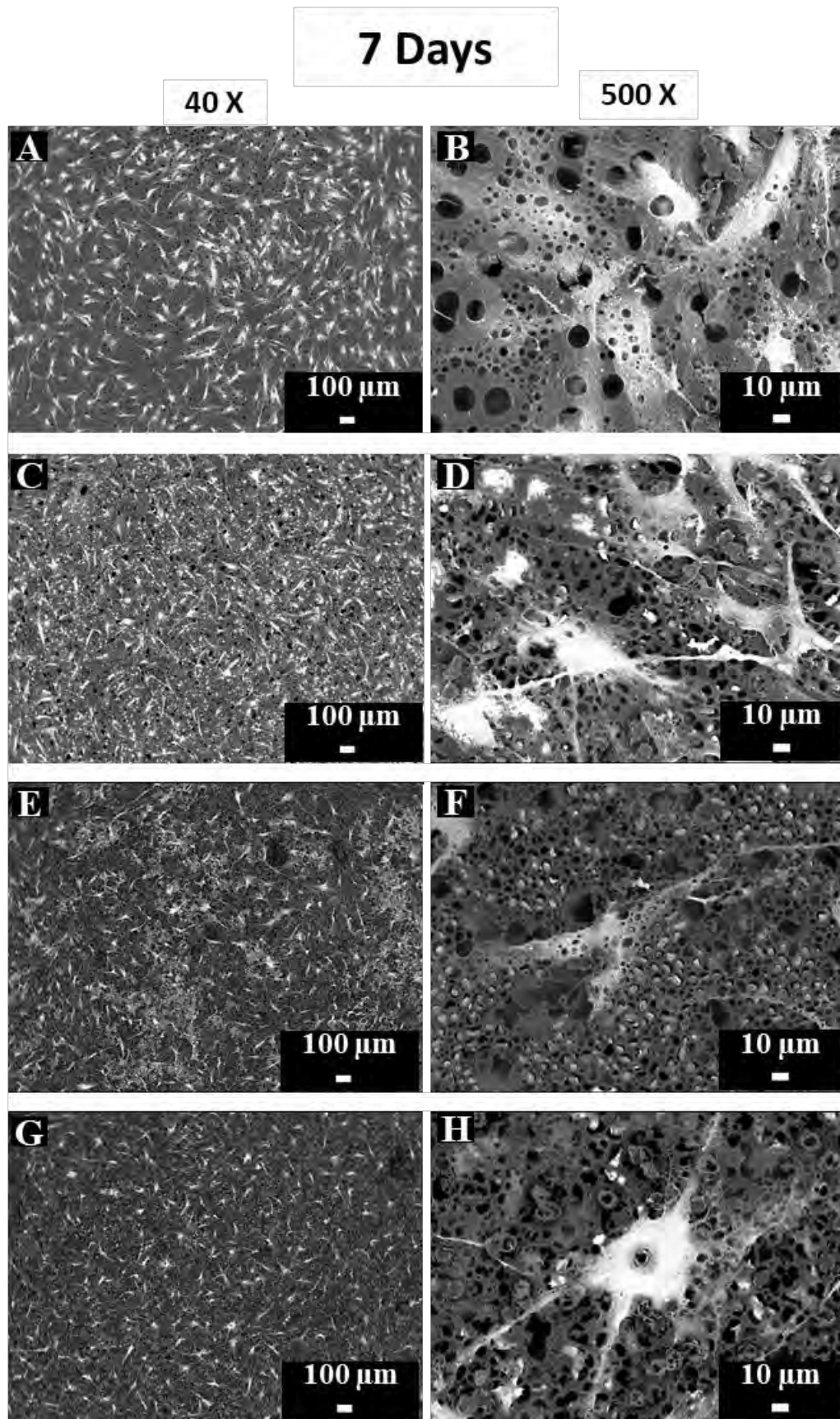


Fig. 4. SEM micrographs of hMSCs after 7 days of culture on PCL/CHT double porous membranes 100/0 (A, B), 90/10 (C, D) 80/20 (E, F), and 70/30 (G, H) at different magnification.

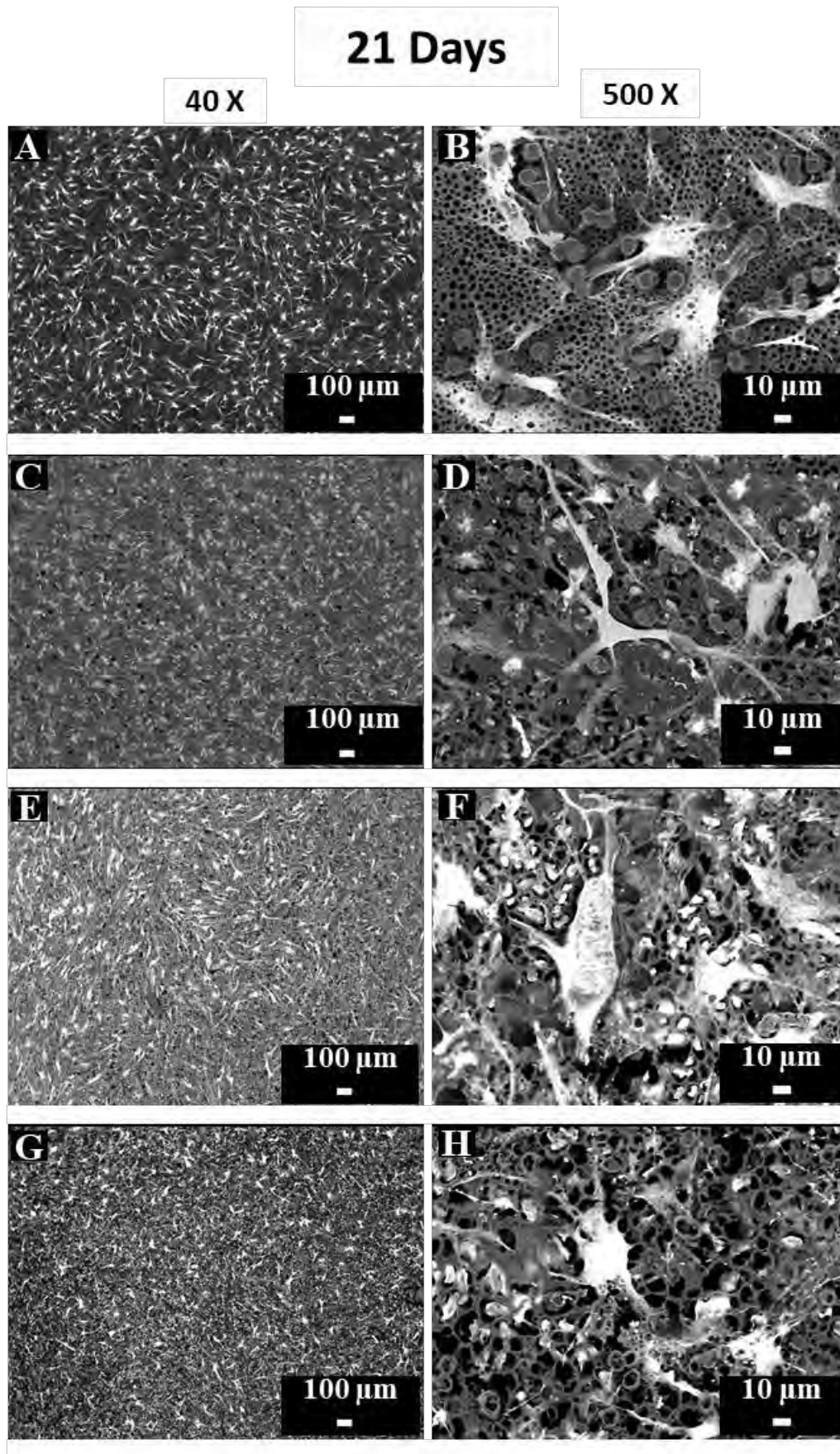


Fig. 5. SEM micrographs of hMSCs after 21 days of culture on PCL/CHT double porous membranes 100/0 (A, B), 90/10 (C, D) 80/20 (E, F), and 70/30 (G, H) at different magnification.

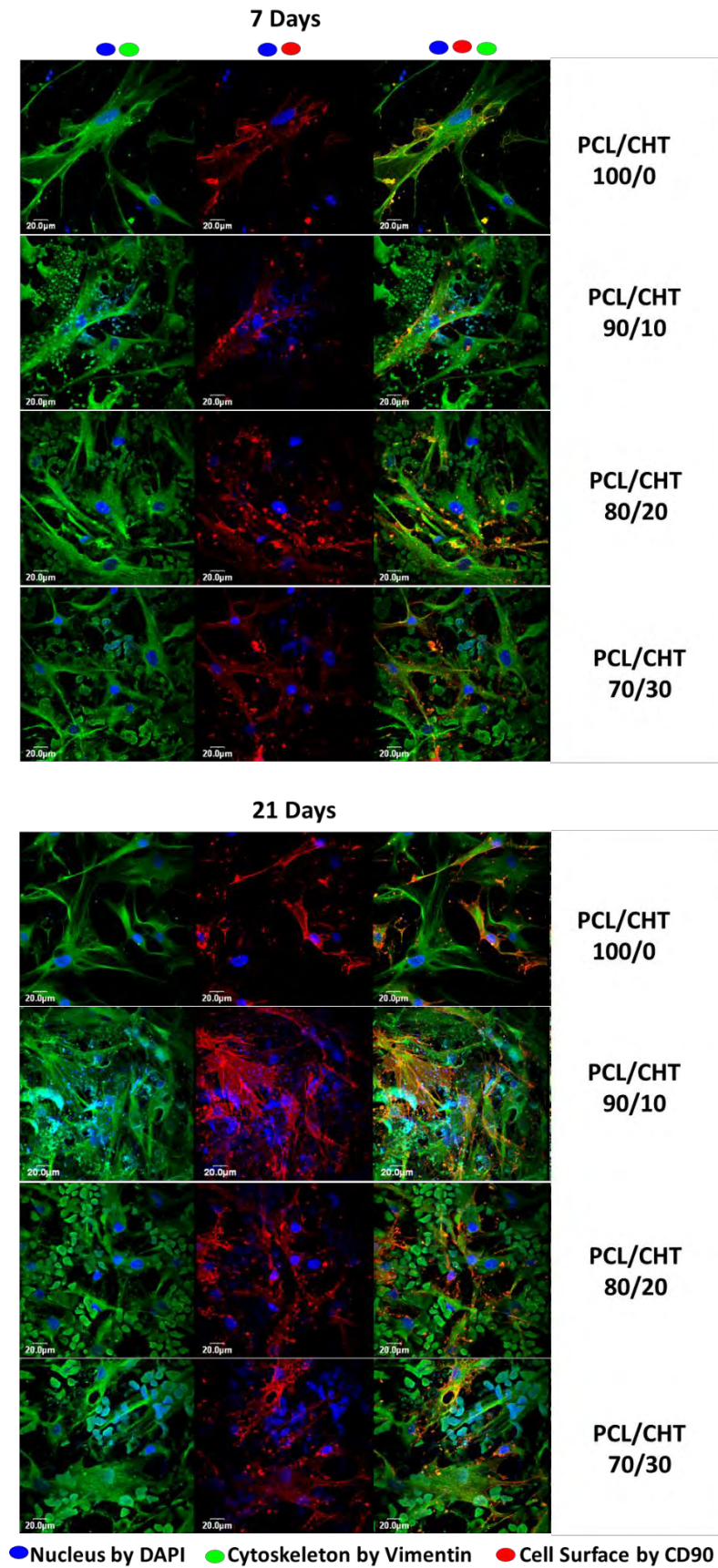


Fig. 6. CLSM images of hMSCs after 7 (a) and 21 (b) days of culture on PCL/CHT double porous membranes. Cells were stained for vimentin (green), CD90 (red) and nuclei (blue).

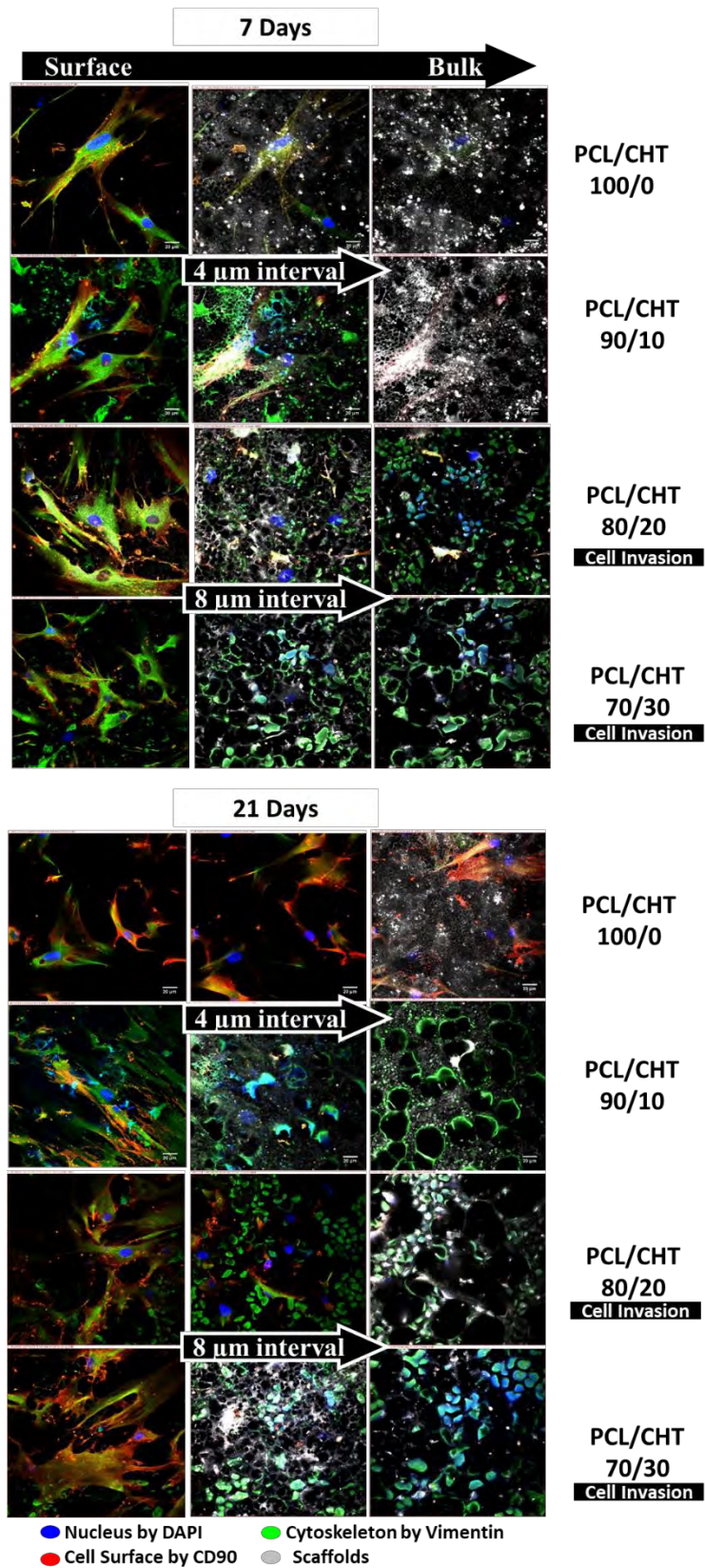


Fig. 7 Distribution in the z-axis of vimentin (green), CD90 (red), nuclei (blue) and scaffolds (grey) after 7 (a) and 21 (b) days of hMSC culture on PCL/CHT double porous membranes. CLSM images were collected at 4 μm and 8 μm intervals to create a stack in the Z axis.

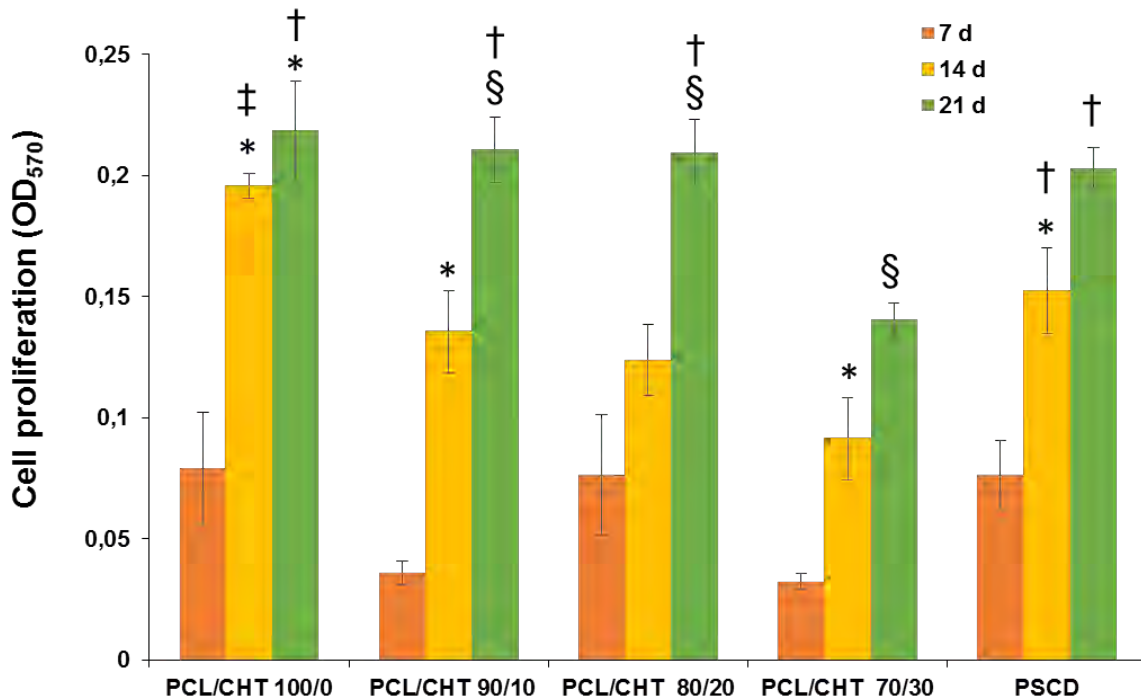


Fig. 8. Cell proliferation of hMSCs at different days of culture on PCL/CHT double porous membranes 100/0, 90/10, 80/20, 70/30, and on polystyrene culture dishes (PSCD) as reference substrate. Data statistically significant according to ANOVA followed by Bonferroni t ' test ($p < 0.05$): (*) vs 7 days, (§) vs 7 and 14 days, on the same substrate; (†) vs PCL/CHT 70/30, (‡) vs all, at the same day of culture.

polystyrene culture dishes (PSCD). The cell viability slightly decreased by increasing the CHT wt.% after 14 days which is related to the increase of mean macrovoid size and surface porosity. However, after 21 days all the membranes (except PCL/CHT 70/30) displayed almost similar cell viability, which was even little higher than the control. This result suggest that the scaffolds created a permissive microenvironment for hMSCs and after 21 days they reached to confluence.

Considering that oxygen deficiency is a serious problem for the cells and inadequate oxygenation induces a decrease of cell metabolism we evaluated the cellular oxygen uptake rate (OUR) with time until 21 days in **Fig. 9** Cells on PCL/CHT 100/0 displayed the highest OUR rate followed by PCL/CHT 90/10, which was also increasing with time compared to the other two blended membranes. For PCL/CHT 80/20 and PCL/CHT 70/30 the oxygen consumption remained significantly high throughout

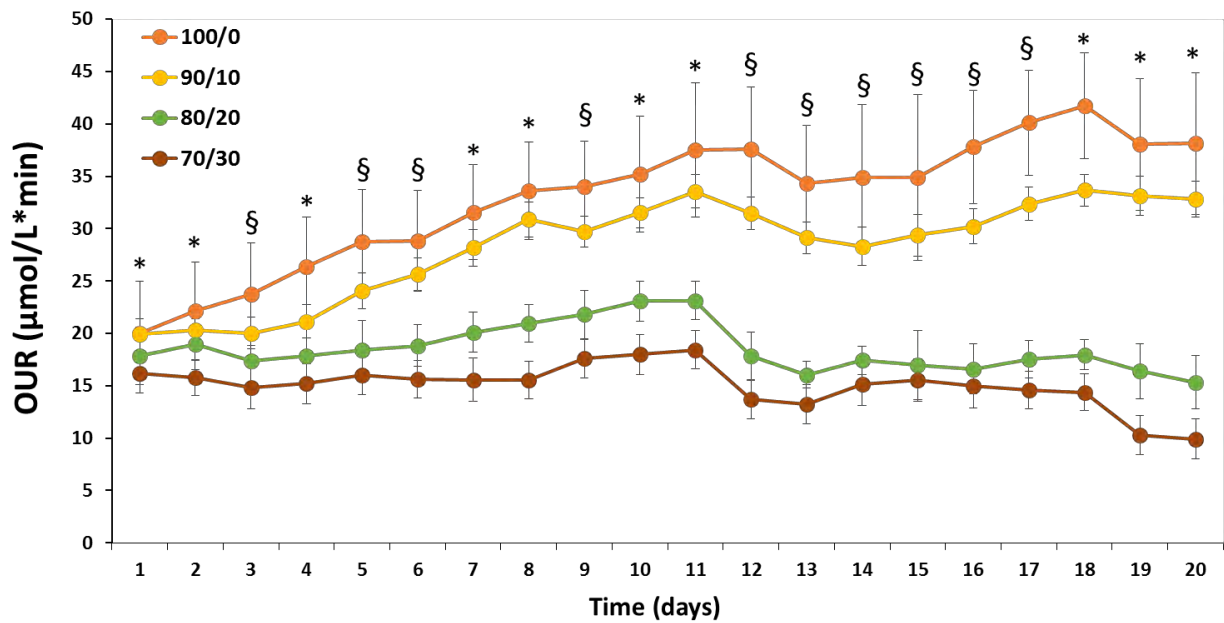


Fig. 9. Oxygen uptake rate ($\mu\text{mol/L}\cdot\text{min}$) in the time of hMSCs cultured on PCL/CHT double porous membranes 100/0, 90/10, 80/20, 70/30. Data statistically significant according to ANOVA followed by Bonferroni t ' test ($p < 0.05$): (*) 100/0 vs all, 90/10 vs 80/20 and 70/30, and 80/20 vs 70/30; (§) 100/0 vs all, 90/10 vs 80/20 and 70/30.

experiment. The OUR values of the different blends after 20 days reached values of $38 \pm 7 \mu\text{mol/L min}$, $33 \pm 2 \mu\text{mol/L min}$, $15 \pm 3 \mu\text{mol/L min}$ and $10 \pm 2 \mu\text{mol/L min}$ for PCL/CHT 100/0, PCL/CHT 90/10, PCL/CHT 80/20 and PCL/CHT 70/30 respectively.

These results are in agreement with the proliferation data and SEMs images that clearly indicate a very high density of the hMSCs on the surface of PCL/CHT 100/0 followed by PCL/CHT 90/10 and no significant dead cell fragments were observed.

3.5 Discussion

The design of bioactive membrane scaffolds mimicking the physiologic environment during tissue formation is an important challenge in biomaterials and tissue engineering research. Herein, we developed double porous polymeric membrane scaffolds that recapitulate the 3D microenvironment able to ensure the long-term stem cell viability and metabolism. A distinguishing feature of the scaffolds is the combination of macrovoids that allow the cell entrapment with a small interconnected microporous network that ensures the selective transfer of oxygen and nutrients and the removal of cell catabolites and products. By changing the CHT wt.%, not only the chemical properties of the scaffolds were modified, but also their structural and morphological properties like macrovoid size, effective surface area (ESA)%, surface porosity% and surface regularity. Finally, all these properties have a direct and strong influence on the morpho-functional behaviour of hMSCs. The formation of the unique double porous morphology by modified non-solvent induced phase inversion can be clarified by understanding the ternary phase diagram triangle (with three component; polymer, solvent and non-solvent) which is conveniently used to analyse the thermodynamics of membrane formation process [143]. In particular, the track-etched membrane placement on the casted solution induced the double porosity during solvent exchange via phase inversion. The pores of the track-etched membrane restricted the non-solvent entry inside the casted polymer, leading to the formation of macrovoids [83,84,142,144]. Changing the polymer composition by adding and increasing the CHT wt.%, the viscosity of the casted solution increased due to the higher molecular weight, cyclic chain [5] and affinity of the natural polymer towards the solvents [152]. That let the non-solvent disable the secondary interaction before initiating the solvent exchange via acid-base neutralization, leading to a delayed diffusion followed by solidification of the polymer chain inside the nascent macrovoids. In the meantime, more non-solvent invasion through the pores of the track-etched membrane, before reaching the solidification, was responsible of a further macrovoid expansion inside the bulk, resulting in bigger macropores eventually made up by coalescence of two nascent neighbouring macrovoids (see section [2.6.2](#)). Consequently, the size of the macrovoids in the bulk was higher than that of the opening ones on the surface [142,144]. On the contrary, without

the use of the commercial track-etched membrane, the phase inversion was quite homogeneous leading to a single porous morphology without macrovoids, followed by dense skin formation [83,143].

The polymer composition influenced mechanical, physico-chemical (See section 2.5) and degradation properties as well the surface morphology and macrovoid size of the developed double porous membrane scaffolds. The mechanical behaviour of PCL was modified by introducing and increasing CHT wt.%, that leads to an increase of the macrovoids size and the porosity, and consequently to a decrease of the polymers bulk density in unit volume. Moreover, the decrease of the tensile strength and Young's modulus is probably due to the thermodynamic miscibility of the two polymers that affects their interfacial adhesion in contact surface and the yield strength of the matrix [161]. Additionally, in wet condition the mechanical properties dramatically change for double porous blended membranes owing to an incorporation of water molecules inside the bulk, through the macrovoids and among the polymeric chains. Water incorporation re-established new hydrogen bonds with the CHT polar functional groups, by disabling the previous polymer-polymer interaction to some extent and leading polymers to slide over another under stress. This phenomenon was previously observed also in CHT and CHT-PCL nanoporous membranes, and is responsible for reduced tensile strength and Young's modulus, and for increased elongation at break [86], in wet condition and increasing CHT wt.%. The microstructures present on the membrane surface deeply affected their wettability. Indeed, the increase of surface macrovoids size and mean diameter of macropores influenced the contact angles according to a path irrespective of the chemical hydrophilicity increase that it is expected to be gained increasing the percentage of CHT [162]. This behaviour is due to the reduction of the solid-liquid interfacial contact in the case of micro- and nano-structured surfaces [163,164].

The enzymatic degradation in lipase and lysozyme with human serum concentration simulated the physiological conditions that would be responsible for enzymatic dissolution of the different double porous membrane scaffolds in vivo as artificial patch [126,128,129]. The percentage of membrane scaffolds dissolution with the two enzymes was evaluated separately, in order to explore their exclusive degradation evolution within the time, considering their different mechanisms of degradation/action. Lipase degrades mainly PCL and polymeric chains that consists of lipid or ester-like chemical structure;

lysozyme mainly CHT consisting of N-acetyl/deacetyl glucosamine linkages via oxidative-reductive chain scission, with a degradation kinetic that is inversely related to the deacetylation degree of CHT [128,131,133]. The slower degradation rate in lysozyme is mainly due to the different degradation mechanism and the lower CHT wt.% in all blends [99]. Nevertheless, the overall enzymatic degradation phenomenon was further governed by the easy accessibility of the enzymatic solution throughout the bulk, which could be beneficial for a scaffold with fast cell growth, needing the scaffold to degrade faster while being replaced by cell-secreted ECM [5]. In particular, the lower lipase degradation of PCL/CHT 100/0 could be due to a higher difficulty of water-soluble enzyme to enter inside the hydrophobic and crystalline PCL chains. Decreasing the concentration of PCL wt.% the degradation increases as CHT chains decrease the crystallinity of PCL chains and also increase the hydrophilicity of the overall blends, creating more space for the enzymatic solution to invade inside the PCL chains [128,129,165,166]. Moreover, increasing the macrovoids size and porosity the enzyme can have a direct access inside the bulk leading to weight loss of 95% of PCL/CHT 70/30 within 10 days. On the other hand, the degradation kinetics by using lysozyme was quite straightforward despite the increase of macrovoids, porosity and hydrophilicity.

The physico-chemical and structural properties of the developed double porous membrane scaffolds, ultimately strongly affected the cellular morpho-functional behaviour and invasion in the polymeric scaffold bulks. We investigated the cell-material interactions and the cell invasion phenomenon inside the macrovoids by culturing hMSCs on the double porous membrane scaffolds. Kang et. al. [167] reported the adipogenesis of murine embryonic stem cells in 3D PCL fibre scaffolds with pore size 6-70 μm . They concluded that the cell viability is determined not only by soluble biomolecules such as growth factors, but also by geometry and morphological structure of the scaffolds in which cells are grown, which in turn modulate the cell shape and cytoskeletal tension thus regulating cell functions. In our case, by increasing CHT wt.% the surface macrovoids size increased leading to a decrease of ESA%. Higher effective surface area (ESA) of the membrane scaffolds affect the cell adhesion on the surface without to influence the cell invasion into the bulk. The increase of CHT wt.% leads to an increase of small pore size distribution and surface porosity that are responsible of higher irregular surface. On

PCL/CHT 100/0 and PCL/CHT 90/10 membrane scaffolds, lower surface porosity% conferred more regular and smoother surfaces, that in addition to higher ESA, enhanced the adhesion of hMSCs. Indeed, on these double porous membrane scaffolds cells adhered on the surface exhibiting their typical spindle-like morphology, as observed in SEM and CLSM images. On the other hand, on PCL/CHT 80/20 and PCL/CHT 70/30 some cells adhered on the surface with wide spreading, others were entrapped inside the macrovoids exhibiting a spherical morphology especially on PCL/CHT 70/30. The cell invasion in the double porous membrane scaffolds reduced the cell proliferation, that was gradually lower on scaffolds with gradual increase of CHT wt.%, as particularly evidenced after 14 days of culture. The proliferation rate increased in the time consistently to the scaffold degradation, reaching maximum values after 21 days on all membrane scaffolds with except for hMSCs cultured on PCL/CHT 70/30 for which the chemical nature of the membrane scaffolds probably plays the pivotal role with respect to the morphological and degradation properties. Indeed, the higher CHT wt.% conferred higher glycosaminoglycan-like ECM matrix that enhanced the cellular spreading of hMSCs, which is inversely related to cell functions and proliferation potential, as it has been already demonstrated for different cells cultured on CHT and CHT-PCL blended membranes [86].

These experimental results suggested that the topographical and physico-chemical properties of the membranes considerably influence hMSCs attachment and proliferation offering cues to the cells.

A further evidence is provided by the OUR data that show a similar trend of cell proliferation by increasing CHT wt.%. In particular cellular oxygen consumption is a good indicator of cell viability and functions since the oxygen is one of the most important nutrients for cells and play an important role in regulating MSC function [168]. The OUR of the hMSCs cultured on the blends increased in the time and with the PCL wt.% coherently with cell adhesion and proliferation data highlighting an enhanced cellular metabolic activity. These results are in agreement with previous findings reported by O'Brien et al. [75] that shown a strong correlation between the scaffold specific surface area and cell attachment indicating that cell attachment and viability are primarily influenced by scaffold specific surface area of pore sizes for MC3T3 cells. An important effect of pore size on the adhesion of osteoblasts in the early

adhesion process has been shown by Murphy et al. [76] suggesting that scaffold specific surface area plays an important role on initial cell adhesion.

Overall the results demonstrated that the scaffolds were able to create a permissive environment for hMSC adhesion and invasion affecting their morphology, proliferation and metabolism without to lose the stem cell phenotype. The macrovoids enabled the cell invasion into the membrane and the microporosity ensured an adequate diffusive mass transfer of nutrients and metabolites, which are essential for the long-term maintenance of cell viability and functions.

3.6 Conclusions

In this study, we developed new double porous (macrovoids interconnected with microporous) membrane scaffolds which consists of variable macrovoids and effective surface area for hMSCs culture for specific concern. Polycaprolactone/Chitosan blend (ratios 100:0, 90:10, 80:20, 70:30) membranes with different properties were prepared by modified liquid induced phase inversion. We found a linear change in scaffolds macrovoids size, effective surface area (ESA)% and surface irregularity by changing the Polycaprolactone/Chitosan blend, which has a direct impact on their physico-chemical and degradation properties. By increasing the Chitosan wt.%, we found that the mechanical property decreased and the surface static contact angle was strikingly increasing which was influenced by the surface irregularity. We investigated the enzymatic degradation by Lipase (*Aspergillus oryzae*) and Lysozyme separately, by maintaining their human serum concentration.

Topographical structure of the membrane scaffolds significantly influences hMSC behavior. We found an increase of cell viability and proliferation by decreasing macrovoid size and by increasing the effective surface area, which is available for specific integrin-ligand interaction. PCL/CHT 100/0 and PCL/CHT 90/10 showed the highest cell viability where the cells proliferated only on the surface with high spreading and exhibiting their typical spindle like morphology. On PCL/CHT 80/20 and PCL/CHT 70/30 some cells adhered on the surface with wide spreading, others were entrapped and proliferated inside the macrovoids with a globular morphology. These results provided evidence that double porous membrane scaffolds offer niches for hMSCs attachment and proliferation. In particular, PCL/CHT

80/20 membrane is characterised by suitable topographical, mechanical and degradation properties that promote high cell viability in long-term cell culture where the cells can invade and proliferate inside the macrovoids, opening a new possibility for 3D tissue engineering. However, future studies are necessary in order to establish the effect of macrovoid size on the viability and metabolic functions of specific cell type. The trend, decreasing cell viability by increasing macrovoid size would not be expected to continue if the macrovoid size cross a certain point where larger macrovoids can provide higher integrin-ligand interaction, outweighing the consequence of effective surface area. This kind of scaffolds can be highly applicable as a 'selective cell co-culture' where according to the cellular dimension, cells which are smaller than the macrovoids dimension can invade and proliferate inside the macrovoids and the bigger cells will be on the surface, eliminating the competition of proliferation between them. Moreover, the use of various cell types would be beneficial to understand and model cell behaviour with 3D structure and could be very useful in future to design potential bioactive scaffolds for specific tissue culture with the cells of interests.

Chapter 4: Fabrication of tuneable micro-structured flat sheet membrane in Organ-on-chip to monitor trans-endothelial hydraulic resistance

4.1 Summary of the chapter

Tissue engineering is an interdisciplinary field, where scientists from different backgrounds collaborate to address the challenge of replacing damaged tissues and organs via the *in vitro* fabrication of functional and transplantable biological structures. Because the development and optimization of tissue engineering strategies relies on the complex interaction of cells, materials and the physical-chemical tissue microenvironment, there is a need for experimental models that allow controlled studies of these aspects. Organs-on-chips have recently emerged as *in vitro* models that capture the complexity of human tissues in a controlled manner, while including functional read-outs related to human organ physiology. Organs-on-chips consist of multiple microfluidic cell culture compartments, which are interfaced by porous membranes or hydrogels in which human cells can be cultured, thereby providing a controlled culture environment that resembles the microenvironment of a certain organ including mechanical, biochemical and geometrical aspects. Because organs-on-chips provide both a well-controlled microenvironment and functional read-outs, they provide a unique opportunity to incorporate, evaluate and optimize materials for tissue engineering. Here we introduce a polymeric blend membrane with a three-dimensional double-porous morphology prepared from a poly(ϵ -caprolactone)/chitosan blends (PCL/CHT) by a modified liquid induced phase inversion technique. The membranes have different physico-chemical, microstructural and morphological properties depending on different PCL/CHT ratios. Big surface pores (macrovoids) provide a suitable microenvironment for the incorporation of cells or growth factors, while an interconnected small porous (macroporous) network allows transfer of essential nutrients, diffusion of oxygen and removal of waste. Human umbilical vein endothelial cells (HUVECs) were seeded on the blend membranes embedded inside an organ-on-chip device. The cellular hydraulic resistance was evaluated by perfusing culture medium at a realistic trans-endothelial pressure of 20 cmH₂O or 2 kPa at 37 °C after one day and three days post-seeding. By introducing and increasing CHT weight-percentage, the resistance of the cellular barrier after three days was significantly improved.

The high tuneability over the membrane physico-chemical and architectural characteristics might potentially allow studies of cell-matrix interaction, cell-transportation and barrier function for optimization of vascular scaffolds using organs-on-chips.

4.2 Introduction

Tissue engineering is expected to have a significant impact on the prevention and treatment of disease, for example through regenerative medicine and the development of artificial organs. The successful engineering of biomaterials or engineered tissues that can be applied in a clinical setting relies on the control and optimization of many physico-chemical parameters, as well as a deep understanding of cell and tissue physiology. To evaluate specific tissue engineered constructs, current *in vitro* methods are relatively limited, because they either rely on simple monolayer cell culture systems (e.g. for the evaluation of cytotoxicity) or on low-throughput bioreactor systems. Because of this, there is a clear need of more advanced *in vitro* models that can be used as tools to evaluate and optimize tissue engineered constructs. Organs-on-chips (OOCs) are considered to better predict cellular responses and potentially mimic a particular organ by introducing organ-like features such as fluid flow and mechanical stress with the corresponding cellular preferences [88,169,170].

Generally, OOCs consist of polydimethylsiloxane (PDMS)-based structures fabricated using soft lithography [171–173] defining microfluidic channels that are often interfaced through a porous membrane material in which human cells can be cultured. Depending on the application, the membrane normally requires micron-sized pores to allow cellular interaction, while thickness and biocompatibility need to closely mimic biological conditions of the human body [174,175]. Moreover, a straightforward way to resemble the microenvironment of a certain organ by tuning mechanical, biochemical and geometrical aspects [89] leads to better predictions [66]. Like all *in vitro* models, OOCs hold the potential of parallelization and high-throughput screening with very limited resources.

In spite of the substantial progress in OOC technologies in general (better sensors, pumps and microfluidics) with a rapidly expanding library of OOCs of different organs, the progress in the development of suitable porous, polymeric membranes is very slow. To date a handful of polymeric

membrane such as polycarbonate (PC) and Polyethylene terephthalate (PET), are applied for interfacial support in OOCs. These membranes are generally prepared by track-etching and are mainly obtained from commercial Transwell inserts [87,176–182] or filter membranes [87,183–188]. Depending on the application, they often provide only a basic, non-physiological cell culture microenvironment due to their limited biocompatible, structural and mechanical properties. All the material properties of the membrane like surface microstructure [189–192], roughness [193–196], hydrophilicity [197,198], mechanical strength [198,199], and porosity [71,74,75,80,145,200] have a significant effect on the cellular adhesion and biocompatibility.

Although polymers have been developed to serve as porous membranes for OOCs and microfluidic systems, only a few, e.g. parylene [201], SU8 [202], PDMS [65,169,203], polylactic acid (PLA) [204], polycaprolactone (PCL) [205] have been reported using electrospinning [206] and conventional microfabrication techniques, such as photolithography and dry etching [207,208]. Despite the good features achieved by the aforementioned materials and the proof-of-concepts developed using those materials, most of them are less suitable for OOCs with specific microstructural requirements and lack controlled three-dimensional cellular adhesion.

Recently, blends of synthetic and natural polymers such as polycaprolactone (PCL) and chitosan (CHT) were found to exhibit excellent abilities to match the needs of their specific target tissues via proper tuning of their properties [19,38,92,108,161]. CHT is widely recognized for its natural ability to promote bioactive functionality, tunable degradation, and structural resemblance of native tissue extra cellular matrix (ECM) [90,149,209]. CHT is produced from the highly abundant natural polymer chitin that supports cell adhesion and function, while also providing properties like being hydrophilic, non-toxic, having a high affinity for proteins, as well as being antibacterial, haemostatic, fungistatic, antitumoural and anticholesterimic [29,151,152]. PCL is approved by the Food and Drug Administration (FDA) for clinical use, and is also very suitable for tissue engineering applications [84,91,155–157] by providing attractive options for the control of morphology, architecture, dynamic modulus and degradation rate to generate potential alternatives via tuning the synthetic/natural ratio in combination with natural polymers [19,38,92,108,161].

Here we report a straightforward way to integrate a three-dimensional porous membrane, intended for use in vascular tissue engineering, in an OOC system. We demonstrate that endothelial cells can be embedded in the scaffolds, and their functionality can be probed by measuring their hydraulic resistance with a microfluidic assay. Our study highlights the great potential of applying of OOCs as models for *in vitro* testing in the field of tissue engineering.

4.3 Materials and Methods:

4.3.1 Materials

Poly (ϵ - caprolactone) with MW 80 KDa (CAPA™ 6800, CAS Number 24980-41-4) was obtained from Perstorp Holding AB, Sweden. Chitosan with medium MW (190 KDa – 310 KDa) and 75 – 85 % degree of de-acetylation (CAS Number 9012-76-4) was purchased from Sigma- Aldrich. Polyethylene Terephthalate (PET) isoporous (track-etched) membranes with pore diameter 10 μ m were commercially obtained from Sterlitech, USA. In the thesis is so called track-etched membrane. Solvents (AcOH, HCOOH), NaOH was obtained from Sigma-Aldrich. Polydimethylsiloxane (PDMS) was purchased from Dow Corning as a kit containing base and curing agent (Sylgard 184, Midland, MI, USA). Toluene was purchased from Merck, Germany. Polyester membrane (8 μ m pore size and 10 μ m thickness) was obtained from GVS Filter Technology. Fluorescent dye (Dextran 4 KDa) was purchased from sigma. Human umbilical vesicle endothelial cells (HUVECs) were obtained from Lonza and the corresponding culture media (EGM-2: basal media with supplement mix, CC-22011) was obtained from Promocell. Collagen-1 (rat-tail), VE-Cadherin goat anti human (Primary antibody) was purchased from Santa Cruz. phosphate buffered saline (PBS), Trypsin-EDTA, Formaldehyde, donkey anti-goat IgG Alexa Fluor 546 (VE-Cadherin secondary antibody), 6-Diamidino-2-Phenylindole (DAPI), and Alexa Fluor 488 Phalloidin were purchased from ThermoFisher. Triton X-100, bovine serum albumin (BSA) were purchased from Sigma Aldrich.

4.3.2 Methods

4.3.2.1 Double porous membrane scaffolds fabrication

The membranes were prepared using a modified liquid induced phase inversion technique using formic acid/ acetic acid as solvent and NaOH as non-solvent as stated in section [2.4.1](#).

4.3.2.2 Membrane characterization by SEM

After preparation of the membrane with double porosity, the repeatability of the membrane surface and bulk morphology was checked by scanning electron microscopy (JEOL 5600LV) (**Fig. 2.**). Diameter of the macrovoids and small porous size distribution were evaluated by ImageJ software on the SEM images.

4.3.2.3 Organ-on-chip fabrication

The chip fabrication was reported in the previous publication from our group [87,210]. Briefly, PDMS base agent and curing agent were mixed in a 10:1 wt% ratio. After degassing, this mixture was poured onto an SU-8 patterned silicon wafer and cured for 4 h at 60 °C. Then the PDMS with channel imprints was cut into top and bottom parts, and four inlets were punched (by 0.5 mm diameter biopsy puncher) into the top parts containing the top channel. Dust was removed using Scotch tape (3M). To assemble the two PDMS parts with an embedded membrane, a PDMS/toluene glue at 5:3 wt ratio [211,212] was prepared which ensures complete leakage-free bonding of the two PDMS parts. At first, the glue was spin-coated onto a glass coverslip (1500 rpm for 60 s, ramped at 1000 rpm s⁻¹; Spin 150, Polos, the Netherlands) and a thin layer was transferred to both PDMS halves using an ink roller. Then the double-porous membrane of 2 mm × 2 mm was cut and placed in the centre of the bottom half. The top part was aligned and gently placed on the bottom part without applying pressure, after which the chips were baked for 3 days at 30 °C (baking was done in low temperature to avoid unwanted damage of the membrane microstructure by melting). The chip design and assembled chip are shown in 3D (by Blender v2.78) in **Fig. 1. (A)**.

After fabrication and before the flux experiments, the chips were verified in order to check good sealing between the membranes and the PDMS or for any unwanted leakages. To do that, a fluorescent dye

(4 kDa dextran Alexa 488, 1 mg/ml in PBS) was pipetted inside the channel and the chips were inspected by performing fluorescence microscopy (EVOS FL, Life Technologies) for one day (Supp. Fig. 6).

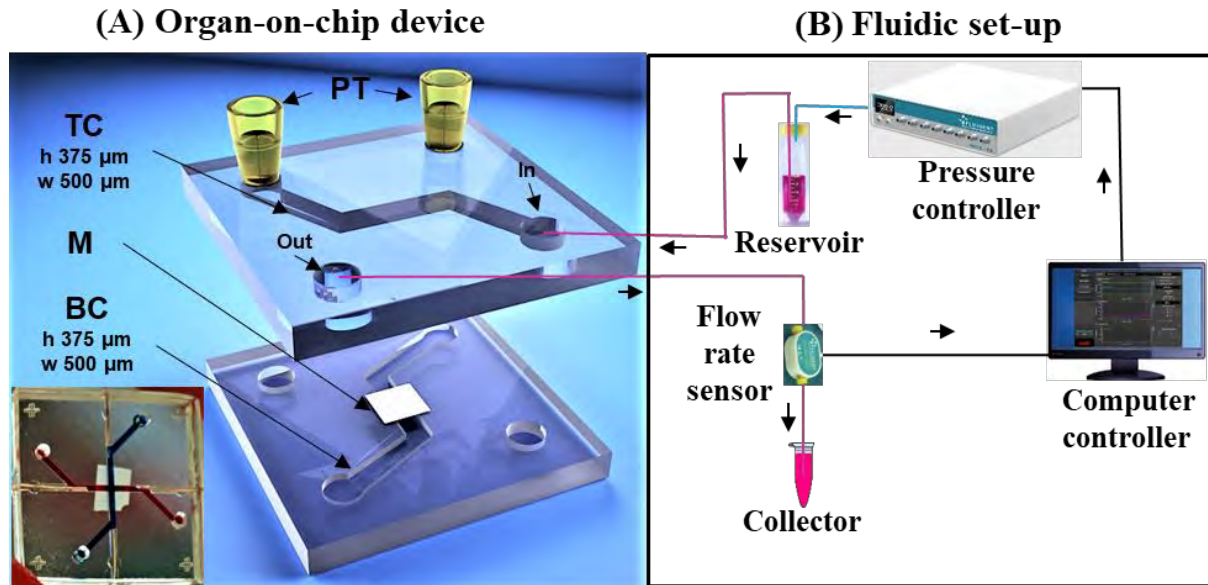


Fig. 1: (A) Organ-on-chip device (inset Picture: BIOS/Lab on a Chip, UTwente); exploded view of the PDMS chip with the top channel (TC), membrane (M), bottom channel (BC) and (PT) blocked pipette tip. The working area of the membrane suspended between two channels is $500 \mu\text{m} \times 500 \mu\text{m}$. (B) Fluidic set up; determination of volumetric flow rate by perfusion of the cell culture medium (EGM-2) through one top channel and collection of the permeate through the bottom channel to the sensor.

4.3.2.4 Hydraulic resistance measurements in different pressure by Fluigent set up

To evaluate the membrane hydraulic performance, volume flow rate of the culture medium (EGM-2) through the membrane at different pressures was conducted by a fluidic setup (Fig. 1. (B)). The fluidic setup was obtained by Fluigent pressure controller to track the flow rate in real time which consists of flow rate platform (FRP) coupled with a flow rate sensor [213]. The experiments were started from 2 kPa (approximately 20 cmH₂O which is within the range of physiological transendothelial pressures or TEP [214–216]) and continued up to 20 kPa. The experimental set up was discussed in section 2.2.5.1. The obtained flux was plotted against pressure (Fig. 3), and the hydraulic resistance of the membranes was determined (Table. 2) from the slope by equations below [85,217,218].

$$J = (Q/t)/A \quad (1)$$

$$\text{And, } J = \frac{\Delta P}{\mu \times R_{Mem}} \quad (2)$$

$$\text{Or, } R_{Mem} = \frac{\Delta P}{J \times \mu} \quad (3)$$

Where, J is Flux (m/s), (Q/t) is the volume flow rate (m³/s), A is membrane surface area (m²), μ is 6.913×10^{-4} Pa·s, the dynamic viscosity of water at 37 °C (all the flow experiments were done with EGM-2 but its viscosity is only 5% higher [214,219], while the resistance of the membrane should not be affected by this), ΔP applied pressure difference (Pa) and R_{Mem} is resistance (m⁻¹) of the membrane.

Polyester membrane (8 μ m pore size and 10 μ m thickness) [220] was also embedded inside the chip system by using the PDMS/toluene glue (which was baked in 60 °C for 4 hours) and the resistance of flow was determined as a control with the same procedure. This polyester membrane is typically used in Transwell insert systems for cell culture purposes.

To assess the membrane hydraulic performance in a high-pressure filtration system, flux of all the membranes mentioned above were also measured in an Amicon cell at room temperature with deionized water at pressure 20 kPa to 60 kPa (**Supp. Fig. 7**). The hydraulic flux and the resistance for water was determined by the above equation where the dynamic viscosity of water at 25 °C was considered as 8.9×10^{-4} Pa·s.

4.3.2.5 Flux before and after the cell seeding by Fluigent set up

The consecutive experiments were done on the same batch of chips with culture medium (EGM-2) at 2 kPa for one day and three days (**Fig. 4**). For each batch, three chips were taken.

4.3.2.5.1 Flux before cell seeding

Chips were transferred in a plastic culture dish and washed with 70% EtOH thoroughly. Then the chips were washed with sterile PBS three times to ensure removal of EtOH from inside of the channel and both the channels were filled with endothelial cell culture medium (EGM-2). One top and one bottom entrance was blocked with sealed yellow pipette tips. The other top channel inlet was connected with the reservoir (30 ml of culture medium) via Tygon tubing. The other bottom channel inlet was connected to the flow rate sensor. Before connecting with the chip, all the tubing and the sensor were filled with

culture medium. Then the flow was started at 2 kPa pressure and the flow rate was recorded after 2-3 minutes to ensure a steady-state measurement.

4.3.2.5.2 Cell seeding

After the flux measurements the channels were washed three times with sterile PBS and kept in PBS suspension for overnight at 4 °C. Then the channels were washed again with sterile PBS and filled with 0.1 mg/ml collagen I in PBS. The channels were inspected for air bubbles (any air bubbles were flushed out by Collagen I solution) and incubated for 30 minutes at 37 °C. Then the chips were taken out from the incubator and flushed with culture medium and incubated for 1 hour at 37 °C. In the meantime, HUVECs were trypsinized and collected from a confluent T175 flask. Then the chips were placed in the sterile hood and 10 µl of cell suspension (4×10^6 cells/ml or 1.5×10^5 cells/cm²) was pipetted slowly inside the top channel and inspected for any bubble formation (any bubble was flushed out by the cell suspension) and incubated in 37 °C for 2 hours. The chips were taken out from the incubator, inspected for complete attachment of the HUVECs by microscope, flushed with fresh culture medium to remove non-attached cells and incubated again. The medium in the channels was changed twice every day (morning and afternoon). Every time before putting inside the incubator, one drop of culture medium was left on top of all the inlets to prevent the channel from drying.

4.3.2.5.3 Flux after Cell seeding and staining

The chips with seeded cells were taken one by one from the incubator and the flow rate was recorded again like the previous procedure. Directly after the perfusion experiment, the chip was washed with PBS and fixed with 4% paraformaldehyde for 15 minutes. Then the channels were washed with PBS and kept in permeabilization buffer (PB; 9:1 v:v ratio of 11 mg/ml BSA with 1% Triton X-100 in PBS) at room temperature for 15 minutes to block any non-specific protein-binding sites. VE-cadherin primary antibody (1:200 in PB) was added inside the channel and incubated at room temperature for 2 hours. The channels were washed with PBS and VE-cadherin secondary antibody, Phalloidin-488 and DAPI were added together in the ratio 1:400, 1 drop/ml and 1:4000 in PB, respectively, and incubated at room temperature for 1 hour. To prevent photo-bleaching, the chips were protected from light exposure from this step onwards. Then the chips were washed with PBS thoroughly and imaged with

confocal microscopy (Zeiss LSM 510, Nikon) in 15× and 85× magnification (**Fig. 5**). The images on the membrane were taken at the intersection point of the two channels. For control, cells on the bare PDMS channel surfaces were also imaged.

4.3.2.5.4 Calculation of the hydraulic resistance of HUVECs

From the flow rate, flux was calculated from **Eq. 1** and plotted for different membranes, before cell seeding and after cell seeding (**Table. 3**). In addition, the resistance of the cellular barrier (R_{Cell}) was calculated from the difference between the total measured resistance (membrane with the cells) and the blank membrane resistance (without cells). The equation has shown below [217,218].

$$R_{cell} = R_{Tot} - R_{Mem} = \left(\frac{\Delta P}{\mu} \times J_{Tot} \right) - \left(\frac{\Delta P}{\mu} \times J_{Mem} \right) \quad (4)$$

4.3.2.5.5 Statistical analysis

All the experiments were done in triplicate (n=3) and the data are shown as mean ± standard deviation. Slope of the blank membrane (**Table.2**) was determined by using LINST equation. To find the significance of flux after cell seeding (**Fig. 4**), one-way ANOVA analysis with Bonferroni correction was done where; ****denotes $p < 0.0001$, ***denotes $0.0001 < p < 0.001$, **denotes $0.001 < p < 0.01$ and *denotes $0.01 < p < 0.05$.

4.4 Results and discussion:

4.4.1 Membrane morphological characteristics

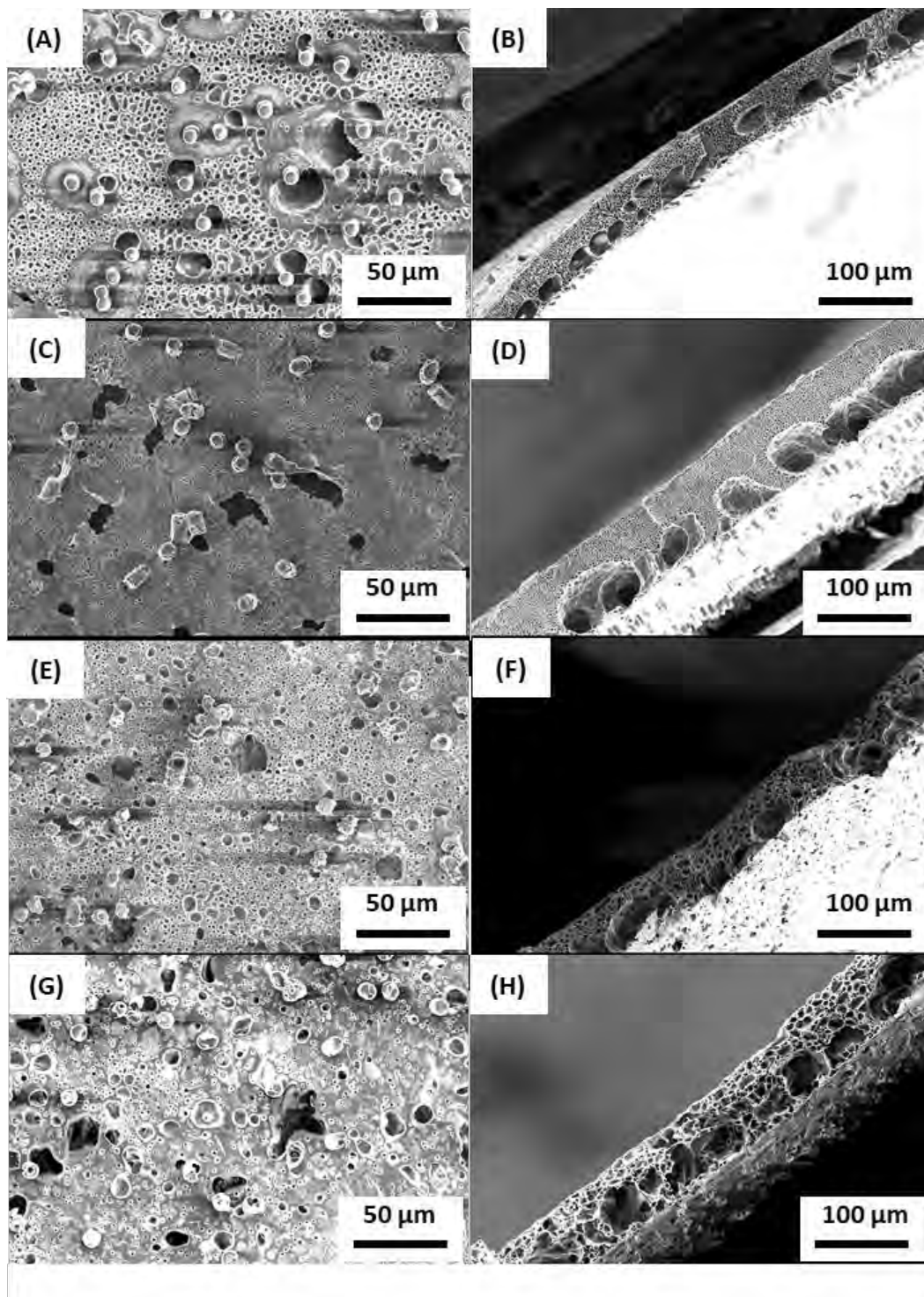


Fig. 2. SEM images of membranes on the Top surface and cross section with double porosity; (A, B) PCL/CHT 100/0, (C, D) PCL/CHT 90/10, (E, F) PCL/CHT 80/20, (G, H) PCL/CHT 70/30 respectively using track-etched membrane (10 μm). All images were taken after removing the track-etched membrane.

Table 1. Relationship between polymer blend ratio and membrane pore size.

	PCL/CHT 100/0	PCL/CHT 90/10	PCL/CHT 80/20	PCL/CHT 70/30
Surface Big Pores Dia. (μm)	21.4 \pm 5.2	14.3 \pm 4.1	15.3 \pm 3.4	15.8 \pm 5.7
Bulk Big Pores Dia. (μm)	30.6 \pm 4.9	54.4 \pm 7.6	51.9 \pm 9.2	56.1 \pm 5.5
*Surface Small Pores Dia. (μm)	2.3 \pm 1.5	0.8 \pm 0.3	1.4 \pm 0.5	1.7 \pm 0.9
Thickness (μm)	55	85	65	80

After the membrane fabrication, the top surface and the cross section characteristics were analyzed by SEM (**Fig. 2** and **Table 1**). It was found that the membrane surface that was covered by the track-etched membrane, contained many open big pores which are interconnected with the small pores network as evident from the cross section images. In case of pure PCL, surface big pores were around 21 μm in diameter and inside the bulk were around 30 μm . On the other hand, all the blend of PCL/CHT, surface big pores were around 14 – 16 μm and inside the bulk 51 – 56 μm . The size of the small pores was around 0.8 – 2 μm . Thickness of all the membranes were around 55 – 85 μm . Overall, by this modified phase inversion technique, a remarkable difference was found between the big pores and the small pores. The morphology also contained some pillars, which were almost the same dimension as the track-etched membrane pores. The amount of pillars was decreasing with increasing CHT %.

The commercial track-etched membrane upon the casted polymer solution triggered a heterogeneous solvent exchange during the solvent-nonsolvent exchange. The solvent exchange is faster where the nonsolvent has a direct contact with the solution through the pores of the track-etched membrane. By introducing and increasing the CHT wt% inside the PCL backbone, several material characteristics can be further tuned like surface pore size and morphology, mechanical property, hydrophilicity, biodegradable properties.

Nonetheless, all these characteristics have direct consequences on cellular viability and adhesion phenomena. As stated earlier, the goal of the current work was to study the suitability of these membranes in vascular tissue engineering by evaluating the adhesion of HUVECs, as well as their functionality in terms of generating hydraulic resistance.

4.4.2 Permeate flux and Hydraulic resistance of the membrane at different pressure regime

The OOC was designed in such a way that the membrane scaffolds are embedded in between two channels where the culture medium were perfused through the top channel at realistic TEP (transendothelial pressure; 2 kPa), mimicking the inner lumen properties. The other end of the top channel was blocked so the medium passes through the membrane porous network to the bottom channel. One exit of the bottom channel was also blocked such that the cell operates in dead-end filtration mode. Firstly, we tested the membrane stand-alone performance, starting from TEP up to 10 times TEP. After that we enhanced the resistance by seeding the endothelial cell and quantifying the additional hydraulic resistance induced by the cells. This kind of membrane scaffolds loaded with endothelial cells can be applied as grafts for disrupted vascular lumen and resist the leakage of fluid from inside of the lumen to outside. Due to the biodegradable porous structure, the cell will grow inside the scaffolds by replacing the scaffolds material and hence repair the disrupted lumen.

4.4.2.1 Permeate flux and Hydraulic resistance of the membranes without cells

The permeate flux of the membranes were plotted (**Fig. 3**) against pressure starting from realistic TEP (2 kPa). All the membranes showed a linear response across the entire pressure range. In the blend, by increasing CHT wt%, the flux was increasing.

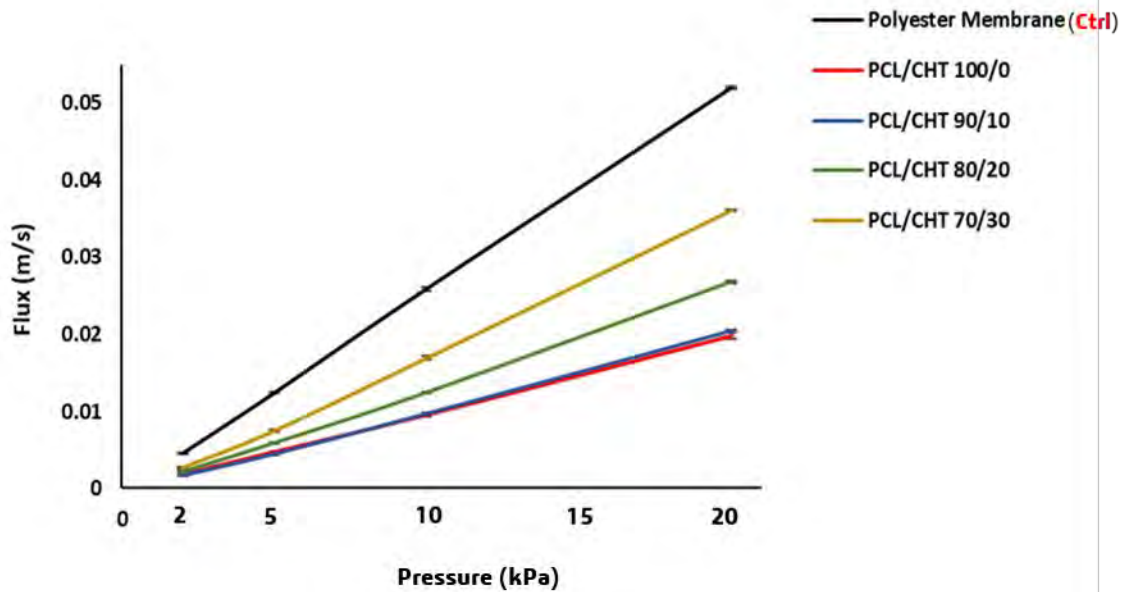


Fig. 3. Flux vs Pressure of four different membrane compare to Polyester membrane (control) measured in Organ-on-chip device by fluidic set up.

The hydraulic resistance of the membrane was obtained from the slopes in **Fig. 3** and depicted in **Table 2**.

Table 2. Resistance determined by the slop of the Flux vs Pressure graph.

	Slope of the Flux vs Press graph ($1/R_{Mem,\mu}$) $m/Pa \cdot s \times 10^{-5}$	Resistance (R) $m^{-1} \times 10^8$
Polyester membrane	0.26 ± 0.001	5.48 ± 0.06
PCL/CHT 100/0	0.1 ± 0.001	14.47 ± 0.39
PCL/CHT 90/10	0.11 ± 0.002	13.65 ± 0.25
PCL/CHT 80/20	0.14 ± 0.003	10.48 ± 0.18
PCL/CHT 70/30	0.19 ± 0.004	7.73 ± 0.19

The pristine membrane does not exhibit any membrane compressibility in the TEP range (2 – 16 kPa) [214–216,221], suggesting in the real-time the bulk microstructure of the membrane will be intact while

the cellular ingrowth should not be affected. The blend membrane has a higher resistance (or lower flux) than the control (Polyester membrane), most probably because the blend membranes have a higher hydraulic length (i.e. the membrane thickness) [222] and different pore morphology. These blend membranes have higher resistance even without the cellular attachment than the membrane like Polyester or Polycarbonate filter membrane which are typically used inside the trans wells inserts systems [214,215] or in OOC system [87,210] to assess cellular barrier. The water flux of the control (polyester membrane) in the manufacturer's protocol [220] is given as - 1000 ml/min/cm² at 10 psi pressure, corresponds to a membrane resistance of $6.25 \times 10^8 \text{ m}^{-1}$, which is very close to what we find in our OOC system. This good agreement confirms that the system allows determining the resistance reliably and that the membrane sealing was intact even up to 10 times TEP.

The flux is very important to applications of membranes in vascular biology as it dictates the amount of fluid flow that can be processed for a given time and dimension at a defined applied pressure without damaging the mechanical integrity of the membrane [223]. Particularly in our blend membrane by increasing CHT wt% the flux was increased likely due to higher hydrophilicity and improved wetting. However, regardless of different chemical property and pore morphology, the resistance of all the blend membranes were quite close to each other. Unlike the polyester membrane, the advantage of the blend microporous structure is that they consists of big pores which are not all the way through the thickness, reducing the flux while facilitate cellular adhesion and incorporation in the same time. Starting from TEP, the applied pressure range (2 - 20 kPa) was well within the range of transmembrane pressure for microfiltration membrane [224]. Copper et. al [225] evaluated the water flux of a PCL-CHT based nanofibrous membranes by electrospining. They found their membranes exhibited flux values in the same order of magnitude with our reported data in the similar pressure range. Madhavan et. al [221] reported vascular grafts made of thin, dense nanofibrous core composed of poly- ϵ -caprolactone, and a thick, porous, hydrogel sleeve composed of genipin-crosslinked collagen-chitosan. They achieved a desired flux 528 ml/cm²/min (corresponds to 0.08 m/s) at average blood pressure of 16 kPa and mentioned flux value in that range considered as ideal for immediate grafting and fast healing. They also mentioned flux value below that range does not require any preclotting before implantation, but

healing could be slower due to limited molecule transport. Whereas unlike the multilayer morphology they reported, the single layer morphology with macroporous structure like us could be an added advantage with optimum flux property and the fast healing.

4.4.2.2 Permeate flux and Hydraulic resistance of membranes with cell cultures

Flux was measured after one and three days of cell culturing and compared with the blank membranes at physiological transendothelial pressure (TEP) 2 kPa (**Fig. 4**). By introducing and increasing the CHT wt% in PCL, the %reduction of flux was depicted in the figure, where it can be found there was a significant decrease of flux took place after three days compare to one day, most likely due to added cellular resistance.

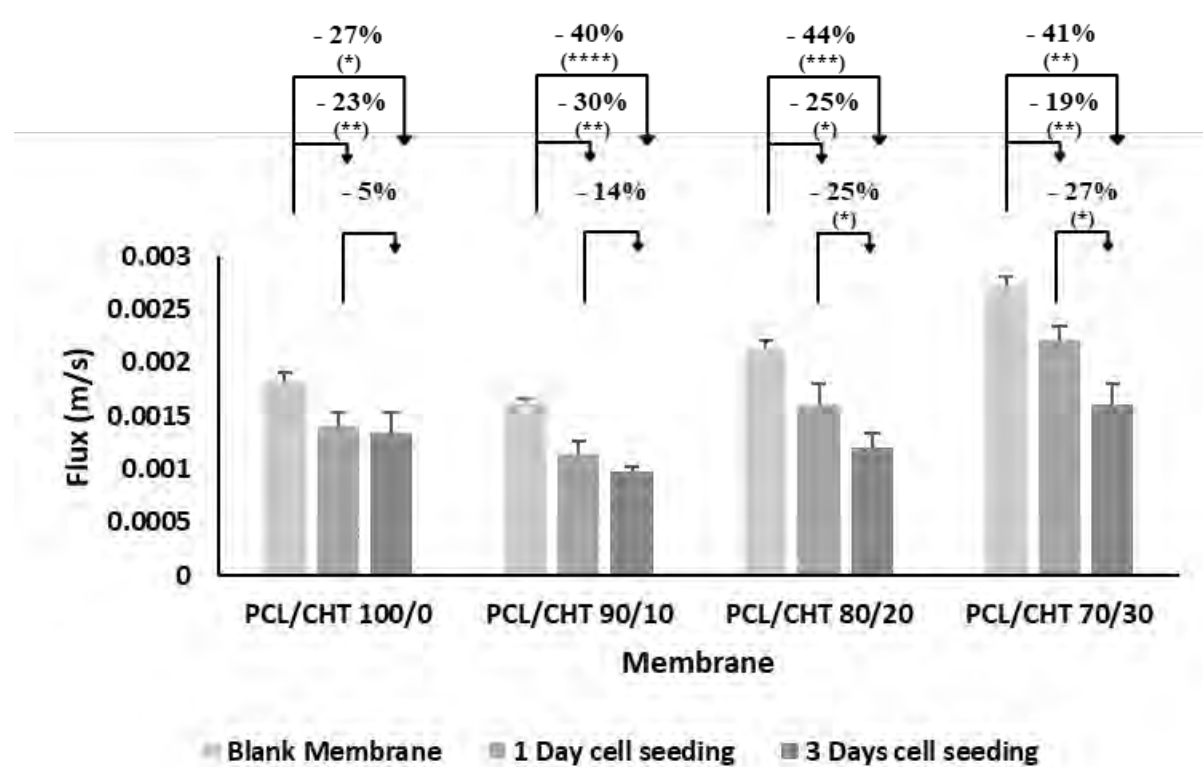


Fig. 4. Flux of four different membranes before cell seeding and after one day and three days of cell seeding. All values were measured at physiological transendothelial pressure (2 kPa). The percentages denote flux reduction compared to the individual blank membrane. (**** $p < 0.0001$, *** $0.0001 < p < 0.001$, ** $0.001 < p < 0.01$ and * $0.01 < p < 0.05$ in one-way ANOVA analysis with Bonferroni correction).

The primary point of interest of this work was to evaluate the additional hydraulic resistance induced by the HUVECs during the flux measurements. These values were derived from the mean flux after one day and three days of cell culture from **Eq. 4** and listed in **Table. 3**.

Table 3. Resistance of HUVECs cellular barrier determined by eq. 4 after 1 and 3 day.

	Resistance of HUVECs (R_{Cell}) $m^{-1} \times 10^8$	
	1 Day	3 Day
PCL/CHT 100/0	4.8	5.8
PCL/CHT 90/10	7.7	11.8
PCL/CHT 80/20	4.5	10.5
PCL/CHT 70/30	2.5	7.4

The cellular resistance (R_{Cell}) increased the total cell-membrane resistance in the OOC system. After one day, by increasing CHT wt%, the cellular resistance of the membrane scaffolds were decreasing perhaps due to enhanced flux property induced by the CHT moieties as discussed above. However, a notable increase in cellular resistance (R_{Cell}) after three days of seeding was observed presumably due to higher numbers of adherent cells and the increase is likely to be more significant by increasing CHT wt%. After three days % R_{Cell} increase compare to one day was as follows; PCL/CHT 100/0 (+20 %), PCL/CHT 90/10 (+50 %), PCL/CHT 80/20 (+130 %) and PCL/CHT 70/30 (+200 %). This could be due to combination of better morphological property or pore spacing as evident from the SEM images (**Fig. 2**) where it was observed that, by increasing CHT wt% the membrane surface has more continuous and smooth space between the pores. Casillo et al. [200] grew endothelial cells on non-porous and porous SiO_2 membranes. The porous membranes had different pore sizes and corresponding pore spacing, and they found membranes with higher pore spacing give better focal adhesion formation. In contrast, they measured cell-cell interactions in the form of tight junctions by ZO-1, which showed an opposite trend. Porosity especially with smaller pore spacing, could thus limit cell adhesion, but enhance barrier function of cells.

By increasing CHT wt%, the hydrophilicity of the membrane was also increased which could have a positive influence on protein adsorption and hence cell adhesion [193,197]. Wala et al. [198] prepared

poly(dimethyl siloxane) (PDMS) films with different hydrophilicity and reported that cell attachment, spreading and growth of 3T3 fibroblasts and HaCaT keratinocytes increased with increasing hydrophilicity of the films. Others found that moderate hydrophilicity often yields the best cell response [197,226]. Adsorption of serum proteins also showed an optimum on films with moderate hydrophilicity [197] which could be the main cause of the increased cell response.

Above all, the big pores inside the scaffold are likely to play a significant role to increase the cellular resistance. During the cell seeding the HUVECs could block the big pores as they have a globular shape of around 15-20 μm in diameter which is almost similar in dimension to the big pores on the surface of the scaffold. Chen et al. [189] showed that pore sizes similar or larger than a single cell have significant influence on clusters formation by involving multiple cells together.

4.4.3 Microscopic observation of cells on the membrane

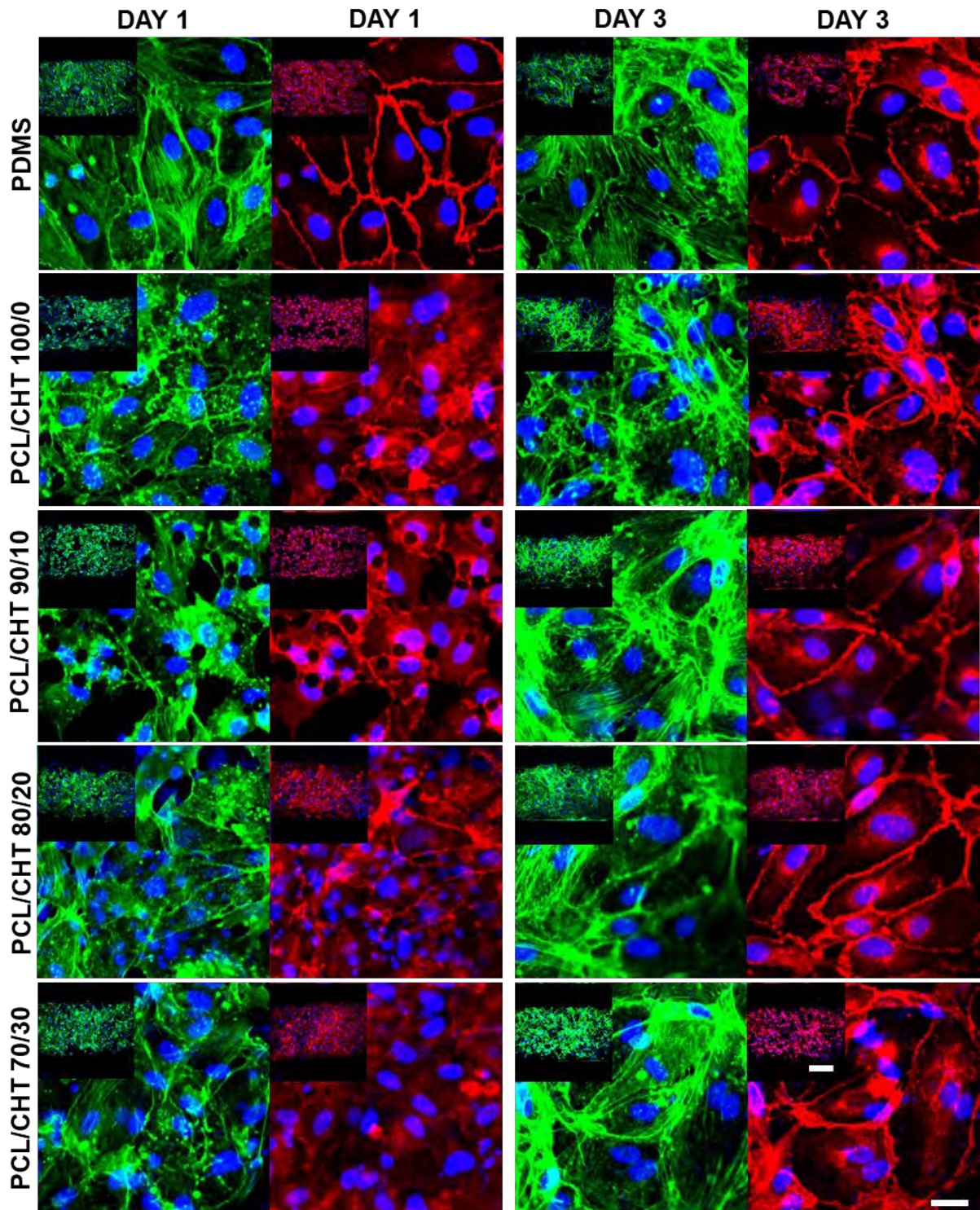


Fig. 5. LCSM representative images of HUVECs on different blends of membranes after staining three different parameters (nucleus by DAPI in blue, cell cytoskeleton by phalloidin 488 in green and cell junctions by VE-Cadherin in red) taken after permeability experiments inside OOC systems after 1 day and 3 day of cell seeding. Bars; 200 μm in inset view (15 \times mag.) and 20 μm in enlarged view (85 \times mag.).

The cellular adhesion was observed after the flux experiments in the confocal images (**Fig. 5**). After one day (in 15× Mag.) all four batches of membranes showed good cellular adhesion and compatibility. The cellular adhesion was increasing by increasing CHT wt%, which could be due to an increase of surface hydrophilicity and functional property like enhanced collagen coating. Whereas in 85× magnification images, the cell-cell interactions looks better on PCL/CHT 100/0 and PCL/CHT 90/10 scaffolds by expressing VE-Cadherin stronger than the other two scaffolds. The cellular morphology was the best on PDMS by strongly expressing VE-Cadherin with confluent cell-cell interactions and cortical F-actin, presumably because the cells prefer a smoother surface during the initial attachments [200].

After three days, the cellular adhesion was clearly higher for PCL/CHT 80/20 and PCL/CHT 70/30 scaffolds than PCL/CHT 100/0 and PCL/CHT 90/10. On PDMS (control) the cellular attachments decreased compared to our membrane scaffolds. This could be due to detachment of the collagen layer from hydrophobic PDMS which eventually detaches the cellular layer. The detachment of the collagen from the PDMS likely occurred due to shear stress during medium changing followed by flux experiments. Normally to establish a strong bonding between PDMS and the collagen layer, chemical modification by amino-silane surface treatment is used inside the chips before collagen coating [169]. In our case, we skipped this chemical surface modification step purposely in order to compare cellular attachment exclusively on the membrane scaffolds and the control (PDMS surface) during long-term cell culture. In 85× magnification, HUVECs on all the scaffolds strongly express junctional VE-cadherin indicating better cell-cell connectivity compared to day one. In addition, the cells were spreading on the surface by increasing CHT wt%, presumably due to its higher hydrophilicity and better pore spacing of the scaffolds which is evident in the confocal images with spreading of actin filament bundles stained by Phalloidin. For comparison, Xiao et. al. [227] seeded HUVECs in three-dimensional β -tricalcium phosphate scaffolds with big pores connected with different interconnection sizes and studied cytoskeletal proteins such as actin to illustrate the spreading and attachment of cells on scaffolds. They found the scaffolds with higher pore spacing exhibited uniform and homogenous actin distribution of cytoplasm. This phenomenon is understandable, as the big pores mainly provide the space for cell growth, whereas the interconnections function as the doorway for cell-cell interaction and eventually

cell growth into the scaffold [227,228]. Du, et al. [38] reported the viability of HUVECs on a gradient nano-fibrous PCL-CHT membrane scaffolds for vascular tissue engineering. They found that the HUVECs have a tendency for high proliferation and adhesion on the luminal side (CHT rich) of the gradient scaffolds due to a better ECM proteoglycan-like structure and adsorption of essential growth factors (VEGF) by the CHT matrix. Our data showed that by increasing CHT wt% in PCL-CHT membranes, the microporous structure was significantly improved promoting higher endothelial cell types growth on the scaffolds. The entire layer of endothelial cell adhesion on the membrane top surface (lumen side) and the scaffold itself as the adventitial side is a potential match to the natural structure of blood vessels.

In the past, several experiments were reported to monitor the hydraulic transportation phenomena across the endothelial cell layer seeded on membrane at TEP range [214–216]. Almost all those experiments were conducted in a trans-well insert system with the conventional track-etched filter membranes. The current study is a further step forward in vascular tissue engineering by demonstrating how these three-dimensional membranes are more convenient candidates with tunable physico-chemical and microstructural properties when analyzed within OOCs.

4.5 Conclusion

We showed a straightforward and simple process to quantify the additional hydraulic resistance of HUVECs seeded on three-dimensional membrane scaffolds in an OOC system. The membrane scaffolds were developed by a modified version of liquid induced phase inversion, using different ratios of polycaprolactone-chitosan. At first, the flux and the corresponding resistance of the membranes were evaluated in the OOC system, starting from realistic trans-endothelial pressure (TEP). The flux was found to increase with increasing CHT content in the blend. The additional hydraulic resistance induced by the living HUVECs was quantified in the same set-up seeded on the membranes after one day and three days using EGM-2 culture medium. Results suggest that by increasing the CHT wt%, the microstructural morphology and the chemical properties are significantly improved leading to an increased hydraulic resistance of the cells due to enhanced cellular adhesion.

Overall, our study demonstrates that OOC systems can be used as *in vitro* platforms to optimize and evaluate the morphology and functionality of various tissue engineering constructs. We anticipate that the use of OOC technology in tissue engineering will increase, because the unique properties of OOCs, with their small size, engineered microenvironments and tissue-level or organ-level functional read-outs. Thus could greatly facilitate the development and optimization of new tissue engineered constructs for regenerative medicine.

4.6 Acknowledgment:

The author would like to acknowledge Marinke van der Helm and Paul ter Braak (BIOS/Lab on a Chip, UTwente) for kindly providing the inset photo in **Figure 1. (A)**.

4.7 Supplementary materials

4.7.1 Verification of the absence of leakage with fluorescent dye

To verify the sealing efficiency of the chip, fluorescent dye was added inside the chip by pipetting with normal hand pressure.

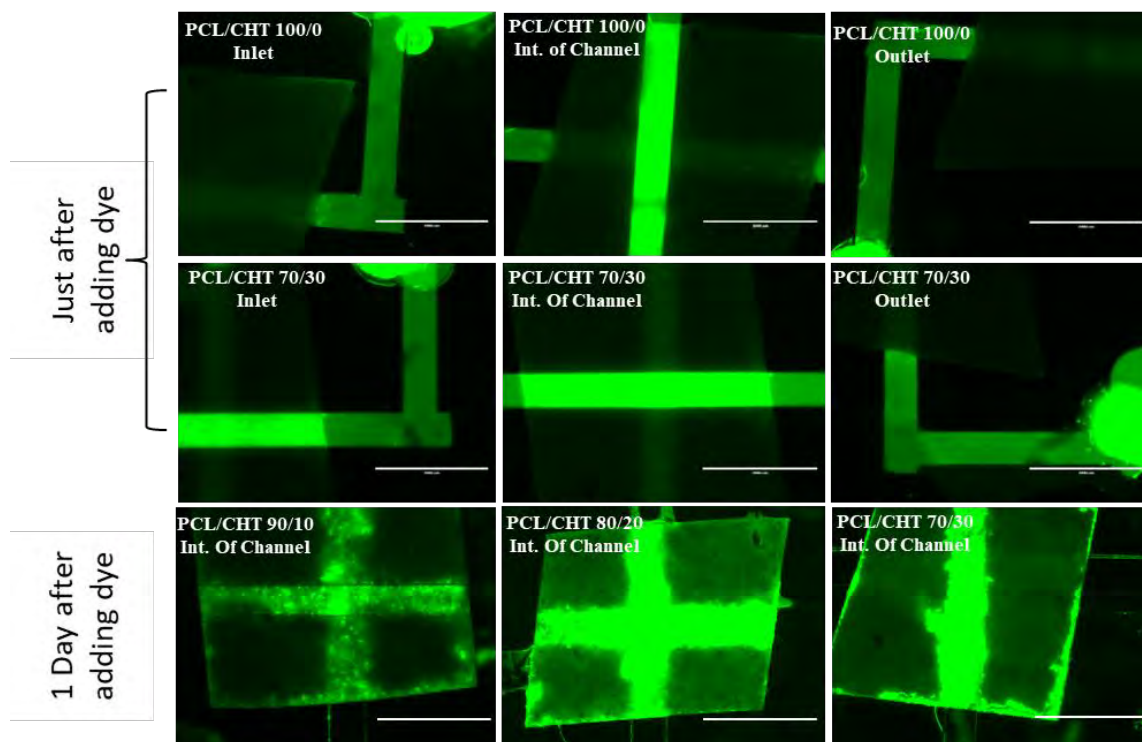


Fig. 6. Leakage test inside the channels by pipetting Fluorescent (Dextran 4 KDa, 1 mg/ml in PBS) dye. Scale bar 2000 μm .

For this experiment, chips with different batch of membrane were taken and they were imaged in EVOS, where no leakage out of the channel was found just after pipetting the dye. Then the chip were kept in room temperature for one day and imaged again. This time the fluorescent dye was slightly dispersed out of channel from inside the membrane area. The normal hand pressure of pipetting inside the channel must be much higher than the pressure of interests (TEP at 2-16 kPa), suggesting at real time Transendothelial pressure (TEP) the probability of leakage inside the channel is almost none.

4.7.2 Permeate flux of the membrane in Amicon cell

The water flux and the corresponding hydraulic resistance was also performed in high-pressure Amicon system where the flux was found much lower than the OOC system at pressure 20 kPa.

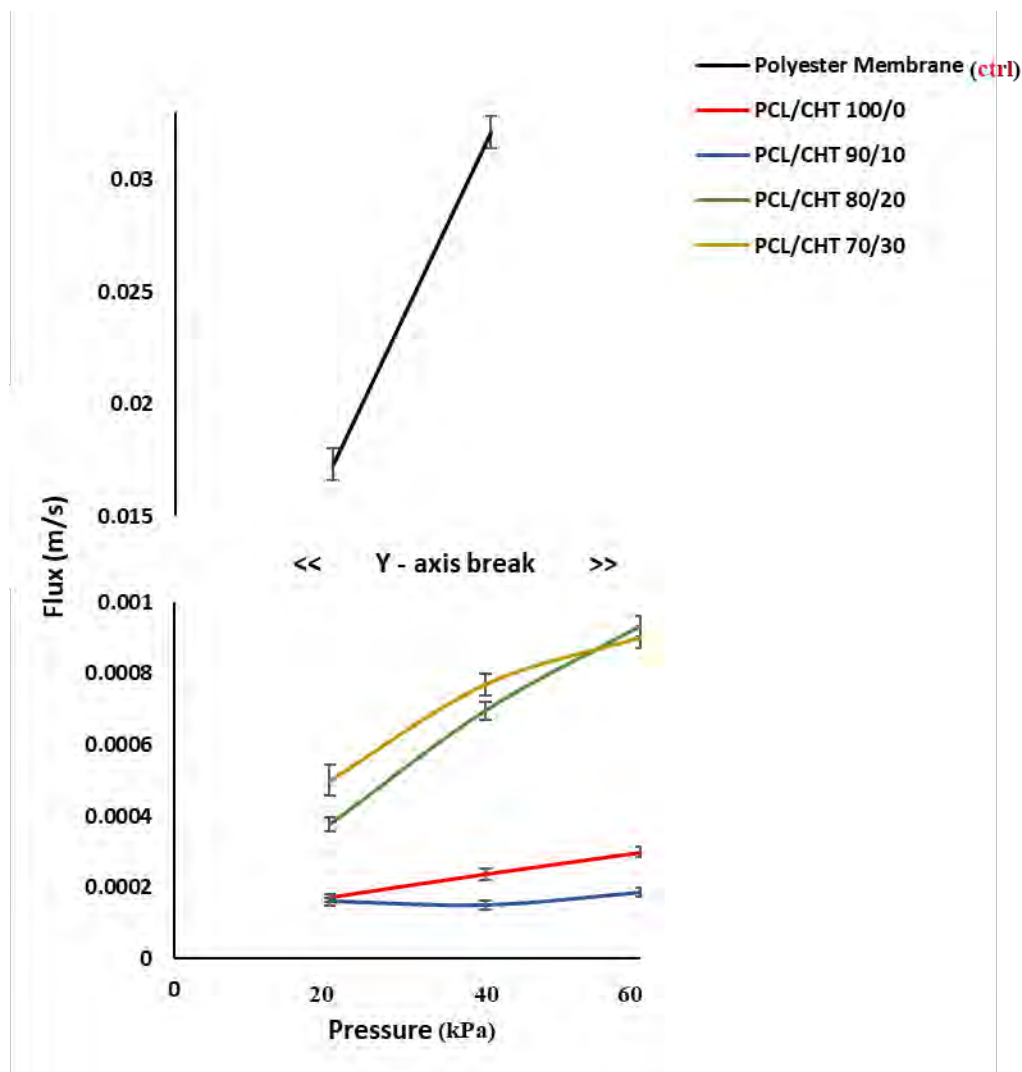


Fig. 7. Flux vs Pressure graph of four different membrane compare to Polyester membrane (control) measured in Amicon cell at 25 °C.

The overall flux of all the membranes follow the similar trend. By increasing CHT wt% flux is increasing due to higher hydrophilicity and improved wetting. Unlike the OOC system, flux was not increasing linearly with pressure due to membrane compaction as big pores are present inside the bulk resulting collapsing of the pores through the thickness. By increasing CHT wt% membrane compaction is increasing as CHT in wet condition is mechanically less stable than PCL, wreaking the PCL structural integrity. PCL/CHT 90/10 has shown the highest compressibility due to smallest small pores. Flux of a Polyester membrane (8 μm pore size and 10 μm thickness) was also measured as a control which is around 30 – 100 times higher than the blend membrane.

Table. 4. Hydraulic resistance (R_{Mem}) of the blend membranes with distilled water at 25 °C by the Eq. 3.

Pressure (kPa)	Resistance (R_{Mem}) m^{-1}			
	PCL/CHT 100/0	PCL/CHT 90/10	PCL/CHT 80/20	PCL/CHT 70/30
20	$1.33 \times 10^{11} \pm$ 0.82×10^{10}	$1.41 \times 10^{11} \pm$ 0.92×10^{10}	$5.99 \times 10^{10} \pm$ 3.2×10^9	$4.52 \times 10^{10} \pm$ 3.6×10^9
40	$1.91 \times 10^{11} \pm$ 1.4×10^{10}	$3.03 \times 10^{11} \pm$ 2.3×10^{10}	$6.47 \times 10^{10} \pm$ 2.4×10^9	$5.85 \times 10^{10} \pm$ 2.2×10^9
60	$2.26 \times 10^{11} \pm$ 1.1×10^{10}	$3.67 \times 10^{11} \pm$ 2.7×10^{10}	$7.23 \times 10^{10} \pm$ 2.2×10^9	$7.49 \times 10^{10} \pm$ 2.5×10^9

Due to the non-linearity of the flux vs pressure graph in the blend membrane, the hydraulic resistance was determined in each corresponding pressure (and water viscosity at 25 °C) by **Eq. 3** and listed in **Table. 4**.

Comparison of hydraulic resistance obtained in Fluigent and Amicon cell:

Below is the Resistance (m^{-1}) of the Polyester membrane by different report -

Manufacturer protocol [220] $4.6 \times 10^8 \text{ m}^{-1}$ (at press 70 kPa or 10 psi and Vis. Water in 25 °C)

Amicon cell $15.2 \times 10^8 \text{ m}^{-1}$ (from slop in **Fig. 8**, using Vis. Water in 25 °C)

In OOC $5.5 \times 10^8 \text{ m}^{-1}$ (from slop in **Fig. 4**, using Vis. Culture medium in 37 °C)

For the polyester membrane (as control), the resistance that obtained from OOC system was quite similar that has been reported in the manufacturer protocol whereas the value in the amicon cell was 3 times higher from the manufacturer protocol. Whereas, in case of PCL-CHT membrane, the resistance in the amicon cell was 100 times higher than that have been obtained in the fluigent system.

Unlike the PCL-CHT membrane, hydraulic flux in the polyester membrane was simpler due to lower hydraulic length (membrane thickness 10 μm) and smooth surface with pores all the way through the membrane thickness. In spite of that, the resistance value in the polyester membrane obtained in the Amicon cell was increasing could be due to added internal instrumental resistance. Whereas PCL-CHT membranes has more complicated surface and bulk morphology than the polyester membrane. Moreover, the blend membrane surface was heterogeneous with combination of pores and pillars where the pillar was decreasing by increasing CHT wt% (the exact proportion of the pores and pillars was unknown). Hence, the resistance that obtained from the Amicon cell is combination of pores and with some pillars. Although similar thing should happen in the OOC system but here the flux experiment was started from 10 times lower pressure and 1256 times lower membrane surface area where it possible that membrane surface majorly faced Pillar (which was giving zero reading and was discarded) and pores (which was giving reading and considered). And as the reading in the OOC was considered majorly from the pores, the resistance should be much lower than the reading of Amicon cell.

General conclusion and perspectives

General conclusion

The aim of the work was to develop three-dimensional biomaterial with unique microstructure properties in term of flat sheet polymeric membranes. Moreover, to understand the cell-matrix interaction by tuning the key material parameter in order to find out the optimum membrane scaffolds for vascular graft and application tissue engineering application. Polymeric membranes as biomaterials have played an increasingly prominent role in the success of biomedical devices and in the development of tissue engineering, which seeks to unlock the regenerative potential innate to human tissues/organs in a state of deterioration and to restore or reestablish normal bodily function. In the last few decades there are many biomaterial have been synthesized and reported to be potentially support the tissue culture and engineering field but in the recent period of time the ever growing demanding for more advance biomaterial will need more detail understanding of material science and their effect on cellular biology. Thus in **chapter 1** was completely dedicated for the bibliography to find the recent progress of the biomaterials in tissue engineering and in biomedical applications in combination of biology, technology and chemical engineering. It was found that the polymeric materials are the great choice as biomaterials due to their different potential varieties leading the option of high tunability in terms of any tissue specific applications. Although there are many natural polymers are already proved for their inbuilt ability to provide ECM like environment. But the combination of synthetic/natural polymers produced today routinely incorporate biologically active components to define the best artificial in vivo milieu with complex and dynamic interactions that foster and regulate cellular adhesion with better material architecture, mechanical and biological properties. The range and degree of polymeric biomaterial have also dramatically increased as more knowledge has accumulated through materials science, matrix biology and tissue engineering. However, achieving clinical translation and commercial success requires regenerative biomaterials to be not only efficacious and safe but also cost-effective and convenient for use and production. In particular, there is increasing interest to use polymeric flat sheet membranes into simplified functional domains and/or biopolymeric assemblies so that these materials can be discretely exploited and manipulated for the production of advance biomimetic biomaterials. In spite of that, tissue-

engineering applications commonly encompass the use of three-dimensional (3D) membrane scaffolds to provide a suitable microenvironment for the incorporation of cells or growth factors to regenerate damaged tissues or organs. In **chapter 1**, all the combination of synthetic/natural polymer used in tissue engineering purposes and the fabrication methods are listed. Those processing technique produce some good porous scaffolds and among them electrospinning, porogen leaching, gas foaming and conversional phase inversion were the technique which were mostly reported. But they still have some limitations as very often those membrane scaffolds produce porosity including non-interconnected/unutilized pores, compromising the mechanical properties with moderate cell culture efficiency.

The research work presented in this dissertation answers to some of these technical and scientific challenges inside the tryptic material/biology as discussed in the introduction. Hence, in **Chapter 2**, we decided to go for further modification of the membrane fabrication technique in order to obtain the optimum porosity to provide the potential architectural environments without compromising the other important mechanical property. It was found that the open pores inside the scaffolds are very important not only to access the bulk microenvironment and tissue ingrowth but also to provide essential nutrients and oxygen inside the bulk. But the big pores are not worthy enough to transfer of the small active molecules inside the bulk. And for that purpose much smaller interconnected pores should be introduced which will not only intact the strength of the materials but also provide suitable microstructural morphology. Thus the idea of double porous membrane scaffolds came, which can readily solve the aforementioned limitations. We found a nice way to produce the double porous morphology by modifying the liquid induced phase inversion by using track-etched commercial membranes. The combination of polycaprolactone and chitosan was chosen as synthetic/natural polymer due to their reputed biocompatibility, biodegradation and ease of tenability. However, the fabrication technique required high polymer/solvent ratio and for that one pot polymer solution in a common solvent was inevitable. But these two polymers are chemically quite different that finding a common solvent and make a polymer solution with optimum viscosity was our preliminary challenge. Thusly for the first time we dissolved two chemically distinct polymer in a common solvent (formic acid/acetic acid

mixture) and successfully produce the flat sheet double porous morphology. The low chemical interaction between the two polymers was responsible to initiate little phase segregation in high CHT% but act also as a plus point to vary the big pore size and overall pore morphology which was evident from the phase inversion diagram. The distinguished architectural properties somewhat overwhelm the scaffolds chemical properties which has a direct impact on the HMSCs viability as well as mechanical and enzymatic biodegradation properties observe in **chapter 3**. These membrane scaffolds serve to mimic the actual in vivo microenvironment where cells interact and behave according to the architectural cues obtained from the surrounding 3D environment. Hence, the material properties of the scaffolds are vital in determining cellular response and fate. 3D scaffolds are generally highly porous with interconnected pore networks to facilitate nutrient and oxygen diffusion and waste removal. We understand that to obtain a high cellular viability the initial cell-matrix attachment is very important which can be attribute by the continuous space between the pore or the pore spacing. But that also depend on the particular cell type. For example in **chapter 3**, we found by increasing CHT wt% the pore spacing or the continuous space upon the membrane surface was not favorable for good initial attachment. Whereas in case of **chapter 4**, the opposite phenomena was observed with the HUVECs. But by increasing CHT wt% both the cell types have shown the similar change in cell structure and morphology which can be manifested by the material chemical property. And the most importantly in **chapter 3**, HMSCs invasion was also observed which was highly depend upon the big pore size on the scaffolds resulting the difference in cell shape and morphology between the cell inside the bulk and upon the surface. The cellular experiments on the membranes were quite promising which indicate this kind of scaffolds will be highly biocompatible for selective co culture and could be useful for different cell culture experiments by changing the phenotype or by providing growth factors to other cell types. Finally, in **chapter 4**, the potential of the membrane scaffolds were tested as a real time vascular patch for biomedical application. HUVECs were seeded on the membranes and their hydraulic resistance were determined in microfluidic organ-on-chip system. These organ-on-chip models, which contain micrometer-sized, fluid-filled channels in which human cells can be cultured, provide opportunities for engineering a controlled culture environment that resembles the microenvironment of a certain organ by tuning mechanical, biochemical and geometrical aspects. The hydraulic resistance was determined

by measuring the flux of the EGM 2 media in real time transmural pressure through the membrane seeded with the cell. By increasing CHT wt% the cellular resistance was increasing due to combination of better morphological-chemical property and also by blocking the big pores. The confocal images was also coherent with flux experiments where higher cell adhesion and cell surface spreading was observed upon the surface with increasing CHT wt%. Results suggests that the membrane scaffold were highly potential to be useful as a in vivo endothelial vessel repairment. As stated earlier, the efficiency of the other cell type like HUVECs could be enhanced by providing growth factors, produced from MSCs where the MSCs could be transduced by genetic engineering. That will be a perfect mimicking of the human physiological condition by indicating that these kind of membrane scaffolds will be highly useful in biomedical industries for advance applications.

Perspectives

On a material point of view, the research work done during this thesis allows to develop and characterize a new material that can be useful for tissue engineering. However, the development have been done for a planar surface. It could be interesting to consider also the development of such double porosities membrane in hollow fiber configuration. The hollow fiber configuration is of great interest for the development of bioreactor for cell culture usually made with non-biodegradable membrane [229,230] but can also be interesting with biodegradable membrane to mimic the shape of vessels. In these perspectives, it could be useful to study how the modified phase inversion techniques used in this work could be adapted for the production of hollow fibers. Others methods of micropatterning could also be studied i) by using template mask obtained by photolithography [231], ii) by microemulsion polymerization [232], iii) by hydrogel formation with Bijels technique [233], iv) by micro-patterning like membrane 3D printing (3D localized additive deposit of polymer solution precipitated with a temperature induced phase separation TIPS)

On a biological point of view, new strategies to favour the cell adhesion can be investigated and different application field could be considered. The studies in the thesis proves the biocompatibility of the materials and its ability to host the cells in the macroporosities. In comparison to electrospun materials made of an assembly of fibers, the membrane materials consist of macrovoids that can host

the cells but also of a “spongy” nanostructure that can act as a reservoir of molecules to deliver multiple molecules. This last property can represent an interest for some tissue engineering application. To investigate this potential benefit, experiments could be performed in the presence of indigenous production of growth factors inside the membrane. For example for the repair of lymphatic wall after lymphatic injuries including chylothorax and lymphedema, bone marrow-derived MSC can be transduced with lentivector to produce lymphangiogenic growth factors: VEGF-C and -D. A strategy could be to pre-load the membrane with MSC expressing lymphangiogenic growth factors to accumulate VEGF-C and/or VEGF-D in the mesopores of the membrane. In a second culture, the adhesion and the growth of the lymphatic endothelial cell (LEC) could be done. This kind of co-culture could allow to produce continuously the growth factor molecules and could be an interesting strategy for “short life” endothelial cells.

The biological properties could then benefit from the specific **transport properties of the materials**. For example, biomolecular sensing that relies on transport properties like has been defined as the new paradigm to consider for scaffolds [20]. It opens up interesting perspectives of studies between chemical engineering, materials science and biology. The use of microfluidic devices or organ in chip devices could help to study the interplay between hydrodynamic and mass transport through cells assemblies. Such devices can give the possibility to study the dynamic of the cells adhesion and growth and the impact of the external operating conditions (flow and concentration). In the microfluidic devices developed in the **chapter 4**, it could be interesting to study the transport of small active molecules or migration of cell through the membrane and the accumulation at the surface. These microfluidic devices could also be useful to have an idea of the flow rate on the adhesion-detachment kinetics of cells on the surface. It could then help to see if there is an interest in having macrovoid that can host the cells and protect the cells from the shear rate.

In general, increasing evidence suggests that membranes as biomaterials for regenerative medicine purposes are yielding an ever-growing list of products and successful clinical approaches to maintain, enhance or restore tissues and organs. These “raw materials” continue to demonstrate great potential and will have an increasingly remarkable impact on synthetic biology, tissue engineering and clinical regenerative

therapies in the future. In addition, synthesized membranes by combining synthetic/natural polymers are directing our nascent understanding of the cellular milieu and how the basic building blocks (e.g., biomacromolecules) of human systems are correctly integrated into the dynamic landscape that represents tissue physiology. Unfortunately, the science of human ECM biology remains in its infancy, with all current and emerging macromolecular assemblies or ECM mimics having serious limitations. As we advance the science of cell–ECM interactions, we will become more precise in our ability to dictate regenerative processes based on tissue ECM materials or information coded within the material, which provides signposts for advanced biomaterial design. Elucidating the molecular pathways through which cells discriminate signals from their ECM will reveal important signposts in designing new biomimetic polymers tuned for a more defined cellular response, allowing for more controlled and efficient tissue regeneration if progress continues. Additionally, materials science strategies are bridging the gaps in various but interrelated scientific fields, and these strategies have become a comprehensive suite of essential tools in the fields of tissue engineering and regenerative medicine. Although several pivotal questions still need to be addressed, and particularly those concerning cell recruitment and functional integration of recruited cells. Meeting the challenge of unravelling these complex mechanisms will be rewarded with therapeutic potential across the field of tissue engineering. A constant influx of new knowledge from biological systems and new structural, chemical, and physical insights into human-derived biomaterials, complemented by recent advances in synthetic technology and biological science, will yield new and more sophisticated biomaterial designs and inspiration in the future. The effect of the field will continue to grow and evolve with the collaborative development of tissue-engineered products that offer simple solutions to complex problems.

References

- [1] Tissue Engineering and Regenerative Medicine, Natl. Inst. Biomed. Imaging Bioeng. (2013). <https://www.nibib.nih.gov/science-education/science-topics/tissue-engineering-and-regenerative-medicine> (accessed January 30, 2019).
- [2] F.-M. Chen, X. Liu, Advancing biomaterials of human origin for tissue engineering, *Prog. Polym. Sci.* 53 (2016) 86–168. doi:10.1016/j.progpolymsci.2015.02.004.
- [3] V. Parpura, Nanoelectronics for the heart: Tissue engineering, *Nat. Nanotechnol.* 11 (2016) 738–739. doi:10.1038/nnano.2016.123.
- [4] K. Sadtler, K. Estrellas, B.W. Allen, M.T. Wolf, H. Fan, A.J. Tam, C.H. Patel, B.S. Lubner, H. Wang, K.R. Wagner, J.D. Powell, F. Housseau, D.M. Pardoll, J.H. Elisseeff, Developing a pro-regenerative biomaterial scaffold microenvironment requires T helper 2 cells, *Science*. 352 (2016) 366–370. doi:10.1126/science.aad9272.
- [5] R. Mondschein, A. Kantikar, C. Williams, S. Verbridge, T. Long, Polymer structure-property requirements for stereolithographic 3D printing of soft tissue engineering scaffolds, *Biomaterials*. 140 (n.d.) 170–188.
- [6] F.T. Moutos, L.E. Freed, F. Guilak, A biomimetic three-dimensional woven composite scaffold for functional tissue engineering of cartilage, *Nat. Mater.* 6 (2007) 162–167. doi:10.1038/nmat1822.
- [7] S. Petit-Zeman, The regeneration of tissues and organs offers a radical new approach to the treatment of injury and disease. It's a new medicine for a new millennium, but does the reality match the hype?, *Nat. Biotechnol.* 19 (2001) 201–206.
- [8] L.L. Hench, Third-Generation Biomedical Materials, *Science*. 295 (2002) 1014–1017. doi:10.1126/science.1067404.
- [9] E. Garreta, R. Oria, C. Tarantino, M. Pla-roca, P. Prado, F. Avilés, J. Campistol, J. Samitier, N. Montserrat, Tissue engineering by decellularization and 3D bioprinting, *Mater. Today*. (2007) 166–178.
- [10] D.A. Grande, Important milestones on the way to clinical translation: Regenerative medicine in 2016, *Nat. Rev. Rheumatol.* 13 (2017) 67–68. doi:10.1038/nrrheum.2016.214.
- [11] M.P. Lutolf, J.A. Hubbell, Synthetic biomaterials as instructive extracellular microenvironments for morphogenesis in tissue engineering, *Nat. Biotechnol.* 23 (2005) 47–55. doi:10.1038/nbt1055.
- [12] S.-W. Choi, J. Xie, Y. Xia, Chitosan-Based Inverse Opals: Three-Dimensional Scaffolds with Uniform Pore Structures for Cell Culture, *Adv. Mater.* 21 (2009) 2997–3001. doi:10.1002/adma.200803504.
- [13] B.G. Childs, H. Li, J.M. van Deursen, Senescent cells: a therapeutic target for cardiovascular disease, (2018). doi:10.1172/JCI95146.
- [14] E. Place, J. George, C. Williams, M. Stevens, Synthetic polymer scaffolds for tissue engineering - *Chemical Society Reviews* (RSC Publishing), *Chem Soc Rev.* 38 (2009) 1139–1151.
- [15] E.R. Welsh, D.A. Tirrell, Engineering the Extracellular Matrix: A Novel Approach to Polymeric Biomaterials. I. Control of the Physical Properties of Artificial Protein Matrices Designed to Support Adhesion of Vascular Endothelial Cells, *Biomacromolecules*. 1 (2000) 23–30. doi:10.1021/bm0002914.
- [16] A. Panitch, T. Yamaoka, M.J. Fournier, T.L. Mason, D.A. Tirrell, Design and Biosynthesis of Elastin-like Artificial Extracellular Matrix Proteins Containing Periodically Spaced Fibronectin CS5 Domains, *Macromolecules*. 32 (1999) 1701–1703. doi:10.1021/ma980875m.
- [17] B. Seal, Polymeric biomaterials for tissue and organ regeneration, *Mater. Sci. Eng. R Rep.* 34 (2001) 147–230. doi:10.1016/S0927-796X(01)00035-3.
- [18] Y. Yao, J. Wang, Y. Cui, R. Xu, Z. Wang, J. Zhang, K. Wang, Y. Li, Q. Zhao, D. Kong, Effect of sustained heparin release from PCL/chitosan hybrid small-diameter vascular grafts on anti-thrombogenic property and endothelialization, *Acta Biomater.* 10 (2014) 2739–2749. doi:10.1016/j.actbio.2014.02.042.

- [19] A. Cooper, N. Bhattarai, M. Zhang, Fabrication and cellular compatibility of aligned chitosan–PCL fibers for nerve tissue regeneration, *Carbohydr. Polym.* 85 (2011) 149–156. doi:10.1016/j.carbpol.2011.02.008.
- [20] S.J. Hollister, Porous scaffold design for tissue engineering, *Nat. Mater.* 4 (2005) 518. doi:10.1038/nmat1421.
- [21] S. Terasaka, Y. Iwasaki, N. Shinya, T. Uchida, Fibrin Glue and Polyglycolic Acid Nonwoven Fabric as a Biocompatible Dural Substitute., *Oper. Neurosurg.* 58 (2006) ONS-134-ONS-139. doi:10.1227/01.NEU.0000193515.95039.49.
- [22] P.B. Maurus, C.C. Kaeding, Bioabsorbable implant material review, *Oper. Tech. Sports Med.* 12 (2004) 158–160. doi:10.1053/j.otsm.2004.07.015.
- [23] J.A. Cooper, H.H. Lu, F.K. Ko, J.W. Freeman, C.T. Laurencin, Fiber-based tissue-engineered scaffold for ligament replacement: design considerations and in vitro evaluation, *Biomaterials.* 26 (2005) 1523–1532. doi:10.1016/j.biomaterials.2004.05.014.
- [24] M. Zilberman, K.D. Nelson, R.C. Eberhart, Mechanical properties and in vitro degradation of bioresorbable fibers and expandable fiber-based stents, *J. Biomed. Mater. Res. B Appl. Biomater.* 74B (2005) 792–799. doi:10.1002/jbm.b.30319.
- [25] L. Wu, H. Li, S. Li, X. Li, X. Yuan, X. Li, Y. Zhang, Composite fibrous membranes of PLGA and chitosan prepared by coelectrospinning and coaxial electrospinning, *J. Biomed. Mater. Res. A.* 92 (2010) 563–574. doi:10.1002/jbm.a.32393.
- [26] F. Danhier, E. Ansorena, J.M. Silva, R. Coco, A. Le Breton, V. Préat, PLGA-based nanoparticles: An overview of biomedical applications, *J. Controlled Release.* 161 (2012) 505–522. doi:10.1016/j.jconrel.2012.01.043.
- [27] B. SAAD, T.. Hirt, M. Welti, G.. Uhlschmid, P. Neuenschwander, U.. Suter, Development of degradable polyesterurethanes for medical applications: In vitro and in vivo evaluations - Saad - 1997 - Journal of Biomedical Materials Research - Wiley Online Library, *J Biomed Mater Res.* 36 (1997) 65–74.
- [28] C. Vauthier, Drug delivery to resistant tumors: the potential of poly(alkyl cyanoacrylate) nanoparticles, *J. Controlled Release.* 93 (2003) 151–160. doi:10.1016/j.jconrel.2003.08.005.
- [29] A. Di Martino, M. Sittinger, M.V. Risbud, Chitosan: A versatile biopolymer for orthopaedic tissue-engineering, *Biomaterials.* 26 (2005) 5983–5990. doi:10.1016/j.biomaterials.2005.03.016.
- [30] C. Ceccaldi, S.G. Fullana, C. Alfarano, O. Lairez, D. Calise, D. Cussac, A. Parini, B. Sallerin, Alginate Scaffolds for Mesenchymal Stem Cell Cardiac Therapy: Influence of Alginate Composition, *Cell Transplant.* 21 (2012) 1969–1984. doi:10.3727/096368912X647252.
- [31] U. Rottensteiner, B. Sarker, D. Heusinger, D. Dafinova, S. Rath, J. Beier, U. Kneser, R. Horch, R. Detsch, A. Boccaccini, A. Arkudas, In vitro and in vivo Biocompatibility of Alginate Dialdehyde/Gelatin Hydrogels with and without Nanoscaled Bioactive Glass for Bone Tissue Engineering Applications, *Materials.* 7 (2014) 1957–1974. doi:10.3390/ma7031957.
- [32] P. Catherine, W. charls, D. David, G. David, L. Gary, Cross-linking electrospun type II collagen tissue engineering scaffolds with carbodiimide in ethanol, *Tissue Eng.* 13 (2007) 1593–605.
- [33] W. Friess, Collagen – biomaterial for drug delivery, *Eur. J. Pharm. Biopharm.* (1998) 24.
- [34] A.O. Elzoghby, Gelatin-based nanoparticles as drug and gene delivery systems: Reviewing three decades of research, *J. Controlled Release.* 172 (2013) 1075–1091. doi:10.1016/j.jconrel.2013.09.019.
- [35] X. Duan, C. McLaughlin, M. Griffith, H. Sheardown, Biofunctionalization of collagen for improved biological response: Scaffolds for corneal tissue engineering, *Biomaterials.* 28 (2007) 78–88. doi:10.1016/j.biomaterials.2006.08.034.
- [36] D.R. Hunt, S.A. Jovanovic, U.M.E. Wikesjö, J.M. Wozney, G.W. Bernard, Hyaluronan Supports Recombinant Human Bone Morphogenetic Protein-2 Induced Bone Reconstruction of Advanced Alveolar Ridge Defects in Dogs. A Pilot Study, *J. Periodontol.* 72 (2001) 651–658. doi:10.1902/jop.2001.72.5.651.
- [37] H. Tan, C.R. Chu, K.A. Payne, K.G. Marra, Injectable in situ forming biodegradable chitosan–hyaluronic acid based hydrogels for cartilage tissue engineering, *Biomaterials.* 30 (2009) 2499–2506. doi:10.1016/j.biomaterials.2008.12.080.

- [38] F. Du, H. Wang, W. Zhao, D. Li, D. Kong, J. Yang, Y. Zhang, Gradient nanofibrous chitosan/poly ϵ -caprolactone scaffolds as extracellular microenvironments for vascular tissue engineering, *Biomaterials*. 33 (2012) 762–770. doi:10.1016/j.biomaterials.2011.10.037.
- [39] J. Zeng, A. Aigner, F. Czubayko, T. Kissel, J.H. Wendorff, A. Greiner, Poly(vinyl alcohol) Nanofibers by Electrospinning as a Protein Delivery System and the Retardation of Enzyme Release by Additional Polymer Coatings, *Biomacromolecules*. 6 (2005) 1484–1488. doi:10.1021/bm0492576.
- [40] S.J. Pomfret, P.N. Adams, N.P. Comfort, A.P. Monkman, Electrical and mechanical properties of polyaniline fibres produced by a one-step wet spinning process, (2000) 5.
- [41] S. Hirano, M. Zhang, M. Nakagawa, T. Miyata, Wet spun chitosan/collagen “fibers, their chemical N-modifications, and blood compatibility, (2000) 7.
- [42] K. Kim, C. Lee, I.W. Kim, J. Kim, Performance modification of a melt-blown filter medium via an additional nano-web layer prepared by electrospinning, *Fibers Polym.* 10 (2009) 60–64. doi:10.1007/s12221-009-0060-6.
- [43] C.J. Ellison, A. Phatak, D.W. Giles, C.W. Macosko, F.S. Bates, Melt blown nanofibers: Fiber diameter distributions and onset of fiber breakup, *Polymer*. 48 (2007) 3306–3316. doi:10.1016/j.polymer.2007.04.005.
- [44] M.J.B. Wissink, R. Beernink, J.S. Pieper, A.A. Poot, G.H.M. Engbers, T. Beugeling, W.G. van Aken, J. Feijen, Binding and release of basic “broblast growth factor from heparinized collagen matrices, (2001) 9.
- [45] F. Causa, P.A. Netti, L. Ambrosio, A multi-functional scaffold for tissue regeneration: The need to engineer a tissue analogue, *Biomaterials*. 28 (2007) 5093–5099. doi:10.1016/j.biomaterials.2007.07.030.
- [46] A.G. Mikes, G. Sarakinos, S.M. Leite, J.P. Vacant, R. Langer, Laminated three-dimensional biodegradable foams for use in tissue engineering, 14 (1993) 8.
- [47] A.G. Mikos, A.J. Thorsen, L.A. Czerwonka, Y. Bao, R. Langer, D.N. Winslow, J.P. Vacanti, Preparation and characterization of poly(l-lactic acid) foams, *Polymer*. 35 (1994) 1068–1077. doi:10.1016/0032-3861(94)90953-9.
- [48] H.G. Kang, S.Y. Kim, Y.M. Lee, Novel porous gelatin scaffolds by overrun/particle leaching process for tissue engineering applications, *J. Biomed. Mater. Res. B Appl. Biomater.* 79B (2006) 388–397. doi:10.1002/jbm.b.30553.
- [49] J.M. Karp, M.S. Shoichet, J.E. Davies, Bone formation on two-dimensional poly(DL-lactide-co-glycolide) (PLGA) films and three-dimensional PLGA tissue engineering scaffolds in vitro, *J. Biomed. Mater. Res.* 64A (2003) 388–396. doi:10.1002/jbm.a.10420.
- [50] D.J. Mooney, D.F. Baldwin, N.P. Suht, J.P. Vacantis, R. Langer, Novel approach to fabricate porous sponges of poly(o,l-lactide-co-glycolic acid) without the use of organic solvents, 17 (1996) 6.
- [51] W.L. Murphy, R.G. Dennis, J.L. Kileny, D.J. Mooney, Salt Fusion: An Approach to Improve Pore Interconnectivity within Tissue Engineering Scaffolds, *Tissue Eng.* 8 (2002) 43–52. doi:10.1089/107632702753503045.
- [52] B.H. Woo, J.W. Kostanski, S. Gebrekidan, B.A. Dani, B. Thanoo, P.P. DeLuca, Preparation, characterization and in vivo evaluation of 120-day poly(d,l-lactide) leuprolide microspheres, *J. Controlled Release*. 75 (2001) 307–315. doi:10.1016/S0168-3659(01)00403-5.
- [53] P.B. Malafaya, T.C. Santos, M. van Griensven, R.L. Reis, Morphology, mechanical characterization and in vivo neo-vascularization of chitosan particle aggregated scaffolds architectures, *Biomaterials*. 29 (2008) 3914–3926. doi:10.1016/j.biomaterials.2008.06.023.
- [54] Y. Ohya, H. Matsunami, T. Ouchi, Cell growth on the porous sponges prepared from poly(depsipeptide-co-lactide) having various functional groups, *J. Biomater. Sci. Polym. Ed.* 15 (2004) 111–123. doi:10.1163/156856204322752264.
- [55] Y. Ohya, H. Matsunami, E. Yamabe, T. Ouchi, Cell attachment and growth on films prepared from poly(depsipeptide-co-lactide) having various functional groups, *J. Biomed. Mater. Res.* 65A (2003) 79–88. doi:10.1002/jbm.a.10446.
- [56] M. Borden, M. Attawia, Y. Khan, C.T. Laurencin, Tissue engineered microsphere-based matrices for bone repair: design and evaluation, (2002) 9.

- [57] J. Guan, K.L. Fujimoto, M.S. Sacks, W.R. Wagner, Preparation and characterization of highly porous, biodegradable polyurethane scaffolds for soft tissue applications, *Biomaterials*. 26 (2005) 3961–3971. doi:10.1016/j.biomaterials.2004.10.018.
- [58] J.-Y. Seong, Y.J. Jun, B. Jeong, Y.S. Sohn, New thermogelling poly(organophosphazenes) with methoxypoly(ethylene glycol) and oligopeptide as side groups, *Polymer*. 46 (2005) 5075–5081. doi:10.1016/j.polymer.2005.04.024.
- [59] B. Jeong, Y.H. Bae, S.W. Kim, Thermoreversible Gelation of PEG–PLGA–PEG Triblock Copolymer Aqueous Solutions, *Macromolecules*. 32 (1999) 7064–7069. doi:10.1021/ma9908999.
- [60] O. Gauthier, R. Muller, D. Vonstchow, B. Lamy, P. Weiss, J. Bouler, E. Aguado, G. Daculsi, In vivo bone regeneration with injectable calcium phosphate biomaterial: A three-dimensional micro-computed tomographic, biomechanical and SEM study, *Biomaterials*. 26 (2005) 5444–5453. doi:10.1016/j.biomaterials.2005.01.072.
- [61] T.A. Holland, J.K.V. Tessmar, Y. Tabata, A.G. Mikos, Transforming growth factor- β 1 release from oligo(poly(ethylene glycol) fumarate) hydrogels in conditions that model the cartilage wound healing environment, *J. Controlled Release*. 94 (2004) 101–114. doi:10.1016/j.jconrel.2003.09.007.
- [62] J. Fukuda, A. Khademhosseini, Y. Yeo, X. Yang, J. Yeh, G. Eng, J. Blumling, C.-F. Wang, D.S. Kohane, R. Langer, Micromolding of photocrosslinkable chitosan hydrogel for spheroid microarray and co-cultures, *Biomaterials*. 27 (2006) 5259–5267. doi:10.1016/j.biomaterials.2006.05.044.
- [63] J. Yeh, Y. Ling, J.M. Karp, J. Gantz, A. Chandawarkar, G. Eng, J. Blumling III, R. Langer, A. Khademhosseini, Micromolding of shape-controlled, harvestable cell-laden hydrogels, *Biomaterials*. 27 (2006) 5391–5398. doi:10.1016/j.biomaterials.2006.06.005.
- [64] D. Dendukuri, D.C. Pregibon, J. Collins, T.A. Hatton, P.S. Doyle, Continuous-flow lithography for high-throughput microparticle synthesis, *Nat. Mater.* 5 (2006) 365–369. doi:10.1038/nmat1617.
- [65] W. Chen, R.H.W. Lam, J. Fu, Photolithographic surface micromachining of polydimethylsiloxane (PDMS), *Lab. Chip*. 12 (2011) 391–395. doi:10.1039/C1LC20721K.
- [66] S.N. Bhatia, D.E. Ingber, Microfluidic organs-on-chips, *Nat. Biotechnol.* 32 (2014) 760–772. doi:10.1038/nbt.2989.
- [67] V.V. Abhyankar, M. Wu, C.-Y. Koh, A.V. Hatch, A Reversibly Sealed, Easy Access, Modular (SEAM) Microfluidic Architecture to Establish In Vitro Tissue Interfaces, *PLOS ONE*. 11 (2016) e0156341. doi:10.1371/journal.pone.0156341.
- [68] J.A. Burdick, A. Khademhosseini, R. Langer, Fabrication of Gradient Hydrogels Using a Microfluidics/Photopolymerization Process, *Langmuir*. 20 (2004) 5153–5156. doi:10.1021/la049298n.
- [69] C.P. Reis, A.J. Ribeiro, R.J. Neufeld, F. Veiga, Alginate microparticles as novel carrier for oral insulin delivery, *Biotechnol. Bioeng.* 96 (2007) 977–989. doi:10.1002/bit.21164.
- [70] G. Steinhoff, U. Stock, N. Karim, H. Mertsching, A. Timke, R.R. Meliss, K. Pethig, A. Haverich, A. Bader, Tissue Engineering of Pulmonary Heart Valves on Allogenic Acellular Matrix Conduits : In Vivo Restoration of Valve Tissue, *Circulation*. 102 (2000) III-50-III-55. doi:10.1161/01.CIR.102.suppl_3.III-50.
- [71] Q.L. Loh, C. Choong, Three-Dimensional Scaffolds for Tissue Engineering Applications: Role of Porosity and Pore Size, *Tissue Eng. Part B Rev.* 19 (2013) 485–502. doi:10.1089/ten.teb.2012.0437.
- [72] L.E. Freed, G. Vunjak-Novakovic, Culture of organized cell communities, *Adv. Drug Deliv. Rev.* 33 (1998) 15–30. doi:10.1016/S0169-409X(98)00017-9.
- [73] T.J. Blokhuis, M.F. Termaat, F.C. den Boer, P. Patka, F.C. Bakker, H.J.T.M. Haarman, Properties of Calcium Phosphate Ceramics in Relation to Their In Vivo Behavior, *J. Trauma Acute Care Surg.* 48 (2000) 179.
- [74] Q. Zhang, H. Lu, N. Kawazoe, G. Chen, Pore size effect of collagen scaffolds on cartilage regeneration, *Acta Biomater.* 10 (2014) 2005–2013. doi:10.1016/j.actbio.2013.12.042.
- [75] F.J. O'Brien, B.A. Harley, I.V. Yannas, L.J. Gibson, The effect of pore size on cell adhesion in collagen-GAG scaffolds, *Biomaterials*. 26 (2005) 433–441. doi:10.1016/j.biomaterials.2004.02.052.
- [76] C.M. Murphy, M.G. Haugh, F.J. O'Brien, The effect of mean pore size on cell attachment, proliferation and migration in collagen–glycosaminoglycan scaffolds for bone tissue engineering, *Biomaterials*. 31 (2010) 461–466. doi:10.1016/j.biomaterials.2009.09.063.

- [77] J. Zeltinger, J.K. Sherwood, D.A. Graham, R. Müller, L.G. Griffith, Effect of Pore Size and Void Fraction on Cellular Adhesion, Proliferation, and Matrix Deposition, *Tissue Eng.* 7 (2001) 557–572. doi:10.1089/107632701753213183.
- [78] A.K. Salem, R. Stevens, R.G. Pearson, M.C. Davies, S.J.B. Tendler, C.J. Roberts, P.M. Williams, K.M. Shakesheff, Interactions of 3T3 fibroblasts and endothelial cells with defined pore features, *J. Biomed. Mater. Res.* 61 (2002) 212–217. doi:10.1002/jbm.10195.
- [79] P. Kasten, I. Beyen, P. Niemeyer, R. Luginbühl, M. Bohner, W. Richter, Porosity and pore size of β -tricalcium phosphate scaffold can influence protein production and osteogenic differentiation of human mesenchymal stem cells: An in vitro and in vivo study, *Acta Biomater.* 4 (2008) 1904–1915. doi:10.1016/j.actbio.2008.05.017.
- [80] S.-W. Choi, Y. Zhang, Y. Xia, Three-dimensional Scaffolds for Tissue Engineering: The Importance of Uniformity in Pore Size and Structure, *Langmuir ACS J. Surf. Colloids.* 26 (2010) 19001–19006. doi:10.1021/la104206h.
- [81] P.X. Ma, J.-W. Choi, Biodegradable Polymer Scaffolds with Well-Defined Interconnected Spherical Pore Network, *Tissue Eng.* 7 (2001) 23–33. doi:10.1089/107632701300003269.
- [82] B.L. Droumaguet, R. Lacombe, H.-B. Ly, B. Carbonnier, D. Grande, Novel Polymeric Materials with Double Porosity: Synthesis and Characterization, *Macromol. Symp.* 340 (2014) 18–27. doi:10.1002/masy.201300117.
- [83] M. Dufresne, P. Bacchin, G. Cerino, J.C. Remigy, G.N. Adrianus, P. Aimar, C. Legallais, Human hepatic cell behavior on polysulfone membrane with double porosity level, *J. Membr. Sci.* 428 (2013) 454–461. doi:10.1016/j.memsci.2012.10.041.
- [84] P. Das, J.-F. Lahitte, J.-C. Remigy, B. Garmy-Susini, S. Desclaux, C. Coetsier, L. De Bartolo, P. Bacchin, Artificial membranes tuning for lymphatic wall repair, in: *Eur. Chapter Meet. Tissue Eng. Regen. Med. Int. Soc. - TERMIS-EU 2016*, Uppsala, Sweden, 2016: p. 101. <https://hal.archives-ouvertes.fr/hal-01360666> (accessed December 13, 2017).
- [85] B.P. Tripathi, P. Das, F. Simon, M. Stamm, Ultralow fouling membranes by surface modification with functional polydopamine, *Eur. Polym. J.* 99 (2018) 80–89. doi:10.1016/j.eurpolymj.2017.12.006.
- [86] S. Salerno, S. Morelli, F. Giordano, A. Gordano, L. De Bartolo, Polymeric membranes modulate human keratinocyte differentiation in specific epidermal layers, *Colloids Surf. B Biointerfaces.* 146 (2016) 352–362. doi:10.1016/j.colsurfb.2016.06.026.
- [87] M.W. van der Helm, M. Odijk, J.-P. Frimat, A.D. van der Meer, J.C.T. Eijkel, A. van den Berg, L.I. Segerink, Direct quantification of transendothelial electrical resistance in organs-on-chips, *Biosens. Bioelectron.* 85 (2016) 924–929. doi:10.1016/j.bios.2016.06.014.
- [88] T. Pasma, D. Grijpma, D. Stamatialis, A. Poot, Flat and microstructured polymeric membranes in organs-on-chips, *J. R. Soc. Interface.* 15 (2018) 20180351. doi:10.1098/rsif.2018.0351.
- [89] A.D. van der Meer, A. van den Berg, Organs-on-chips: breaking the in vitro impasse, *Integr. Biol.* 4 (2012) 461. doi:10.1039/c2ib00176d.
- [90] F. Chen, X. Li, X. Mo, C. He, H. Wang, Y. Ikada, Electrospun chitosan-P(LLA-CL) nanofibers for biomimetic extracellular matrix, *J. Biomater. Sci. Polym. Ed.* 19 (2008) 677–691. doi:10.1163/156856208784089661.
- [91] S. Hong, G. Kim, Fabrication of electrospun polycaprolactone biocomposites reinforced with chitosan for the proliferation of mesenchymal stem cells, *Carbohydr. Polym.* 83 (2011) 940–946. doi:10.1016/j.carbpol.2010.09.002.
- [92] V.N. Malheiro, S.G. Caridade, N.M. Alves, J.F. Mano, New poly(ϵ -caprolactone)/chitosan blend fibers for tissue engineering applications, *Acta Biomater.* 6 (2010) 418–428. doi:10.1016/j.actbio.2009.07.012.
- [93] D.M. García Cruz, J.L. Gomez Ribelles, M. Salmerón Sánchez, Blending polysaccharides with biodegradable polymers. I. Properties of chitosan/polycaprolactone blends, *J. Biomed. Mater. Res. B Appl. Biomater.* 85 (2008) 303–313. doi:10.1002/jbm.b.30947.
- [94] A. Cooper, N. Bhattarai, F. M. Kievit, M. Rossol, M. Zhang, Electrospinning of chitosan derivative nanofibers with structural stability in an aqueous environment, *Phys. Chem. Chem. Phys.* 13 (2011) 9969–9972. doi:10.1039/C0CP02909B.
- [95] T. Honma, T. Senda, Y. Inoue, Thermal properties and crystallization behaviour of blends of poly(ϵ -caprolactone) with chitin and chitosan, *Polym. Int.* 52 (2003) 1839–1846. doi:10.1002/pi.1380.

- [96] S.D. Vrieze, P. Westbroek, T.V. Camp, L.V. Langenhove, Electrospinning of chitosan nanofibrous structures: feasibility study, *J. Mater. Sci.* 42 (2007) 8029–8034. doi:10.1007/s10853-006-1485-6.
- [97] R. Jayakumar, M. Prabakaran, S.V. Nair, H. Tamura, Novel chitin and chitosan nanofibers in biomedical applications, *Biotechnol. Adv.* 28 (2010) 142–150. doi:10.1016/j.biotechadv.2009.11.001.
- [98] M. Rahmouni, F. Chouinard, F. Nekka, V. Lenaerts, J.C. Leroux, Enzymatic degradation of cross-linked high amylose starch tablets and its effect on in vitro release of sodium diclofenac, *Eur. J. Pharm. Biopharm.* 51 (2001) 191–198. doi:10.1016/S0939-6411(01)00127-8.
- [99] T. Honma, L. Zhao, N. Asakawa, Y. Inoue, Poly(ϵ -Caprolactone)/Chitin and Poly(ϵ -Caprolactone)/Chitosan Blend Films With Compositional Gradients: Fabrication and Their Biodegradability, *Macromol. Biosci.* 6 (2006) 241–249. doi:10.1002/mabi.200500216.
- [100] K.T. Shalumon, K.H. Anulekha, C.M. Girish, R. Prasanth, S.V. Nair, R. Jayakumar, Single step electrospinning of chitosan/poly(caprolactone) nanofibers using formic acid/acetone solvent mixture, *Carbohydr. Polym.* 80 (2010) 413–419. doi:10.1016/j.carbpol.2009.11.039.
- [101] I. Olabarrieta, D. Forsström, U.W. Gedde, M.S. Hedenqvist, Transport properties of chitosan and whey blended with poly(ϵ -caprolactone) assessed by standard permeability measurements and microcalorimetry, *Polymer.* 42 (2001) 4401–4408. doi:10.1016/S0032-3861(00)00680-7.
- [102] A. Sarasam, S.V. Madihally, Characterization of chitosan–polycaprolactone blends for tissue engineering applications, *Biomaterials.* 26 (2005) 5500–5508. doi:10.1016/j.biomaterials.2005.01.071.
- [103] A.R. Sarasam, P. Brown, S.S. Khajotia, J.J. Dmytryk, S.V. Madihally, Antibacterial activity of chitosan-based matrices on oral pathogens, *J. Mater. Sci. Mater. Med.* 19 (2008) 1083–1090. doi:10.1007/s10856-007-3072-z.
- [104] A.R. Sarasam, R.K. Krishnaswamy, S.V. Madihally, Blending Chitosan with Polycaprolactone: Effects on Physicochemical and Antibacterial Properties, *Biomacromolecules.* 7 (2006) 1131–1138. doi:10.1021/bm050935d.
- [105] A.R. Sarasam, A.I. Samli, L. Hess, M.A. Ihnat, S.V. Madihally, Blending chitosan with polycaprolactone: porous scaffolds and toxicity, *Macromol. Biosci.* 7 (2007) 1160–1167. doi:10.1002/mabi.200700001.
- [106] H. She, X. Xiao, R. Liu, Preparation and characterization of polycaprolactone-chitosan composites for tissue engineering applications, *J. Mater. Sci.* 42 (2007) 8113–8119. doi:10.1007/s10853-007-1706-7.
- [107] L. Van der Schueren, B. De Schoenmaker, Ö.I. Kalaoglu, K. De Clerck, An alternative solvent system for the steady state electrospinning of polycaprolactone, *Eur. Polym. J.* 47 (2011) 1256–1263. doi:10.1016/j.eurpolymj.2011.02.025.
- [108] L. Van der Schueren, I. Steyaert, B. De Schoenmaker, K. De Clerck, Polycaprolactone/chitosan blend nanofibres electrospun from an acetic acid/formic acid solvent system, *Carbohydr. Polym.* 88 (2012) 1221–1226. doi:10.1016/j.carbpol.2012.01.085.
- [109] H. Strathmann, K. Kock, P. Amar, R.W. Baker, The formation mechanism of asymmetric membranes, *Desalination.* 16 (1975) 179–203. doi:10.1016/S0011-9164(00)82092-5.
- [110] W.S. Rasband, ImageJ, U. S. National Institutes of Health, Bethesda, Maryland, USA, (1997). <https://imagej.nih.gov/ij/>.
- [111] M.N.V.R. Kumar, R.A.A. Muzzarelli, C. Muzzarelli, H. Sashiwa, A.J. Domb, Chitosan Chemistry and Pharmaceutical Perspectives, *Chem. Rev.* 104 (2004) 6017–6084. doi:10.1021/cr030441b.
- [112] P.J. Flory, Principles of Polymer Chemistry, Cornell University Press, Ithaca, NY, 1953.
- [113] Using the ATR for Qualitative and Quantitative Analysis of Samples, AZoM.Com. (2017). <https://www.azom.com/article.aspx?ArticleID=13585> (accessed February 5, 2019).
- [114] C. Vogel, E. Wessel, H.W. Siesler, FT-IR Imaging Spectroscopy of Phase Separation in Blends of Poly(3-hydroxybutyrate) with Poly(l-lactic acid) and Poly(ϵ -caprolactone), *Biomacromolecules.* 9 (2008) 523–527. doi:10.1021/bm701035p.
- [115] Y. Wan, X. Lu, S. Dalai, J. Zhang, Thermophysical properties of polycaprolactone/chitosan blend membranes, *Thermochim. Acta.* 487 (2009) 33–38. doi:10.1016/j.tca.2009.01.007.

- [116] H. Zhang, X. Luo, X. Lin, X. Lu, Y. Zhou, Y. Tang, Polycaprolactone/chitosan blends: Simulation and experimental design, *Mater. Des.* 90 (2016) 396–402. doi:10.1016/j.matdes.2015.10.108.
- [117] M. Borjigin, C. Eskridge, R. Niamat, B. Strouse, P. Bialk, E.B. Kmiec, Electrospun fiber membranes enable proliferation of genetically modified cells, *Int. J. Nanomedicine.* 8 (2013) 855–864. doi:10.2147/IJN.S40117.
- [118] V.M. Correlo, L.F. Boesel, M. Bhattacharya, J.F. Mano, N.M. Neves, R.L. Reis, Properties of melt processed chitosan and aliphatic polyester blends, *Mater. Sci. Eng. A.* 403 (2005) 57–68. doi:10.1016/j.msea.2005.04.055.
- [119] N. Niamsa, A. Puntumchai, V. Sutthikhum, Y. Srisuwan, Y. Baimark, Preparation and characterization of biodegradable chitosan and methoxy poly(ethylene glycol)-b-poly (ϵ -caprolactone) blend homogeneous films, *J. Appl. Polym. Sci.* 109 (2008) 418–423. doi:10.1002/app.28117.
- [120] Y. Chatani, Y. Okita, H. Tadokoro, Y. Yamashita, Structural Studies of Polyesters. III. Crystal Structure of Poly- ϵ -caprolactone, *Polym. J.* 1 (1970) 555. doi:10.1295/polymj.1.555.
- [121] S. Ramakrishna, K. Fujihara, W.E. Teo, T.C. Lim, Z. Ma, An Introduction to Electrospinning and Nanofibers, World Sci. Publ. Singap. (2005). <http://sci-hub.tw/10.1007/s10853-007-1706-7> (accessed March 10, 2018).
- [122] F.S. Kittur, K.V. Harish Prashanth, K. Udaya Sankar, R.N. Tharanathan, Characterization of chitin, chitosan and their carboxymethyl derivatives by differential scanning calorimetry, *Carbohydr. Polym.* 49 (2002) 185–193. doi:10.1016/S0144-8617(01)00320-4.
- [123] M. Mucha, A. Pawlak, Thermal analysis of chitosan and its blends, *Thermochim. Acta.* 427 (2005) 69–76. doi:10.1016/j.tca.2004.08.014.
- [124] T. Nishi, T.T. Wang, Melting Point Depression and Kinetic Effects of Cooling on Crystallization in Poly(vinylidene fluoride)-Poly(methyl methacrylate) Mixtures, *Macromolecules.* 8 (1975) 909–915. doi:10.1021/ma60048a040.
- [125] H.S. Azevedo, F.M. Gama, R.L. Reis, In Vitro Assessment of the Enzymatic Degradation of Several Starch Based Biomaterials, *Biomacromolecules.* 4 (2003) 1703–1712. doi:10.1021/bm0300397.
- [126] H.S. Azevedo, R.L. Reis, Understanding the Enzymatic Degradation of Biodegradable Polymers and Strategies to Control Their Degradation Rate, *Biodegrad. Syst. Tissue Eng. Regen. Med.* 177–201 (2005). doi:10.1201/9780203491232.ch12.
- [127] J.S. Chawla, M.M. Amiji, Biodegradable poly(ϵ -caprolactone) nanoparticles for tumor-targeted delivery of tamoxifen, *Int. J. Pharm.* 249 (2002) 127–138. doi:10.1016/S0378-5173(02)00483-0.
- [128] Ana R Costa-Pinto, Ana M Martins, Magda J Castelhana-Carlos, Vitor M Correlo, Paula C Sol, Adhemar Longatto-Filho, Mrinal Battacharya, Rui L Reis, Nuno M Neves, In vitro degradation and in vivo biocompatibility of chitosan–poly(butylene succinate) fiber mesh scaffolds, *J. Bioact. Compat. Polym.* 29 (2014) 137–151. doi:10.1177/0883911514521919.
- [129] A.M. Martins, Q.P. Pham, P.B. Malafaya, R.A. Sousa, M.E. Gomes, R.M. Raphael, F.K. Kasper, R.L. Reis, A.G. Mikos, The role of lipase and alpha-amylase in the degradation of starch/poly(epsilon-caprolactone) fiber meshes and the osteogenic differentiation of cultured marrow stromal cells, *Tissue Eng. Part A.* 15 (2009) 295–305. doi:10.1089/ten.tea.2008.0025.
- [130] K. Tomihata, Y. Ikada, In vitro and in vivo degradation of films of chitin and its deacetylated derivatives, *Biomaterials.* 18 (1997) 567–575. doi:10.1016/S0142-9612(96)00167-6.
- [131] K.M. Vårum, M.M. Myhr, R.J.N. Hjerde, O. Smidsrød, In vitro degradation rates of partially N-acetylated chitosans in human serum, *Carbohydr. Res.* 299 (1997) 99–101. doi:10.1016/S0008-6215(96)00332-1.
- [132] H. Sashiwa, H. Saimoto, Y. Shigemasa, R. Ogawa, S. Tokura, Lysozyme susceptibility of partially deacetylated chitin, *Int. J. Biol. Macromol.* 12 (1990) 295–296. doi:10.1016/0141-8130(90)90016-4.
- [133] S. Hirano, H. Tsuchida, N. Nagao, N-acetylation in chitosan and the rate of its enzymic hydrolysis, *Biomaterials.* 10 (1989) 574–576. doi:10.1016/0142-9612(89)90066-5.
- [134] X. Zhong, C. Ji, A.K.L. Chan, S.G. Kazarian, A. Ruys, F. Dehghani, Fabrication of chitosan/poly(ϵ -caprolactone) composite hydrogels for tissue engineering applications, *J. Mater. Sci. Mater. Med.* 22 (2011) 279–288. doi:10.1007/s10856-010-4194-2.

- [135] L. Santambrogio, ed., *Immunology of the Lymphatic System*, Springer-Verlag, New York, 2013. [//www.springer.com/gp/book/9781461432340](http://www.springer.com/gp/book/9781461432340) (accessed March 16, 2018).
- [136] B. Alberts, *Molecular Biology of the Cell*, Courier Corporation, 1989.
- [137] C. Hansen, *Hansen Solubility Parameters: A user's handbook*, Second, Boca Raton, Fla: CRC Press, 2007. <https://www.hansen-solubility.com/> (accessed March 16, 2018).
- [138] R. Ravindra, K.R. Krovvidi, A.A. Khan, Solubility parameter of chitin and chitosan, *Carbohydr. Polym.* 36 (1998) 121–127. doi:10.1016/S0144-8617(98)00020-4.
- [139] R.J. Lehnert, A. Kandelbauer, Comments on “Solubility parameter of chitin and chitosan” *Carbohydrate Polymers* 36 (1998) 121–127, *Carbohydr. Polym.* 175 (2017) 601–602. doi:10.1016/j.carbpol.2017.07.079.
- [140] C. Bordes, V. Fréville, E. Ruffin, P. Marote, J.Y. Gauvrit, S. Briançon, P. Lanteri, Determination of poly(ϵ -caprolactone) solubility parameters: Application to solvent substitution in a microencapsulation process, *Int. J. Pharm.* 383 (2010) 236–243. doi:10.1016/j.ijpharm.2009.09.023.
- [141] C.N. Costa, V.G. Teixeira, M.C. Delpech, J.V.S. Souza, M.A.S. Costa, Viscometric study of chitosan solutions in acetic acid/sodium acetate and acetic acid/sodium chloride, *Carbohydr. Polym.* 133 (2015) 245–250. doi:10.1016/j.carbpol.2015.06.094.
- [142] H. Strathmann, K. Kock, The formation mechanism of phase inversion membranes, *Desalination*. 21 (1977) 241–255. doi:10.1016/S0011-9164(00)88244-2.
- [143] G.R. Guillen, Y. Pan, M. Li, E.M.V. Hoek, Preparation and Characterization of Membranes Formed by Nonsolvent Induced Phase Separation: A Review, *Ind. Eng. Chem. Res.* 50 (2011) 3798–3817. doi:10.1021/ie101928r.
- [144] J.C. Remigy, M. Meireles, X. Thibault, Morphological characterization of a polymeric microfiltration membrane by synchrotron radiation computed microtomography, *J. Membr. Sci.* 305 (2007) 27–35. doi:10.1016/j.memsci.2007.06.059.
- [145] A. Di Luca, B. Ostrowska, I. Lorenzo-Moldero, A. Lepedda, W. Swieszkowski, C. Van Blitterswijk, L. Moroni, Gradients in pore size enhance the osteogenic differentiation of human mesenchymal stromal cells in three-dimensional scaffolds, *Sci. Rep.* 6 (2016). doi:10.1038/srep22898.
- [146] H. Liu, H. Peng, Y. Wu, C. Zhang, Y. Cai, G. Xu, Q. Li, X. Chen, J. Ji, Y. Zhang, H.W. OuYang, The promotion of bone regeneration by nanofibrous hydroxyapatite/chitosan scaffolds by effects on integrin-BMP/Smad signaling pathway in BMSCs, *Biomaterials*. 34 (2013) 4404–4417. doi:10.1016/j.biomaterials.2013.02.048.
- [147] A.I. Caplan, Adult mesenchymal stem cells for tissue engineering versus regenerative medicine, *J. Cell. Physiol.* 213 (2007) 341–347. doi:10.1002/jcp.21200.
- [148] A. Piscioneri, S. Morelli, M. Mele, M. Canonaco, E. Bilotta, P. Pantano, E. Drioli, L. De Bartolo, Neuroprotective effect of human mesenchymal stem cells in a compartmentalized neuronal membrane system, *Acta Biomater.* 24 (2015) 297–308. doi:10.1016/j.actbio.2015.06.013.
- [149] R.S. Teotia, D. Kalita, A.K. Singh, S.K. Verma, S.S. Kadam, J.R. Bellare, Bifunctional Polysulfone-Chitosan Composite Hollow Fiber Membrane for Bioartificial Liver, *ACS Biomater. Sci. Eng.* 1 (2015) 372–381. doi:10.1021/ab500061j.
- [150] M. Prabhakar, M. Rodriguez-perez, J. Saja, J. Mano, Preparation and characterization of poly(L-lactic acid)-chitosan hybrid scaffolds with drug release capability - Prabhakaran - 2007 - *Journal of Biomedical Materials Research Part B: Applied Biomaterials* - Wiley Online Library, *Jour Biomed Mater Res B*. 81B (n.d.) 427–434.
- [151] A. Anitha, S. Sowmya, P.T.S. Kumar, S. Deepthi, K.P. Chennazhi, H. Ehrlich, M. Tsurkan, R. Jayakumar, Chitin and chitosan in selected biomedical applications, *Prog. Polym. Sci.* 39 (2014) 1644–1667. doi:10.1016/j.progpolymsci.2014.02.008.
- [152] M. Dash, F. Chiellini, R.M. Ottenbrite, E. Chiellini, Chitosan—A versatile semi-synthetic polymer in biomedical applications, *Prog. Polym. Sci.* 36 (2011) 981–1014. doi:10.1016/j.progpolymsci.2011.02.001.
- [153] A. Atala, F. Kasper, A. Mikos, Engineering Complex Tissues, *Sci Trans Med.* 4 (2012) 160.
- [154] M. Okamoto, Synthetic biopolymer nanocomposites for tissue engineering scaffolds, *Prog. Polym. Sci.* (2013) 17.

- [155] Z. Li, B.H. Tan, Towards the development of polycaprolactone based amphiphilic block copolymers: molecular design, self-assembly and biomedical applications, *Mater. Sci. Eng. C.* (2014) 15.
- [156] S. Morelli, A. Piscioneri, A. Messina, S. Salerno, M.B. Al-Fageeh, E. Drioli, L.D. Bartolo, Neuronal growth and differentiation on biodegradable membranes, *J. Tissue Eng. Regen. Med.* 9 (2015) 106–117. doi:10.1002/term.1618.
- [157] Y. Xiao, D. Li, X. Chen, J. Lu, H. Fan, X. Zhang, Preparation and cytocompatibility of chitosan-modified polylactide, *J. Appl. Polym. Sci.* 110 (2008) 408–412. doi:10.1002/app.28493.
- [158] M.A. Meyers, J. McKittrick, P.-Y. Chen, Structural Biological Materials: Critical Mechanics-Materials Connections, *Science.* 339 (2013) 773–779. doi:10.1126/science.1220854.
- [159] S. Mitragotri, J. Lahann, Physical approaches to biomaterial design, *Nat. Mater.* 8 (2009) 15–23. doi:10.1038/nmat2344.
- [160] J.M. Holzwarth, P.X. Ma, Biomimetic nanofibrous scaffolds for bone tissue engineering, *Biomaterials.* 32 (2011) 9622–9629. doi:10.1016/j.biomaterials.2011.09.009.
- [161] V.M. Correlo, L.F. Boesel, M. Bhattacharya, J.F. Mano, N.M. Neves, R.L. Reis, Properties of melt processed chitosan and aliphatic polyester blends, *Mater. Sci. Eng. A.* 403 (2005) 57–68. doi:10.1016/j.msea.2005.04.055.
- [162] D. Öner, T.J. McCarthy, Ultrahydrophobic Surfaces. Effects of Topography Length Scales on Wettability, *Langmuir.* 16 (2000) 7777–7782. doi:10.1021/la000598o.
- [163] A. Marmur, The Lotus Effect: Superhydrophobicity and Metastability, *Langmuir.* 20 (2004) 3517–3519. doi:10.1021/la036369u.
- [164] L. Feng, Y. Zhang, J. Xi, Y. Zhu, N. Wang, F. Xia, L. Jiang, Petal Effect: A Superhydrophobic State with High Adhesive Force, *Langmuir.* 24 (2008) 4114–4119. doi:10.1021/la703821h.
- [165] F. He, S. Li, M. Vert, R. Zhuo, Enzyme-catalyzed polymerization and degradation of copolymers prepared from ϵ -caprolactone and poly(ethylene glycol), *Polymer.* 44 (2003) 5145–5151. doi:10.1016/S0032-3861(03)00562-7.
- [166] E. Murray, B.C. Thompson, S. Sayyar, G.G. Wallace, Enzymatic degradation of graphene/polycaprolactone materials for tissue engineering, *Polym. Degrad. Stab.* 111 (2015) 71–77. doi:10.1016/j.polymdegradstab.2014.10.010.
- [167] X. Kang, Y. Xie, H.M. Powell, L. James Lee, M.A. Belury, J.J. Lannutti, D.A. Kniss, Adipogenesis of murine embryonic stem cells in a three-dimensional culture system using electrospun polymer scaffolds, *Biomaterials.* 28 (2007) 450–458. doi:10.1016/j.biomaterials.2006.08.052.
- [168] G.F. Muschler, C. Nakamoto, L.G. Griffith, ENGINEERING PRINCIPLES OF CLINICAL CELL-BASED TISSUE ENGINEERING:, *J. Bone Jt. Surg.-Am.* Vol. 86 (2004) 1541–1558. doi:10.2106/00004623-200407000-00029.
- [169] W.F. Quirós-Solano, N. Gaio, O.M.J.A. Stassen, Y.B. Arik, C. Silvestri, N.C.A.V. Engeland, A.V. der Meer, R. Passier, C.M. Sahlgren, C.V.C. Bouten, A. van den Berg, R. Dekker, P.M. Sarro, Microfabricated tuneable and transferable porous PDMS membranes for Organs-on-Chips, *Sci. Rep.* 8 (2018) 13524. doi:10.1038/s41598-018-31912-6.
- [170] M.W. van der Helm, Electrical and microfluidic technologies for organs-on-chips: Mimicking blood-brain barrier and gut tissues, (2018). doi:10.3990/1.9789036544672.
- [171] Y. Xia, G.M. Whitesides, Soft Lithography, *Annu. Rev. Mater. Sci.* 28 (1998) 153–184. doi:10.1146/annurev.matsci.28.1.153.
- [172] D. Huh, Y. Torisawa, G.A. Hamilton, H.J. Kim, D.E. Ingber, Microengineered physiological biomimicry: organs-on-chips, *Lab. Chip.* 12 (2012) 2156–2164. doi:10.1039/c2lc40089h.
- [173] A.K. Capulli, K. Tian, N. Mehandru, A. Bukhta, S.F. Choudhury, M. Suchyta, K.K. Parker, Approaching the In Vitro Clinical Trial: Engineering Organs on Chips, *Lab. Chip.* 14 (2014) 3181–3186. doi:10.1039/c4lc00276h.
- [174] D. Huh, G.A. Hamilton, D.E. Ingber, From 3D cell culture to organs-on-chips, *Trends Cell Biol.* 21 (2011) 745–754. doi:10.1016/j.tcb.2011.09.005.
- [175] D. Huh, H.J. Kim, J.P. Fraser, D.E. Shea, M. Khan, A. Bahinski, G.A. Hamilton, D.E. Ingber, Microfabrication of human organs-on-chips, *Nat. Protoc.* 8 (2013) 2135–2157. doi:10.1038/nprot.2013.137.

- [176] V.V. Abhyankar, M. Wu, C.-Y. Koh, A.V. Hatch, A Reversibly Sealed, Easy Access, Modular (SEAM) Microfluidic Architecture to Establish In Vitro Tissue Interfaces, *PLOS ONE*. 11 (2016) e0156341. doi:10.1371/journal.pone.0156341.
- [177] H. Lee, D.S. Kim, S.K. Ha, I. Choi, J.M. Lee, J.H. Sung, A pumpless multi-organ-on-a-chip (MOC) combined with a pharmacokinetic-pharmacodynamic (PK-PD) model, *Biotechnol. Bioeng.* 114 (2017) 432–443. doi:10.1002/bit.26087.
- [178] P. Loskill, T. Sezhan, K.M. Tharp, F.T. Lee-Montiel, S. Jeeawoody, W.M. Reese, P.-J.H. Zushin, A. Stahl, K.E. Healy, WAT-on-a-chip: a physiologically relevant microfluidic system incorporating white adipose tissue, *Lab. Chip*. 17 (2017) 1645–1654. doi:10.1039/c6lc01590e.
- [179] K.-Y. Shim, D. Lee, J. Han, N.-T. Nguyen, S. Park, J.H. Sung, Microfluidic gut-on-a-chip with three-dimensional villi structure, *Biomed. Microdevices*. 19 (2017) 37. doi:10.1007/s10544-017-0179-y.
- [180] L. Zhu, H. Xia, Z. Wang, E.L.S. Fong, J. Fan, W.H. Tong, Y.P.D. Seah, W. Zhang, Q. Li, H. Yu, A vertical-flow bioreactor array compacts hepatocytes for enhanced polarity and functions, *Lab. Chip*. 16 (2016) 3898–3908. doi:10.1039/c6lc00811a.
- [181] K.J. Pocock, X. Gao, C. Wang, C. Priest, C.A. Prestidge, K. Mawatari, T. Kitamori, B. Thierry, Low-temperature bonding process for the fabrication of hybrid glass–membrane organ-on-a-chip devices, *J. MicroNanolithography MEMS MOEMS*. 15 (2016) 044502. doi:10.1117/1.JMM.15.4.044502.
- [182] B.M. Maoz, A. Herland, O.Y.F. Henry, W.D. Leineweber, M. Yadid, J. Doyle, R. Mannix, V.J. Kujala, E.A. FitzGerald, K.K. Parker, D.E. Ingber, Organs-on-Chips with combined multi-electrode array and transepithelial electrical resistance measurement capabilities, *Lab. Chip*. 17 (2017) 2294–2302. doi:10.1039/c7lc00412e.
- [183] Y.I. Wang, H.E. Abaci, M.L. Shuler, Microfluidic blood-brain barrier model provides in vivo-like barrier properties for drug permeability screening, *Biotechnol. Bioeng.* 114 (2017) 184–194. doi:10.1002/bit.26045.
- [184] D. Sticker, M. Rothbauer, S. Lechner, M.-T. Hehenberger, P. Ertl, Multi-layered, membrane-integrated microfluidics based on replica molding of a thiol–ene epoxy thermoset for organ-on-a-chip applications, *Lab. Chip*. 15 (2015) 4542–4554. doi:10.1039/C5LC01028D.
- [185] Y. Ma, J.-Z. Pan, S.-P. Zhao, Q. Lou, Y. Zhu, Q. Fang, Microdroplet chain array for cell migration assays, *Lab. Chip*. 16 (2016) 4658–4665. doi:10.1039/C6LC00823B.
- [186] S. Lee, S.-P. Jin, Y.K. Kim, G.Y. Sung, J.H. Chung, J.H. Sung, Construction of 3D multicellular microfluidic chip for an in vitro skin model, *Biomed. Microdevices*. 19 (2017) 22. doi:10.1007/s10544-017-0156-5.
- [187] M. Jie, H.-F. Li, L. Lin, J. Zhang, J.-M. Lin, Integrated microfluidic system for cell co-culture and simulation of drug metabolism, *RSC Adv.* 6 (2016) 54564–54572. doi:10.1039/C6RA10407J.
- [188] J.A. Brown, S.G. Codreanu, M. Shi, S.D. Sherrod, D.A. Markov, M.D. Neely, C.M. Britt, O.S. Hoilett, R.S. Reiserer, P.C. Samson, L.J. McCawley, D.J. Webb, A.B. Bowman, J.A. McLean, J.P. Wikswo, Metabolic consequences of inflammatory disruption of the blood-brain barrier in an organ-on-chip model of the human neurovascular unit, *J. Neuroinflammation*. 13 (2016). doi:10.1186/s12974-016-0760-y.
- [189] C.S. Chen, M. Mrksich, S. Huang, G.M. Whitesides, D.E. Ingber, Geometric control of cell life and death, *Science*. 276 (1997) 1425–1428.
- [190] M. Hulsman, F. Hulshof, H. Unadkat, B.J. Papenburg, D.F. Stamatialis, R. Truckenmüller, C. van Blitterswijk, J. de Boer, M.J.T. Reinders, Analysis of high-throughput screening reveals the effect of surface topographies on cellular morphology, *Acta Biomater.* 15 (2015) 29–38. doi:10.1016/j.actbio.2014.12.019.
- [191] M.B. Esch, D.J. Post, M.L. Shuler, T. Stokol, Characterization of in vitro endothelial linings grown within microfluidic channels, *Tissue Eng. Part A*. 17 (2011) 2965–2971. doi:10.1089/ten.tea.2010.0371.
- [192] K.E. Broaders, A.E. Cerchiari, Z.J. Gartner, Coupling between apical tension and basal adhesion allow epithelia to collectively sense and respond to substrate topography over long distances, *Integr. Biol. Quant. Biosci. Nano Macro*. 7 (2015) 1611–1621. doi:10.1039/c5ib00240k.

- [193] M. Lampin, null Warocquier-Clérout, C. Legris, M. Degrange, M.F. Sigot-Luizard, Correlation between substratum roughness and wettability, cell adhesion, and cell migration, *J. Biomed. Mater. Res.* 36 (1997) 99–108.
- [194] D.P. Dowling, I.S. Miller, M. Ardhaoui, W.M. Gallagher, Effect of surface wettability and topography on the adhesion of osteosarcoma cells on plasma-modified polystyrene, *J. Biomater. Appl.* 26 (2011) 327–347. doi:10.1177/0885328210372148.
- [195] T.P. Kunzler, T. Drobek, M. Schuler, N.D. Spencer, Systematic study of osteoblast and fibroblast response to roughness by means of surface-morphology gradients, *Biomaterials.* 28 (2007) 2175–2182. doi:10.1016/j.biomaterials.2007.01.019.
- [196] R. Lange, F. Lüthen, U. Beck, J. Rychly, A. Baumann, B. Nebe, Cell-extracellular matrix interaction and physico-chemical characteristics of titanium surfaces depend on the roughness of the material, *Biomol. Eng.* 19 (2002) 255–261.
- [197] J.H. Lee, G. Khang, J.W. Lee, H.B. Lee, Interaction of Different Types of Cells on Polymer Surfaces with Wettability Gradient, *J. Colloid Interface Sci.* 205 (1998) 323–330. doi:10.1006/jcis.1998.5688.
- [198] J. Wala, D. Maji, S. Das, Influence of physico-mechanical properties of elastomeric material for different cell growth, *Biomed. Mater. Bristol Engl.* 12 (2017) 065002. doi:10.1088/1748-605X/aa7e81.
- [199] A.J. Engler, S. Sen, H.L. Sweeney, D.E. Discher, Matrix elasticity directs stem cell lineage specification, *Cell.* 126 (2006) 677–689. doi:10.1016/j.cell.2006.06.044.
- [200] S.M. Casillo, A.P. Peredo, S.J. Perry, H.H. Chung, T.R. Gaborski, Membrane Pore Spacing Can Modulate Endothelial Cell-Substrate and Cell-Cell Interactions, *ACS Biomater. Sci. Eng.* 3 (2017) 243–248. doi:10.1021/acsbiomaterials.7b00055.
- [201] M.Y. Kim, D.J. Li, L.K. Pham, B.G. Wong, E.E. Hui, Microfabrication of High-Resolution Porous Membranes for Cell Culture, *J. Membr. Sci.* 452 (2014) 460–469. doi:10.1016/j.memsci.2013.11.034.
- [202] M.B. Esch, J.H. Sung, J. Yang, C. Yu, J. Yu, J.C. March, M.L. Shuler, On chip porous polymer membranes for integration of gastrointestinal tract epithelium with microfluidic “body-on-a-chip” devices, *Biomed. Microdevices.* 14 (2012) 895–906. doi:10.1007/s10544-012-9669-0.
- [203] H. Wei, B. Chueh, H. Wu, E.W. Hall, C. Li, R. Schirhagl, J.-M. Lin, R.N. Zare, Particle sorting using a porous membrane in a microfluidic device, *Lab. Chip.* 11 (2011) 238–245. doi:10.1039/C0LC00121J.
- [204] V. Pensabene, L. Costa, A.Y. Terekhov, J.S. Gnecco, J.P. Wikswo, W.H. Hofmeister, Ultrathin Polymer Membranes with Patterned, Micrometric Pores for Organs-on-Chips, *ACS Appl. Mater. Interfaces.* 8 (2016) 22629–22636. doi:10.1021/acsami.6b05754.
- [205] V. Pensabene, S.W. Crowder, D.A. Balikov, J.B. Lee, H.J. Sung, Optimization of electrospun fibrous membranes for in vitro modeling of blood-brain barrier, *Conf. Proc. Annu. Int. Conf. IEEE Eng. Med. Biol. Soc. IEEE Eng. Med. Biol. Soc. Annu. Conf.* 2016 (2016) 125–128. doi:10.1109/EMBC.2016.7590656.
- [206] Q. Cheng, B.L.-P. Lee, K. Komvopoulos, S. Li, Engineering the Microstructure of Electrospun Fibrous Scaffolds by Microtopography, *Biomacromolecules.* 14 (2013) 1349–1360. doi:10.1021/bm302000n.
- [207] J. Garra, T. Long, J. Currie, T. Schneider, R. White, M. Paranjape, Dry etching of polydimethylsiloxane for microfluidic systems, *J. Vac. Sci. Technol. A.* 20 (2002) 975–982. doi:10.1116/1.1460896.
- [208] S.J. Hwang, D.J. Oh, P.G. Jung, S.M. Lee, J.S. Go, J.-H. Kim, K.-Y. Hwang, J.S. Ko, Dry etching of polydimethylsiloxane using microwave plasma, *J. Micromechanics Microengineering.* 19 (2009) 095010. doi:10.1088/0960-1317/19/9/095010.
- [209] M. Prabakaran, M.A. Rodriguez-Perez, J.A. de Saja, J.F. Mano, Preparation and characterization of poly(L-lactic acid)-chitosan hybrid scaffolds with drug release capability, *J. Biomed. Mater. Res. B Appl. Biomater.* 81B (2007) 427–434. doi:10.1002/jbm.b.30680.
- [210] M.W. van der Helm, M. Odijk, J.-P. Frimat, A.D. van der Meer, J.C.T. Eijkel, A. van den Berg, L.I. Segerink, Fabrication and Validation of an Organ-on-chip System with Integrated Electrodes to Directly Quantify Transendothelial Electrical Resistance, *JoVE J. Vis. Exp.* (2017) e56334–e56334. doi:10.3791/56334.

- [211] B. Chueh, D. Huh, C.R. Kyrtos, T. Houssin, N. Futai, S. Takayama, Leakage-Free Bonding of Porous Membranes into Layered Microfluidic Array Systems, *Anal. Chem.* 79 (2007) 3504–3508. doi:10.1021/ac062118p.
- [212] L.M. Griep, F. Wolbers, B. de Wagenaar, P.M. ter Braak, B.B. Weksler, I.A. Romero, P.O. Couraud, I. Vermes, A.D. van der Meer, A. van den Berg, BBB ON CHIP: microfluidic platform to mechanically and biochemically modulate blood-brain barrier function, *Biomed. Microdevices.* 15 (2013) 145–150. doi:10.1007/s10544-012-9699-7.
- [213] FRP Flow Sensor: FLOW-RATE PLATFORM | Fluigent 2018, Fluigent. (n.d.). <https://www.fluigent.com/product/microfluidic-components/frp-flow-rate-platform/> (accessed December 17, 2018).
- [214] H.W. Sill, Y.S. Chang, J.R. Artman, J.A. Frangos, T.M. Hollis, J.M. Tarbell, Shear stress increases hydraulic conductivity of cultured endothelial monolayers, *Am. J. Physiol.-Heart Circ. Physiol.* 268 (1995) H535–H543. doi:10.1152/ajpheart.1995.268.2.H535.
- [215] Z. Pang, D.A. Antonetti, J.M. Tarbell, Shear stress regulates HUVEC hydraulic conductivity by occludin phosphorylation, *Ann. Biomed. Eng.* 33 (2005) 1536–1545. doi:10.1007/s10439-005-7786-0.
- [216] P.M. Lockett, J. Fischbarg, J. Bhattacharya, S.C. Silverstein, Hydraulic conductivity of endothelial cell monolayers cultured on human amnion, *Am. J. Physiol.-Heart Circ. Physiol.* 256 (1989) H1675–H1683. doi:10.1152/ajpheart.1989.256.6.H1675.
- [217] P. Desmond, J.P. Best, E. Morgenroth, N. Derlon, Linking composition of extracellular polymeric substances (EPS) to the physical structure and hydraulic resistance of membrane biofilms, *Water Res.* 132 (2018) 211–221. doi:10.1016/j.watres.2017.12.058.
- [218] P. Desmond, L. Böni, P. Fischer, E. Morgenroth, N. Derlon, Stratification in the physical structure and cohesion of membrane biofilms — Implications for hydraulic resistance, *J. Membr. Sci.* 564 (2018) 897–904. doi:10.1016/j.memsci.2018.07.088.
- [219] E. Fröhlich, G. Bonstingl, A. Höfler, C. Meindl, G. Leitinger, T.R. Pieber, E. Roblegg, Comparison of two in vitro systems to assess cellular effects of nanoparticles-containing aerosols, *Toxicol. In Vitro.* 27–360 (2013) 409–417. doi:10.1016/j.tiv.2012.08.008.
- [220] Product lines, GVS Filter Technol. (n.d.). <http://www.gvs.com> (accessed September 18, 2018).
- [221] K. Madhavan, W.H. Elliott, W. Bonani, E. Monnet, W. Tan, Mechanical and biocompatible characterizations of a readily available multilayer vascular graft, *J. Biomed. Mater. Res. B Appl. Biomater.* 101 (2013) 506–519. doi:10.1002/jbm.b.32851.
- [222] H. Bazyar, P. Lv, J.A. Wood, S. Porada, D. Lohse, R.G.H. Lammertink, Liquid–liquid displacement in slippery liquid-infused membranes (SLIMs), *Soft Matter.* 14 (2018) 1780–1788. doi:10.1039/C7SM02337E.
- [223] R.S. Barhate, S. Ramakrishna, Nanofibrous filtering media: Filtration problems and solutions from tiny materials, *J. Membr. Sci.* 296 (2007) 1–8. doi:10.1016/j.memsci.2007.03.038.
- [224] D. Borge, N. Daels, S. De Vrieze, P. Dejans, T. Van Camp, W. Audenaert, J. Hogue, P. Westbroek, K. De Clerck, S.W.H. Van Hulle, Performance assessment of electrospun nanofibers for filter applications, *Desalination.* 249 (2009) 942–948. doi:10.1016/j.desal.2009.06.064.
- [225] A. Cooper, R. Oldinski, H. Ma, J.D. Bryers, M. Zhang, Chitosan-based nanofibrous membranes for antibacterial filter applications, *Carbohydr. Polym.* 92 (2013) 254–259. doi:10.1016/j.carbpol.2012.08.114.
- [226] P. Premnath, A. Tavangar, B. Tan, K. Venkatakrishnan, Tuning cell adhesion by direct nanostructuring silicon into cell repulsive/adhesive patterns, *Exp. Cell Res.* 337 (2015) 44–52. doi:10.1016/j.yexcr.2015.07.028.
- [227] X. Xiao, W. Wang, D. Liu, H. Zhang, P. Gao, L. Geng, Y. Yuan, J. Lu, Z. Wang, The promotion of angiogenesis induced by three-dimensional porous beta-tricalcium phosphate scaffold with different interconnection sizes via activation of PI3K/Akt pathways, *Sci. Rep.* 5 (2015) 9409. doi:10.1038/srep09409.
- [228] M. Mastrogiacomo, S. Scaglione, R. Martinetti, L. Dolcini, F. Beltrame, R. Cancedda, R. Quarto, Role of scaffold internal structure on in vivo bone formation in macroporous calcium phosphate bioceramics, *Biomaterials.* 27 (2006) 3230–3237. doi:10.1016/j.biomaterials.2006.01.031.

- [229] S.L. Nyberg, R.A. Shatford, M.V. Peshwa, J.G. White, F.B. Cerra, W.-S. Hu, Evaluation of a hepatocyte-entrapment hollow fiber bioreactor: A potential bioartificial liver, *Biotechnol. Bioeng.* 41 (1993) 194–203. doi:10.1002/bit.260410205.
- [230] L. De Bartolo, S. Salerno, E. Curcio, A. Piscioneri, M. Rende, S. Morelli, F. Tasselli, A. Bader, E. Drioli, Human hepatocyte functions in a crossed hollow fiber membrane bioreactor, *Biomaterials.* 30 (2009) 2531–2543. doi:10.1016/j.biomaterials.2009.01.011.
- [231] D. Falconnet, G. Csucs, H. Michelle Grandin, M. Textor, Surface engineering approaches to micropattern surfaces for cell-based assays, *Biomaterials.* 27 (2006) 3044–3063. doi:10.1016/j.biomaterials.2005.12.024.
- [232] F.J.E. Sanz, J.F. Lahitte, J.-C. Remigy, Membrane synthesis by microemulsion polymerisation stabilised by commercial non-ionic surfactants, *Desalination.* 199 (2006) 127–129. doi:10.1016/j.desal.2006.03.156.
- [233] M.N. Lee, A. Mohraz, Bicontinuous Macroporous Materials from Bijel Templates, *Adv. Mater.* 22 (2010) 4836–4841. doi:10.1002/adma.201001696.

Scientific Output

Publications

- **Pritam Das**, Jean-Christophe Remigy, Jean-François Lahitte, Barbara Garmy-Susini, Clémence Coetsier, Sandrine Desclaux, Patrice Bacchin, Double porous poly (ϵ - caprolactone)/chitosan blend membrane as tissue engineering scaffold: from material development to human dermal lymphatic endothelial cell growth. (Submitted)
- **Pritam Das**, Simona Salerno, Jean-Christophe Remigy, Jean-François Lahitte, Patrice Bacchin, Loredana De Bartolo, Double porous, biodegradable poly (ϵ -caprolactone)/chitosan 3D scaffolds: understanding hMSCs attachment, proliferation and invasion by varying pore size and morphology of the scaffolds. (In preparation)
- **Pritam Das**, Andries D. van der Meer, Aisen Vivas, Yusuf B. Arik, Jean-Christophe Remigy, Jean-François Lahitte, Rob G. H. Lammertink, Patrice Bacchin, Fabrication of tuneable micro-structured flat sheet membrane in Organ-on-chip to monitor trans-endothelial hydraulic resistance. (Submitted)

Conferences

- June 2018: North American Membrane Society conference, Lexington, KY, USA.
 - Oral Presentation: **Pritam Das**, Jean-Christophe Remigy, Jean-François Lahitte, Simona Salerno, Loredana De Bartolo, Patrice Bacchin, Double porous membrane as bio-artificial vascular patch: development, characterization and understanding cell-matrix interaction by varying pore size and morphology.
 - Poster Presentation: **Pritam Das**, Andries D. van der Meer, Jean-Christophe Remigy, Jean-François Lahitte, Rob G. H. Lammertink, Patrice Bacchin, Direct quantification of transendothelial electrical resistance to estimate the barrier function in organ-on-chip embedded with double porous membrane.
- September 2017: European Society for Biomaterials International conference, Athens, Greece.
 - Oral Presentation: **Pritam Das**, Simona Salerno, Patrice Bacchin, Loredana De Bartolo, Development of double porous material by poly (ϵ -caprolactone)/chitosan blends for tissue engineering application
- June 2016: Termis-European Chapter International Conference, Uppsala, Sweden.
 - Poster Presentation: **Pritam Das**, Jean-François Lahitte, Jean Christophe Remigy, Barbara Garmy Susini, Sandrine Desclaux, Clémence Coetsier, Loredana De Bartolo, Patrice Bacchin, Artificial membranes tuning for lymphatic wall repair, 2016: p. 101. <https://hal.archives-ouvertes.fr/hal-01360666>.
- Nov 2015: La Journée Des Doctorants (JDD), INP-ENSIACET, Toulouse, France.
 - Poster Presentation : **Pritam Das**, Patrice Bacchin, Jean-François Lahitte, Barbara Garmy-Susini, Jean Christophe Remigy, Clémence Coietsier, Artificial Membranes Tuning for Controlled Biological Cells Interactions.

Thank You.

I would like to thank my funding Erasmus Mundus Doctorate in Membrane Engineering (EUDIME-5th Ed.) under the European commission (EACEA).

These three years will be always special and memorable of my entire life. It was the fastest three years of my life so far with lots of experiences including academic and social field. I have opportunity to travel many places, to meet with many people from different cultural background and to learn my positive aspect of life, which is one of my best hobby. I have a nice time not only to improve my professional working experiences but also to build character with deeper moral values. For that, I will always appreciate the great European culture that gives me always the charm to find sense behind what I see, hear or do.

At first, I would like to convey my deepest regards to Prof. Patrice Bacchin. You are great supervisors. Apart from all the fruitful scientific discussion, you always strengthen my confidence and always give me space at first and value my opinion. I am really grateful to your enthusiasm, determination to research and always encouraging personality. This are the sign of a true leader and that is what I am still learning from you. I will highly acknowledge Dr. Jean-François Lahitte, Prof. Jean-Christophe Remegy, Dr. Clémence Coitsoir and Dr. Barbara Gergy-susini. Please accept my kind gratitude for all the scientific discussion and for your great supervision.

This doctoral program also give me opportunity to do fruitful international collaboration in other top-notch departments in the partner universities. Hence, I would deeply thankful to Dr. Loredana de Bartolo, Dr. Simona Salerno from my first host university and Dr. Andries van der Meer and Prof. Rob G.H. Lammertink from my second host university. I thank to you for all the fruitful scientific discussion, your support, determination and ever-motivating personality.

Therefore, I highly appreciate the attitude and the substance of genius and the excitement in regard to research for all of my respected supervisors. Without your consistence guidance, this dissertation would not have been possible.

I also would like to thank all the technicians, my fellow colleagues/friends and all other members of the three Universities. Thank you for having a great time with me. Thank you being an integral part of this three years and your support no matter which situation it was.

Thank you to the entire thesis committee member to review my thesis work and I highly acknowledge that you find time to be present in my defense.

It is the end of three years of my doctorate and I am really happy for one of the most special occasion of my life. But I am not super excited. It is the beginning and the last three years just increase my hunger for knowledge and to do research. Hence many things to do ahead. It started since long ago and I do not remember when. But I still remember in the first day in my bachelor in the chemistry practical lab. That I used to do crazy chemical reactions just to get excitement what happen next and followed by a simple question always from my mind 'WHY!!?'. No matter which profession, hobby or passion I will choose in my life, I will continue my research.

And finally I have no word to say my parents but accept my deepest regards to make me what I am. Your never-ending love and support are the primary elements which lead a small kid from an average school in India to earn his master from one of the elite university of India and followed by research graduate from well-known universities in abroad. You always motivate me to be highly educated and wanted to see me as your doctorate son. Hence here it is, please accept the small gift.

About the Author

Pritam Das was born in 23rd September 1990 at Serampore, West Bengal, India. In March 2013, he received his Master of Science degree (M.Sc.) in chemistry (with organic specialization) from R.K.M.C. Narendrapur under Calcutta University, India. After that he got the opportunity to do his Master of Technology degree (M.Tech.) from Indian institute of Technology (IIT) Kharagpur, India in polymer technology as an interdisciplinary subject. During his M.Tech. he went to Libniz institute for polymer research Dresden, Germany to do his Master thesis under DAAD-IIT fellowship. He was working on water filtration application by chemical nanostructured surface modification of microporous membrane under Prof. Manfred Stamm. After his Master studies, he got opportunity to peruse his doctorate degree funded by Erasmus Mundus Doctorate in Membrane Engineering (EUDIME 5th ed.) under European Commission (EACEA). This doctorate degree allows him to do his work with collaboration between three Universities under the consortium. He started his doctoral work at first in University Paul Sabatier as home university under Prof. Patrice Bacchin, Dr. Jean-françois Lahitte, Prof. Jean-christophe Remigy and Dr. Clémence Coitsoir. That time his work was to develop tunable micro-structured polymeric membranes with modified phase inversion technique. After that, he went to ITM-CNR under University of Calabria as his first host university to work under supervision of Dr. Loredana de Bartolo and Dr. Simona Salerno. He was able to apply those micro-structured membranes for tissue culture application with human stem cell. Finally, he went to University of Twente as his second host university to work under Dr. Andries van der Meer and Prof. Rob G.H. Lammeetink. That time he was mainly focus to apply those membranes as potent biomaterials in microfluidic Organ-on-chip system for human vascular grafts application. In December 2018, he will defend his final thesis and successfully obtain his joint doctoral degree from three universitie.